

NONINVASIVE DETECTION OF PHYSIOLOGICALLY SIGNIFICANT
PUMPING STATES IN AN IMPLANTABLE ROTARY BLOOD PUMP

OOI HUI LEE

FACULTY OF ENGINEERING
UNIVERSITY OF MALAYA
KUALA LUMPUR

2014

NONINVASIVE DETECTION OF PHYSIOLOGICALLY
SIGNIFICANT PUMPING STATES IN AN IMPLANTABLE
ROTARY BLOOD PUMP

OOI HUI LEE

DISSERTATION SUBMITTED IN FULFILMENT
OF THE REQUIREMENT FOR THE DEGREE OF
MASTER OF ENGINEERING SCIENCE

FACULTY OF ENGINEERING
UNIVERSITY OF MALAYA
KUALA LUMPUR

2014

UNIVERSITI MALAYA

ORIGINAL LITERARY WORK DECLARATION

Name of Candidate: Ooi Hui Lee

Registration/Matrix No.: KGA120085

Name of Degree: Master of Engineering Science

Title of Project Paper/Research Report/Dissertation/Thesis ("this Work"):

Noninvasive Classification of Physiologically Significant Pumping States in an Implantable Rotary Blood Pump

Field of Study: Biomedical Engineering (Engineering and Engineering Trades)

I do solemnly and sincerely declare that:

- (1) I am the sole author/writer of this Work;
- (2) This work is original;
- (3) Any use of any work in which copyright exists was done by way of fair dealing and for permitted purposes and any excerpt or extract from, or reference to or reproduction of any copyright work has been disclosed expressly and sufficiently and the title of the Work and its authorship have been acknowledged in this Work;
- (4) I do not have any actual knowledge nor do I ought reasonably to know that the making of this work constitutes an infringement of any copyright work;
- (5) I hereby assign all and every rights in the copyright to this Work to the University of Malaya ("UM"), who henceforth shall be owner of the copyright in this Work and that any reproduction or use in any form or by any means whatsoever is prohibited without the written consent of UM having been first had and obtained;
- (6) I am fully aware that if in the course of making this Work I have infringed any copyright whether intentionally or otherwise, I may be subject to legal action or any other action as may be determined by UM.

Candidate's Signature

Date

Subscribed and solemnly declared before,

Witness's Signature

Date

Name:

Designation:

ABSTRACT

Heart failure is a serious health problem that could potentially be life threatening as the inflected heart lacks the ability to supply sufficient oxygen rich blood to the rest of the body. This spurred the emergence of implantable rotary blood pump (IRBP) that is designed to provide an alternative route for blood flow as opposed to the native route that may be obstructed or problematic due to different circumstances. In particular, much interest has been garnered on the subject of pump state detection due to the potential deleterious outcomes that is associated with over-pumping. The full unloading of the left ventricle (LV) over long period of time in a pump state known as aortic valve non-opening (ANO) may cause aortic valve fusion and thrombosis. Excessive pumping in a pump state known as ventricular suction may induce several complications such as arrhythmia induction, shift of septum, tricuspidal anastomosis and dislodging of thrombi. In this study, over-pumping states such as ANO and ventricular suction are investigated by employing the pump speed signal that is acquired noninvasively from four greyhounds that consists of different levels of systemic vascular resistance (SVR) and total blood volume. A nested classification strategy is applied in two stages, with the first one involves the detection of ventricular suction whereas the second stage was focused on distinguishing ANO state from the normal ventricular ejection (VE) state. The classification task is implemented by evaluating newly introduced indices (Ran_2 , Ran_3 , Sta_1 , Rms_1 , Rms_3 , Rmr_1 , Rmr_2 , Rmr_3) in addition to the existing indices for the different pump states. Four types of classification algorithms, namely linear discriminant analysis (LDA), logistic regression (LR), back propagation neural network (BPNN) and k-nearest neighbor (KNN) are applied to the computed indices to assess their performance in identification of the different pump states. From the study it is observed that ventricular suction detection achieved accuracy of 94% when implemented individually using the duration index. The

performance for combination of indices was noted to have improved up to 99.5% (five indices). As for ANO pump states, combination of root mean square and standard deviation has successfully performed the detection with accuracy of 93%. Further addition of indices of (five indices) will produce accuracy of 94.6%.

University of Malaya

ABSTRAK

Kegagalan jantung merupakan masalah kesihatan serius yang mengancam nyawa disebabkan jantung kehilangan kebolehan untuk membekalkan oksigen yang secukupnya melalui aliran darah ke seluruh badan. Ini mendorong ciptaan implan pam darah putaran (IRBP) untuk menyediakan laluan alternatif untuk pengaliran darah dari laluan asal yang tersumbat atau bermasalah. Khususnya, subjek pengesanan keadaan pam telah banyak menarik minat atas sebab risiko kesan buruk yang dikaitkan dengan pengempaman yang keterlaluan. 'Unloading' yang sepenuhnya dalam ventrikel kiri pesakit untuk tempoh masa yang panjang dalam keadaan injap aortik yang bertutup (ANO) akan mendorong gabungan injap aortik dan trombosis. Pengempaman secara berlebihan dalam keadaan pam yang dikenal sebagai penyedutan ventrikel akan menyebabkan komplikasi seperti aritmia, pengalihan septum, anastomosis dalam injap trikuspid dan pengasingan trombus. Dalam kajian ini, keadaan pam yang keterlaluan seperti ANO dan penyedutan ventrikel telah diselidik dengan menggunakan isyarat kelajuan pam yang diperoleh dengan cara bukan invasif dari haiwan 'greyhound' yang mengadungi pelbagai tahap rintangan sistem vaskular (SVR) and jumlah isipadu darah. Klasifikasi berperingkat telah digunakan dalam dua tahap, tahap pertama melibatkan keadaan penyedutan ventrikel manakala tahap kedua menumpukan perhatian kepada perbezaan keadaan ANO daripada keadaan penolakan ventrikel (VE) yang normal. Tugas klasifikasi telah dilaksanakan dengan penilaian indeks baru (Ran_2 , Ran_3 , Sta_1 , Rms_1 , Rms_3 , Rmr_1 , Rmr_2 , Rmr_3) selain indeks yang sedia ada untuk keadaan pam yang berbeza. Empat jenis algoritma klasifikasi, iaitu analisis diskriminan linear (LDA), regresi logistik (LR), rangkaian neural perambatan balik (BPNN) dan k-jiran terdekat (KNN) telah digunakan pada untuk penilaian prestasi indeks teresebut dalam pengenalanpastian keadaan pam. Pemerhatian dari kajian menunjukkan bahawa pengesanan keadaan ventrikel penyedutan mencapai ketepatan sebanyak 94% apabila indeks tempoh

digunakan secara individu, prestasi kombinasi indeks diperhatikan telah meningkat kepada 99.5% (lima indeks). Bagi keadaan ANO, kombinasi punca min kuasa dua dan sisihan piawai telah berjaya melaksanakan pengesanan dengan ketepatan 93%. Penambahan indeks seterusnya dalam kombinasi (lima indeks) dapat meningkatkan ketepatan sehingga 94.6%.

University of Malaya

ACKNOWLEDGEMENTS

First and foremost, I would like to extend my deepest appreciation and gratitude to both of my supervisors, Dr. Ng Siew Cheok and Dr. Lim Einly for their intellectual support and inspiration. Their invaluable guidance, tremendous patience, insightful recommendation and encouragement, not to mention the time spent throughout the time of this study are highly appreciated.

Also, I am highly indebted to Dr. Lim Einly for her willingness to take me in under her grant with Ministry of Higher Education Malaysia (grant number: UM /HIR (MOHE) /ENG /50) that offered me financial support and sponsorship throughout the course of my MEngSc study.

My gratitude also extends to her collaborators: Prof. Robert F. Salamonsen, Prof. Alberto Avolio and Prof. Nigel Lovell for overseeing the writing and revision process of publication by offering insightful recommendations. I would like to thank the University of New South Wales (UNSW) for granting me permission to use its experimental data in my study as presented in this dissertation.

Next, my special thank goes to fellow colleagues and lab mates in NeuroLab and Asian Cardiac Engineering Lab in Department of Biomedical Engineering, Faculty of Engineering, University of Malaya for providing the vibrant and wonderful working environment that is conducive to my research progress. It has been a pleasure working with these wonderful individuals.

Lastly, I would like to devote my appreciations and blessings to my family and friends who have rendered their whole-heart support and encouragement at all times in my pursuit of this study.

CONSENT LETTER

8 June, 2014

Ms. Ooi Hui Lee
Department of Biomedical Engineering
Faculty of Engineering
University of Malaya



To Whom it May Concern,

Letter of consent for the use of experimental data in thesis

An animal experiment involving greyhounds was conducted for the purpose of studying control aspects of a left ventricular assist device (LVAD). It was carried out in strict accordance with the Code of Conduct for Scientific Procedures using Animals and the protocol was approved by the Alfred Medical Research and Education Precinct (AMREP).

As a PI of the study, I hereby grant permission on the use of the said data in the Master of Engineering Science thesis of Miss Ooi Hui Lee entitled 'Noninvasive Detection of Physiologically Significant Pumping States in an Implantable Rotary Blood Pump' for fulfilment of study completion to the Faculty of Engineering, University of Malaya.

Yours sincerely,

Nigel Lovell

Nigel Lovell.

DR NIGEL LOVELL
SCIENTIA PROFESSOR
GRADUATE SCHOOL OF
BIOMEDICAL ENGINEERING

UNSW SYDNEY 2052 AUSTRALIA
Email: N.Lovell@unsw.edu.au
Telephone: +61(0)2 9385 3922
Facsimile: +61(0)2 9663 2108

Location: Room 508, Samuels Bldg
Gate 11, Botany Street, Randwick

TABLE OF CONTENTS

ORIGINAL LITERARY WORK DECLARATION	ii
ABSTRACT	iii
ABSTRAK	v
ACKNOWLEDGEMENTS	vii
CONSENT LETTER	viii
TABLE OF CONTENTS	ix
LIST OF FIGURES	xi
LIST OF TABLES	xiii
LIST OF SYMBOLS AND ACRONYMS	xv
LIST OF APPENDICES	xvi
CHAPTER 1: INTRODUCTION	1
1.1 Overview	1
1.2 Problem Statement	3
1.3 Research Scope	4
1.4 Research Objective	4
1.5 Dissertation Outline	4
CHAPTER 2: LITERATURE REVIEW	6
2.1 Overview	6
2.2 History of Rotary Blood Pump	6
2.3 Complications of LVAD with Cardiovascular Physiology	8
2.4 Types of Pump States	10
2.5 Noninvasive Signals	15
2.6 Ventricular Suction	15
2.7 Aortic Valve Non-opening	25
2.8 Current Limitations	27
2.9 Summary	29
CHAPTER 3: METHODS	30
3.1 Overview	30
3.2 Signal Acquisition	30
3.2.1 Acquisition of Non-invasive Pump Speed Signal	31
3.2.2 Acquisition of Invasive Signals as Reference Signals	32
3.3 Cardiac Signal Processing	32

3.4	Classification Algorithms	37
3.4.1	Linear Discriminant Analysis	38
3.4.2	Logistic Regression	39
3.4.3	Back Propagation Neural Network	40
3.4.4	K-Nearest Neighbor	41
3.5	Validation of Classification	42
3.6	Feature Selection	45
3.7	Assessment and Evaluation	48
3.8	Summary	50
CHAPTER 4: VENTRICULAR SUCTION DETECTION		51
4.1	Overview	51
4.2	Suction State Determination	51
4.3	Suction State in Pump Speed Waveform	52
4.4	Suction Indices	52
4.5	Results	55
4.5.1	Classification Strategy	55
4.5.2	Individual Index	56
4.5.3	Optimization of Classifiers	57
4.5.4	Comparison of Different Classifiers	61
4.5.5	Classification Time	63
4.6	Discussion	63
4.7	Summary	68
CHAPTER 5: ANO DETECTION		70
5.1	Overview	70
5.2	ANO State Determination	70
5.3	ANO Pump State in Pump Speed Waveform	71
5.4	ANO Indices	73
5.5	Results	74
5.5.1	Individual Index	74
5.5.2	Combination of Indices	75
5.5.3	Computation Time	80
5.6	Discussion	81
5.7	Summary	84
CHAPTER 6: CONCLUSION		86
6.1	Overview	86
6.2	Recommendation for Future Work	87
APPENDICES		89
LIST OF PUBLICATIONS AND PAPERS PRESENTED		97
REFERENCES		98

LIST OF FIGURES

Figure 1.1	An example of LVAD that connects left ventricle with aorta (The Alfred Intensive Care Unit, 2011).	2
Figure 2.1	Events of cardiac cycle under normal condition for left ventricular function (Guyton & Hall, 2006).	10
Figure 2.2	Example of pump differential pressure (pump dP), arterial pressure (AoP), left ventricular pressure (LVP), pump flow (Qp), proximal aortic flow (Qa) and pump speed waveforms during ventricular ejection (VE) (Ayre, Lovell, Morris, Wilson, & Woodard, 2001).	12
Figure 2.3	Example of pump differential pressure (pump dP), arterial pressure (AoP), left ventricular pressure (LVP), pump flow (Qp), proximal aortic flow (Qa) and pump speed waveforms showing aortic valve non-opening (ANO) (Ayre et al., 2001).	13
Figure 2.4	Figurative summary of different pump states for rotary blood pump (Karantonis, 2008).	14
Figure 2.5	Waveforms of noninvasive signals (speed and current) and invasive signals (aortic pressure (AoP), left ventricular pressure (LVP), pump inlet pressure (Pin), aortic flow (Qa) and pump flow (Qp)) for different pumping states (Karantonis, Lovell, Ayre, Mason, & Cloherty, 2006).	16
Figure 2.6	Patterns of different states (regurgitation, normal and suction) from deriving the relationship between bypass flow and motor current waveforms (Yuhki et al., 1999).	17
Figure 2.7	Resulting signal waveforms due to change in pump speed (a) pump flow (left), pulsatility index(center), and mean value of the pump flow (right) (b) load coefficient (left), pulsatility index of the load coefficient (center) and mean value of the load coefficient (right) (Choi, 2003).	18
Figure 2.8	Waveforms of indices based on pump speed to determine different pump states with porcine data (Karantonis, Cloherty, et al., 2006).	21
Figure 2.9	Waveforms of indices based on pump speed to determine normal and suction states on human data (Karantonis, Mason, et al., 2007).	22
Figure 2.10	Transition of pump state from VE to ANO during the increase of pump speed (Ayre et al., 2001).	26
Figure 3.1	Snapshot of a speed ramp signal taken from greyhound data (Ooi, Ng, & Lim, 2013).	31
Figure 3.2	Multiclass classification strategy for overall classification of all pump states	33
Figure 3.3	Nested binary classification strategy for overall classification of all pump states	33
Figure 3.4	Flowchart of overall pump state classification	34
Figure 3.5	Implementation of pump speed waveform during cardiac cycle estimation for indices extraction.	34

Figure 3.6	Effects of different moving average size on cycle estimation.(a) shows moving average of 0.5s has under-estimated the number of cycles and (b) shows moving average of 2s has over-estimated the number of cycles (Ooi et al., 2014).	35
Figure 3.7	Single data represented by segment that consists of multiple cycles for indices computation.	36
Figure 3.8	Five data represented by five individual cycles in single cycle index computation	37
Figure 3.9	An example of LDA implementation on two classes that considers the between-class variance and within class variance.	38
Figure 3.10	Plot of sigmoid function for the classification implementation	39
Figure 3.11	An example of a neural network model	40
Figure 3.12	An example of nearest distance computation for KNN classification.	42
Figure 3.13	Working steps of k fold cross validation (k=3).	45
Figure 3.14	Workflow of SFFS in finding the optimal set of indices for the final implementation in pump state detection.	47
Figure 4.1	Reference signal used for distinguishing suction state and non-suction state.	52
Figure 4.2	Examples of identified ventricular suction instances obtained from pump speed signal.	52
Figure 4.3	Accuracy of suction classification for all tested indices for greyhound data.	58
Figure 4.4	Comparison of different classifiers in terms of sensitivity, specificity and accuracy for individual index implementation.	62
Figure 4.5	Comparison of accuracy from different classifiers when implemented with multiple indices.	62
Figure 5.1	Reference signal criteria between ANO and VE state	71
Figure 5.2	Transition from VE state to ANO state for pump speed waveform (Ooi et al., 2014).	72
Figure 5.3	Examples of identified ANO instances obtained from pump speed signal (Ooi et al., 2014).	72
Figure 5.4	Percentage of statistical performance during implementation of combination of multiple ANO indices for (a) LDA, (b) LR, (c) BPNN and (d) KNN	78
Figure 5.5	Decision boundaries of evaluated classification algorithms for ANO detection (Ooi et al., 2014). Distribution of data with VE state is represented by darker dots whereas distribution of data with ANO state is denoted by dots with lighter color.	79

LIST OF TABLES

Table 3.1	Confusion matrix of all possible classification outcomes.	48
Table 4.1	Descriptions of all features used in the present study.	53
Table 4.2	Statistical performance of index mean of Dur_3 for multi-class classification. Sensitivity, specificity and accuracy are denoted as P1, P2 and P3 respectively.	55
Table 4.3	Statistical performance of binary classification of different indices on greyhound data from taken from compared classifiers. Results are arranged as sensitivitiy/specificity(accuracy)	57
Table 4.4	Comparison of statistical performance for different regularization under LR.	59
Table 4.5	Comparison of statistical performance for different learning rate under BPNN.	59
Table 4.6	Comparison of statistical performance for different number of iteration under BPNN.	60
Table 4.7	Comparison of statistical performance for different hidden under BPNN.	60
Table 4.8	Comparison of statistical performance for different values of k parameter under KNN.	61
Table 4.9	Statistical Performance of multiple indices for suction detection. Sensitivity, specificity and accuracy are denoted as P1, P2 and P3 respectively.	62
Table 4.10	Comparison of computation time for all classifiers during the implementation of suction indices.	63
Table 5.1	List of evaluated ANO indices with respective description and formula (Ooi et al., 2014).	73
Table 5.2	Statistical performance of individual ANO indices during implementation in greyhound data. Sensitivity, specificity and accuracy are denoted as P1, P2 and P3 respectively.	74
Table 5.3	The highest classification accuracy among the compared classifiers for each combination is displayed (Ooi et al., 2014). The last row indicates the number of combination set that exceed 90% accuracy.	76
Table 5.4	Combinations of indices performs well in terms of overall accuracy from the different classifiers (Ooi et al., 2014). Number of indices is stated in the second row. X denotes the presence of the specified index in the combination sets with respect to each classifier. The last row shows the accuracy obtained from the corresponding index combination sets as indicated in each column.	77
Table 5.5	Comparison of computation time for all classifiers during the implementation of ANO indices.	80

Table A.1	List of statistical performance for multiclass classification. Sensitivity, specificity and accuracy are denoted as P1, P2 and P3 respectively. Statistical measures from the first column are used to extract indices computed in the multiple cycle that are found in second column	90
Table B.1	Statistical performance of the evaluation of the individual suction indices using LDA. The results are shown as sensitivity / specificity (overall accuracy).	93
Table B.2	Statistical performance of the evaluation of the individual suction indices using LR. The results are shown as sensitivity / specificity (overall accuracy).	94
Table B.3	Statistical performance of the evaluation of the individual suction indices using BPNN. The results are shown as sensitivity / specificity (overall accuracy).	95
Table B.4	Statistical performance of the evaluation of the individual suction indices using KNN. The results are shown as sensitivity / specificity (overall accuracy).	96

LIST OF SYMBOLS AND ACRONYMS

ANO	aortic valve non-opening.
AoP	aortic pressure.
AoQ	aortic flow.
BAI	blood assistant index.
BPNN	Back Propagation Neural Network.
CART	classification and regression tree.
CVP	central venous pressure.
emf	electromotive force.
FA	full assist.
FN	false negative.
FP	false positive.
GMM	Gaussian Mixture Model.
INP	inlet pressure.
IRBP	implantable rotary blood pump.
KNN	K-Nearest Neighbor.
LAP	left atrial pressure.
LDA	Linear Discriminant Analysis.
LR	Logistic Regression.
LV	left ventricle.
LVAD	left ventricular assist device.
LVP	left ventricular pressure.
OUP	outlet pressure.
PA	partial assist.
PAP	pulmonary arterial pressure.
PVC-C	Partial Ventricular Collapse Continuously.
PVC-I	Partial Ventricular Collapse Intermittently.
rms	root mean square.
SBS	Sequential Backward Selection.
SFBS	Sequential Floating Backward Selection.
SFFS	Sequential Floating Forward Selection.
SFS	Sequential Forward Selection.
STI	state transition index.
SVR	systemic vascular resistance.
TN	true negative.
TP	true positive.
VAD	ventricular assist device.
VE	ventricular ejection.
WDI	waveform deformation index.

LIST OF APPENDICES

Appendix A	Complete list of result for suction detection with multi class classification	90
Appendix B	Complete list of result for suction detection with all evaluated classifiers	93

University of Malaya

CHAPTER 1

INTRODUCTION

1.1 Overview

The heart supports life by providing sufficient oxygen supply and nutrients to the rest of the cells in the body for sustenance. It takes place via a predefined route of circulation through blood flow continuously and the process critically influences the biological mechanism of virtually every living thing. Without the supplements of oxygen-rich blood, organs in the body will fail to meet the required metabolic demand, thereby causing potential deterioration in the functions of the body. Hence, failure and impairment of this vital organ will often lead to complications of varying degree and subsequently compromising the overall health of the individual.

In fact, heart disease has one of the highest mortality rate in the world by claiming an average of 17 million lives each year (Mackay, Mensah, Mendis, Greenlund, & Organization, 2004). Based on the statistics and trend, it is estimated that 23.6 million lives worldwide may be lost due to heart diseases by the year 2030 (Mendis et al., 2011). Due to the severity of risks posed by heart diseases, various methods have been implemented over the years for patient recovery as well as improving their quality of life. While there are observed improvements in terms of surgical approaches from medical perspective over the years of research, the optimal option for those inflicted with end-stage heart diseases remains to be heart transplantation (AlOmari et al., 2013). However, scarcity of donor organs has not been able to fully meet the demand of the ever rising cases of patients in need, causing only a minority of them are able to benefit from such procedure (Barr et al., 2005). Hence, this spurs the development of ventricular assist device (VAD) that

performs pumping action to aid the native heart.

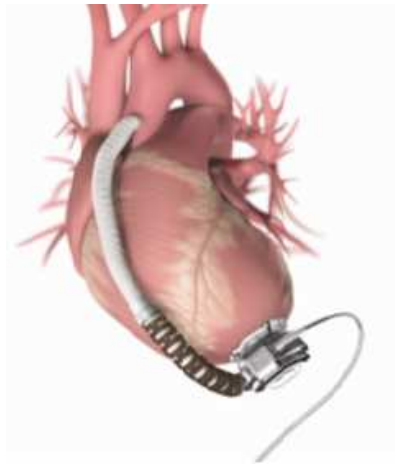


Figure 1.1: An example of LVAD that connects left ventricle with aorta (The Alfred Intensive Care Unit, 2011).

VAD is essentially a mechanical circulatory system that is used to augment the cardiac output of patients with heart failure. Specifically, left ventricular assist device (LVAD) is designed to support the failing left ventricle (AlOmari et al., 2013) that is responsible for the circulation of oxygenated blood. Particularly, implantable rotary blood pump (IRBP) is a type of VAD with continuous flow that works with smaller size, lighter weight and minimal blood trauma, therefore being the popular choice these days (AlOmari et al., 2013). Generally, VAD is a promising option due to its potential to provide either temporary solution for recovery (Andrade, Al-Saloos, Jeewa, Sandor, & Cheung, 2010; Farrar et al., 2002), bridge to transplant (Matoba, Okubo, & Nosé, 2004; Navia et al., 2002; Nosé, Yoshikawa, Murabayashi, & Takano, 2000) or as destination therapy (Lietz et al., 2007; Long et al., 2005; S. J. Park et al., 2005) in instances where heart transplantation is not viable (Boston, Simaan, Antaki, Yu, & Choi, 1998). As shown in Figure 1.1, the device is positioned to the left ventricle and the aorta, creating an alternative path for the blood flow that may be hindered in the native heart due to patient conditions. Implantation of VAD enables patients with heart diseases to continue with their lives instead of being bound to the hospital, hence it is imperative that research efforts are made on

improving the control design on the device. It can be seen that popularity of IRBP has soared with the increasing types of such device being introduced for different clinical applications in recent years (Kumpati, McCarthy, & Hoercher, 2001; Nosé et al., 2000, 2010).

Ultimately, the long term goal of LVAD is to provide intrinsic adaptation and sensitivity with respect to changes in the venous return and cardiac conditions. Ideally, automatic adjustment is desired on the pump output to reduce dependence on clinical observation (AlOmari et al., 2013). However, in practice, the current main constraints of LVAD lies in its limited durability and risk of complications such as bleeding, thromboembolism and infections (Kamdar et al., 2009).

1.2 Problem Statement

Non-pulsatile IRBP such as axial pump and centrifugal pump continuously draw the blood out from the ventricle and supply it to aorta via the pump outlet. Control strategies in LVAD are imperative as it will greatly affect its performance on the patients. Successful implantation in the long term should allow minimal physician monitoring, with effective control system that avoid occurrence of potentially abnormal pump states. Due to the lack of the overall sensitivity and unphysiological responses to changes in the preloads and afterloads (Salamonsen, Mason, & Ayre, 2011), the concern spurs the need to achieve pump state detections that prevent harmful consequences such as ventricular suction state (Karantonis, Lovell, et al., 2006; Ferreira, Boston, & Antaki, 2007; Choi, 2003; Mason, Hilton, & Salamonsen, 2008; Voigt, Benkowski, & Morello, 2005; Ng, Lim, Mason, Avolio, & Lovell, 2013; Wang & Simaan, 2013; Tzallas et al., 2012), ANOstate (Granegger, Moscato, Mahr, Wieselthaler, & Schima, 2011; Granegger, Schima, Zimpfer, & Moscato, 2013; Bishop et al., 2010) and regurgitation state (Karantonis, Lovell, et al., 2006).

1.3 Research Scope

In this study, the scope is focused on investigation of abnormal pump states resulted from over-pumping occurrences. Specifically, detection of ventricular suction and ANO from a wide range of operating conditions will be studied based on the noninvasively acquired pump speed signal.

1.4 Research Objective

With the research motivation highlighted, the current study aims to achieve the following two objectives.

- To noninvasively detect ANO occurrence for different cardiac conditions.
- To noninvasively detect ventricular suction for different cardiac conditions.

1.5 Dissertation Outline

The dissertation entitled Noninvasive Detection of Physiologically Significant Pumping States in an Implantable Rotary Blood Pump is essentially organized into six chapters.

Chapter 1 gives a brief overview on the background of the LVAD and highlights the motivation of study. Problem statements, research scope and objectives for the study as well as dissertation outline are included as well.

Meanwhile, Chapter 2 reviews the previous literature that has been conducted on the subject of LVAD. Emphasis is given on the different pump states during the implantation of the device, especially on over-pumping states.

Next, Chapter 3 discusses the techniques and implemented approaches that was applied to the scope of the study. Overall workflow of the study and reasoning in experimentation process are documented in an organized manner to give reader an understanding to the applied methods.

Chapter 4 documents the implementation of ventricular suction detection. Results of the employed methods with appropriate settings are presented and supported with adequate comparative analysis.

For Chapter 5, a detailed elaboration is given to classification among the non-suction states. Findings and observations on the implementation of ANO detection are detailed and relevant analysis is conferred to discuss the evaluation results.

Last but not least, Chapter 6 concludes the dissertation with summary and conclusive remark from conducting this study. Suggestion and recommendations are proposed for possible future work.

University of Malaysia

CHAPTER 2

LITERATURE REVIEW

2.1 Overview

This chapter is divided into several sections. Section 2.2 chronicles different types of rotary blood pump with regards to their strength and weakness in applications. Section 2.3 delves deeper into the complications encountered for these devices encountered and their effects from the physiological perspective. Next, different pump states are discussed in details with respect to rotary blood pump to explain the different categorization that previous researchers have used in their work in Section 2.4. Meanwhile, Section 2.5 explains the significance of noninvasive approach in the study. Section 2.6 covers all the previous work that has been proposed to solve the occurrence of ventricular collapse during blood pump implementation. On the other hand, Section 2.7 details the literature that has been used on ANO events for rotary blood pump support. Limitations and constraints of current literature are discussed in Section 2.8. Lastly, Section 2.9 presents a brief summary of the chapter and subsequently research motivations.

2.2 History of Rotary Blood Pump

Pulsatility was at first believed to be the most optimal approach for the device and hence most first generation LVADs (Allen, Murray, & Olsen, 1996; Borovetz, Kormos, Griffith, & Hung, 1988; Dixon & Farris, 1991) operate the pumping in pulsatile manner, offering effective mechanical unloading of failing heart (Nosé et al., 2000). Such devices are usually used in a limited, critical care mode with close monitoring from health specialists to perform the required manual adjustment to prescribe appropriate settings (Boston, Antaki, & Simaan, 2003). Due to the bearings and moving parts, these pulsatile

LVADs have limited durability and faced issues for long term use.

This eventually led to increasing use of continuous flow devices that allow wider applications due to its small size and more durable characteristics. The second generation LVADs do not require extensive dissection and hence lowering the incidence of post-operative bleeding and device-related infections (Kamdar et al., 2009). In order to ensure sufficient perfusion for end-organ function in human body, continuous flow centrifugal pump is introduced for further improvements.

Supported by ceramic bearings, MicroMed DeBakey is a continuous axial flow pump that has previously been used in the study of cardiac contractility (Naiyanetr et al., 2010), suction events (Voigt et al., 2005; Vollkron, Voigt, Ta, Wieselthaler, & Schima, 2007) and fixed pulmonary hypertension in cardiac implantation (Zimpfer et al., 2007).

Meanwhile, the implantable, magnetically accentuated axial flow pump Incor (Berlin Heart AG, Germany) (Schmid et al., 2005) was previously proposed for use in studying control strategy of rotary blood pump on different modes of operations (Arndt, Nüsser, Graichen, Müller, & Lampe, 2008; Arndt, Nüsser, & Lampe, 2010).

VentrAssist (VentraCor, Sydney) is a third generation centrifugal pump with hydrodynamically suspended impeller used in several studies on ventricular collapse (Ayre et al., 2001; Karantonis, Cloherty, et al., 2006; Karantonis, Lovell, et al., 2006; Karantonis, Lovell, Ayre, Mason, & Cloherty, 2007; Karantonis, Mason, et al., 2007; Karantonis et al., 2008).

Other LVADs that have been utilized in similar studies are centrifugal pump (Kyocera Corp, Kyoto, Japan) (Yuhki et al., 1999), Gyro P1710 pumps (Baylor college of Medicine) (Tanaka et al., 2006), Taita T-LVAD (Lin, Chou, Chen, & Jan, 2001), Nimbus/UoP axial flow blood pump (Choi, 2003) and Heartmate (Boston et al., 2003).

2.3 Complications of LVAD with Cardiovascular Physiology

Different levels of cardiac output are required for patients with varying physiological demands, which depend on contractility, preload and afterload. Contractility is the intrinsic ability of heart muscle to contract while preload is the end diastolic pressure that stretches the filled ventricle to its maximum. As such, the level of contractility of heart is often related to the preload and venous return, where the blood returns to the heart (Boston et al., 2003). Due to the structure of the heart, greater contraction force is generated with increasing amount of stretching during filling to pump more blood from its chamber into the aorta, as concurred by the Frank-Sterling mechanism (Guyton & Hall, 2006). The afterload is the tension developed in the artery leading from the wall of the left ventricle during ejection (Guyton & Hall, 2006), usually it is estimated by the systemic vascular resistance (SVR). In response to afterload, the heart will produce higher pressure and less volume to ensure constant total work per beat is performed by the heart (Boston et al., 2003).

With the advances of technologies LVADs with smaller size, more efficient and more reliable non-pulsatile pumps were developed, however careful pump speed control is still required due to its poor sensitivity to ventricular preload (venous return) and high sensitivity to ventricular afterload (Baloa, Liu, Boston, Simaan, & Antaki, 2000; Boston et al., 1998; Choi, Boston, & Antaki, 2007; Choi, 2003). Difficulties may arise to determine the appropriate set point for pump speed as it depends on preload and afterload that varies with time (Boston et al., 2000).

Some existing LVAD applies pulsatility indices on the measurement of pump pressure head for pump speed regulation (Arndt et al., 2010). Hence, occurrence of ventricular collapse can be avoided as long as the venous return does not decrease suddenly. In order to promote better washout of the left ventricle and opening of the aortic valve, the motor

speed is reduced periodically to allow temporary regurgitation of the blood flow inside the pump (Arndt et al., 2010).

Excessive pumping from devices will lead to myocardial suction that causes arrhythmia induction, shift of septum, tricuspidal anastomosis and dislodging of thrombi, among other complications. To avoid suction occurrence, manual speed adjustment is often included in the setting that accommodate the expected lowest venous return (Arndt et al., 2010). However, the performance of the pump is compromised as a result (Arndt et al., 2010). Despite offering such auxiliary features, there is still room for improvement in emerging technologies that continuously seek improvement for the implementation of IRBP in the long term.

Being an inherently preload insensitive device, the lack of reliable implantable pressure sensors has spurred the rising needs for alternative measures to control LVAD and detect pump states that are detrimental to heart conditions of patient (Mason et al., 2008). In order to make sure that LVAD does not hinder their daily activities, it is imperative that wider variation in demand for cardiac output can be met by adjusting the pump speed (Ferreira, Boston, & Antaki, 2009). The lack of available pressure sensors for preload condition detection indicates that efforts for adaptation to venous return changes in existing control approaches still left much to be desired (Ferreira, Simaan, Boston, & Antaki, 2006). Hence, adjustment of pump flow for accommodating the required physiological demands of patients via pump speed remains a challenge today (Ferreira, Simaan, et al., 2006).

It is suffice to say that the speed of LVAD needs to be sufficiently high to prevent regurgitation or backflow, where the blood from aorta return to the left ventricle through the pump (Ferreira, Chen, Simaan, Boston, & Antaki, 2006). On the other hand, there is a limitation of high speed that can be applied as suction may occur if the pump attempts to drive more blood such that it exceeds the available volume, resulting in ventricular col-

lapse that may lead to cardiac tissue damage (Ferreira, Chen, et al., 2006). Also known as anatomic collapse of the ventricle, this condition may also develop due to contact between the cannula tip and left ventricular wall besides over-pumping of LVAD (Boston et al., 2003). Having pump speed that is excessively high will cause most or all of the blood entering the left ventricle (LV) to exit through the inflow conduit of LVAD, leaving no blood volume flowing in its native route across aortic valve. With the decreased blood pressure or volume in the native heart, there is insufficient pressure for LV to open up aortic valve, leading to deleterious neurologic events such as thrombus formation. Prolonged closure of aortic valve may eventually lead to fusion, resulting in stenosis or regurgitation that further disturb blood flow (Bishop et al., 2010). At low speed, there is no proper cardiac output with sufficient perfusion pressure. Hence, it is imperative that pump speed is increased adequately to allow maximized pump flow without inducing suction.

2.4 Types of Pump States

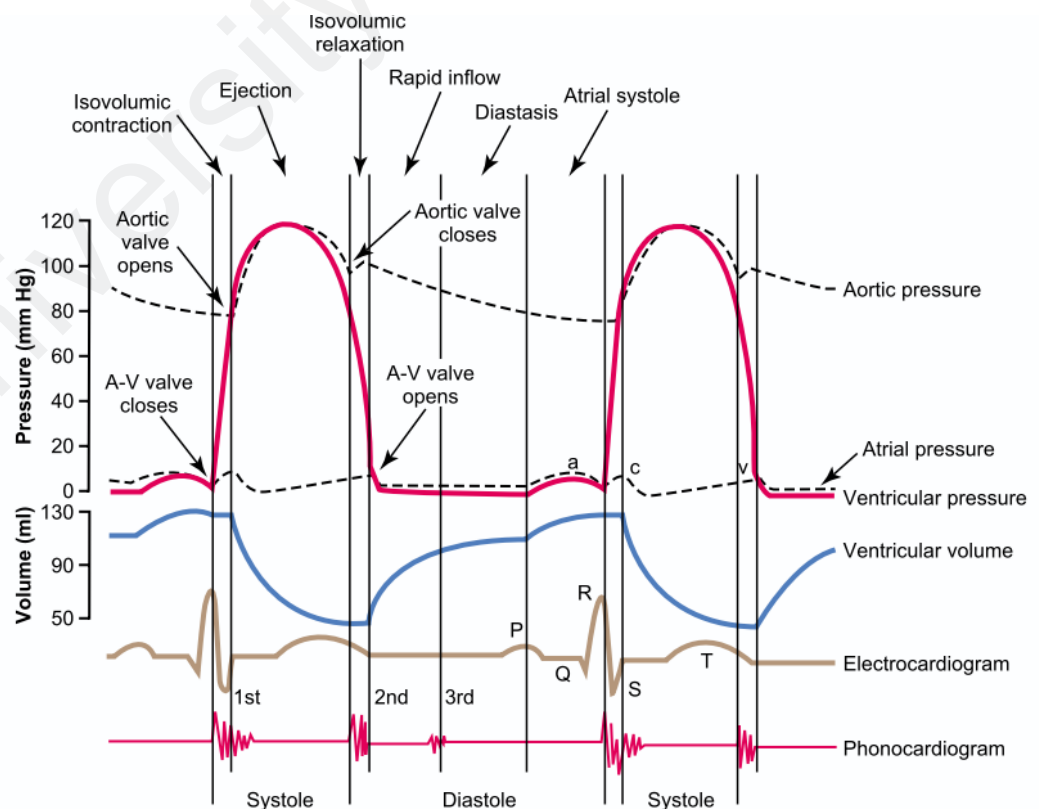


Figure 2.1: Events of cardiac cycle under normal condition for left ventricular function (Guyton & Hall, 2006).

In each heartbeat, cardiac events take place with a period of relaxation (diastole) and followed by a period of contraction (systole) (Guyton & Hall, 2006) in Figure 2.1 to ensure successful blood pumping. During this recurring occurrence of diastole and systole, several physiological states may take place.

As portrayed in Figure 2.1, VE is the ideal state, in which net positive flow is present to satisfy physiological needs. This pump state can be interpreted from several signals in Figure 2.2. Pressurization of the right and left ventricles begin with cardiac cycle, blood flows through the ascending aorta as the rising left ventricular pressure (LVP) opens the tricuspid valve (Ayre et al., 2001). Pressure across the pump decreases the instant aortic valves open, causing the continued increase in pump flow throughout systole. End pressurization of left ventricle triggered the abrupt decrease in flow across aorta (Ayre et al., 2001).

Partial collapse of ventricle may occur at high pump speeds, involving obstruction of the pump inlet cannula as the ventricle walls suck together (Karantonis, Cloherty, et al., 2006). Aortic pressure drops to a level that is close to zero at end-systole and the aortic valve remained close. In some cases, suction of the ventricle walls takes place several times for a cardiac cycle, due to the increased stress that was placed on the native heart (Karantonis, Lovell, et al., 2006). The oscillatory nature of pump flow is driven by the transient preload, causing volume loading of an over-pumped left ventricle while the arterial pressure is only supported by pump flow. Partial Ventricular Collapse Intermittently (PVC-I) is caused by the respiration on cardiac behavior, hence it occurs only over a fraction of the respiratory cycle instead of every heartbeat (Karantonis, Lovell, et al., 2006). The aortic pressure is of zero pulsatility and aortic valves are closed for the remainder of the respiratory cycle. On the contrary, Partial Ventricular Collapse Continuously (PVC-C) is the pump state where suction event occurs for each cardiac cycle (Karantonis, Cloherty, et al., 2006).

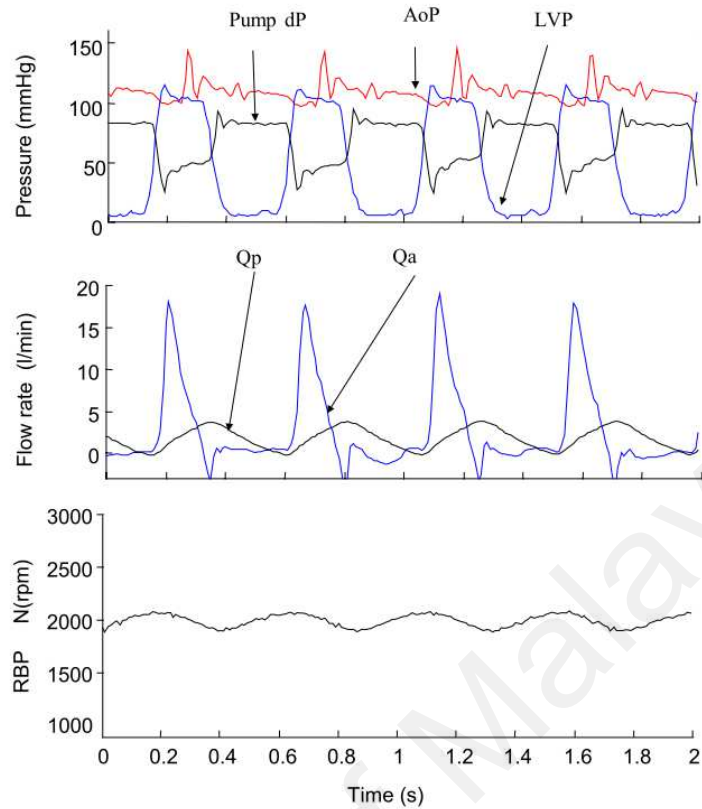


Figure 2.2: Example of pump differential pressure (pump dP), arterial pressure (AoP), left ventricular pressure (LVP), pump flow (Q_p), proximal aortic flow (Q_a) and pump speed waveforms during VE (Ayre et al., 2001).

ANO is the pump state in which aortic valves remain closed throughout the entire cardiac cycle with zero or slightly negative aortic flow due to insufficient LVP (Ayre et al., 2001). Instead of showing the ideal waveform in Figure 2.2, the reduced LVP was lower than aortic pressure such that it was unable to open the aortic valves. This is caused by decreased myocardial contractility, increased power pump or a decrease in blood returning from the left atrium (Ayre et al., 2001), as indicated in Figure 2.3. In the long term, the prolonged closure of aortic valves has adverse effects such as stenosis, regurgitation or even fusion (Rose, Park, Bank, & Miller, 2000) that further disrupt blood flow. Compared to VE, the level of native heart modulation on the speed signal in ANO pump state is generally lower (Karantonis, Cloherty, et al., 2006). Due to larger influence by the respiratory system, it is subjected to greater variation in mean value (Karantonis,

Cloherty, et al., 2006). In the events when aortic valves do not open, thrombogenesis is likely to develop, leading to deleterious neurologic events (Bishop et al., 2010).

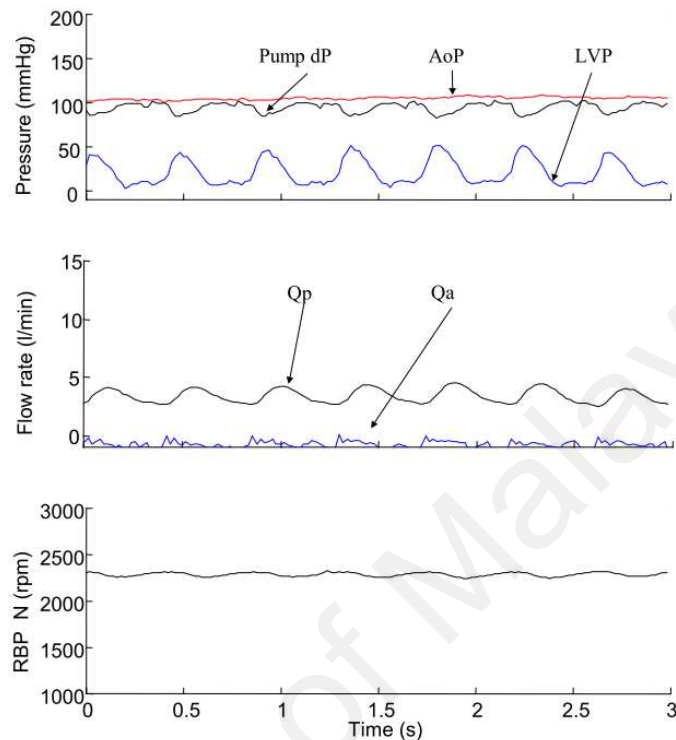


Figure 2.3: Example of pump differential pressure (pump dP), arterial pressure (AoP), left ventricular pressure (LVP), pump flow (Q_p), proximal aortic flow (Q_a) and pump speed waveforms showing ANO (Ayre et al., 2001).

Due to the lower pressure in open aortic valves as compared to that of LVAD cannula, more blood is preferably directed through the aortic valve (Salamonsen et al., 2012). Since the sensitivity of pump pulsatility for further increase of left ventricular stroke work falls off once the aortic valves are open (Salamonsen et al., 2012), it is imperative to detect the state of the aortic valve.

Figure 2.4 illustrates the transition of the different described pump states as the pump speed of LVAD changes. High speed will result in over-pumping causing potential ANO or ventricular suction state to occur whereas maintaining excessively low speed does not aid pumping action of the heart due to the backward flow.

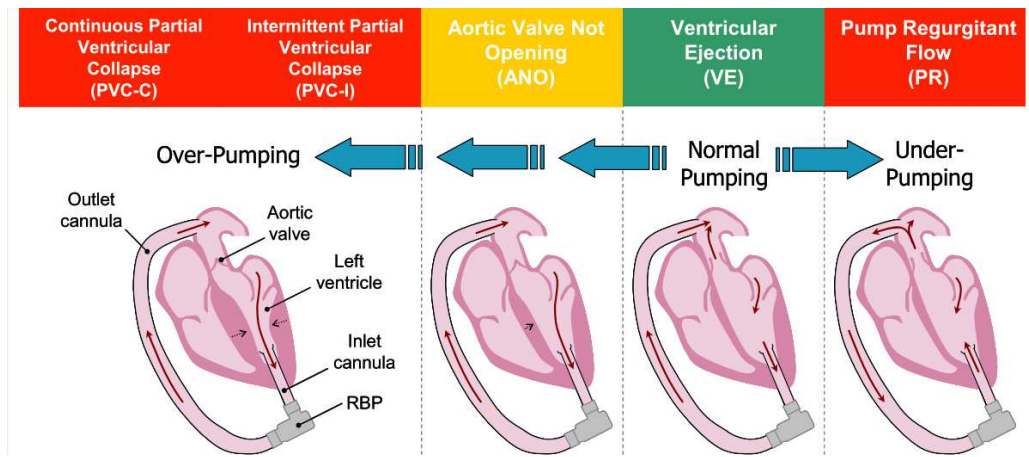


Figure 2.4: Figurative summary of different pump states for rotary blood pump (Karan-tonis, 2008).

Investigation by (Boston et al., 1998) only focused on suction state and non-suction states in the classification of optimal operating speeds in animal experiments. Meanwhile, (Lin et al., 2001) proposed the use of four stages (time of mitral valve close, time of aortic valve open, time of aortic valve close, time of mitral valve open) to determine the pump states. Mean pump flow was calculated for each stage to establish the relationship between pump voltage and the derived flow index. On the other hand, three pump states were categorized in the study by (Choi, 2003), namely ‘before suction’, ‘imminent suction’ and ‘suction’ for the proposed four-input data fusion system. In the subsequent studies (Choi, Boston, & Antaki, 2005; Choi et al., 2007) from the same author, two pump operating conditions, namely normal and suction status were characterized. Similarly, (Ferreira et al., 2007, 2009; Ferreira, Chen, et al., 2006) named ‘no suction’, ‘moderate suction’ and ‘severe suction’ as the three studied pump status in the suction identification work. These categories were further improvised by predefined expert classification class of ‘No suction’, ‘Moderate suction’, ‘Severe Suction’, ‘Not Classified’ and ‘Not useful’ on a different study using frequency and time-frequency based indices (Ferreira, Simaan, et al., 2006). In a study by (Voigt et al., 2005), the physiological states are classified as five different classes, namely ‘certainly no suction’, ‘most probably no suction’, ‘not de-

cidable', 'most probably suction' and 'suction'. Meanwhile, (Vollkron et al., 2007, 2005) uses five states, namely 'suction', 'most probably no suction', 'not decidable', 'most probably suction' and 'suction' in the development of suction detection system based on the beat-to-beat analysis of pump flow signal. In the study by (Yuhki et al., 1999), three different states have been identified, namely regurgitation, normal and suction during the development of control algorithm for pump state classification. A suction study by (Mason et al., 2008) had categorized its patient data into 'normal', 'pre-suction' and 'suction', this help identifying the different pump states occurring at the time of experimentation. In the work of (Karantonis, Cloherty, et al., 2006), initially a total of five pump states was identified, namely regurgitant pump flow, VE, ANO, PVC-I and PVC-C. However, the proposed classification result had categorized the five states into only 'suction' and 'non-suction'.

2.5 Noninvasive Signals

Conventional explicit control based on flow set point would require invasive acquisition of venous flow signal and pump flow signal (Balboa et al., 2000). However, due to the limited reliability of the transducers in the long term implantation and the complications caused, it should be avoided whenever possible (Ayre et al., 2001). Study on noninvasive signals is advocated by others as well (Balboa et al., 2000; Choi, 2003; Choi et al., 2005, 2007). It is observed that invasive signals are used in addition to noninvasive signals for aiding the verification of state determination in recent trends, as illustrated in Figure 2.5.

2.6 Ventricular Suction

In the study by (Boston et al., 1998), control system is integrated with four heuristic indices, namely flow pulsatility index, diminishing return index, minimum flow index and harmonic magnitude ratio index. Combination of a number of techniques, such as Bayesian methods, fuzzy logic or Dempster-Shafer based fusion approach were used to

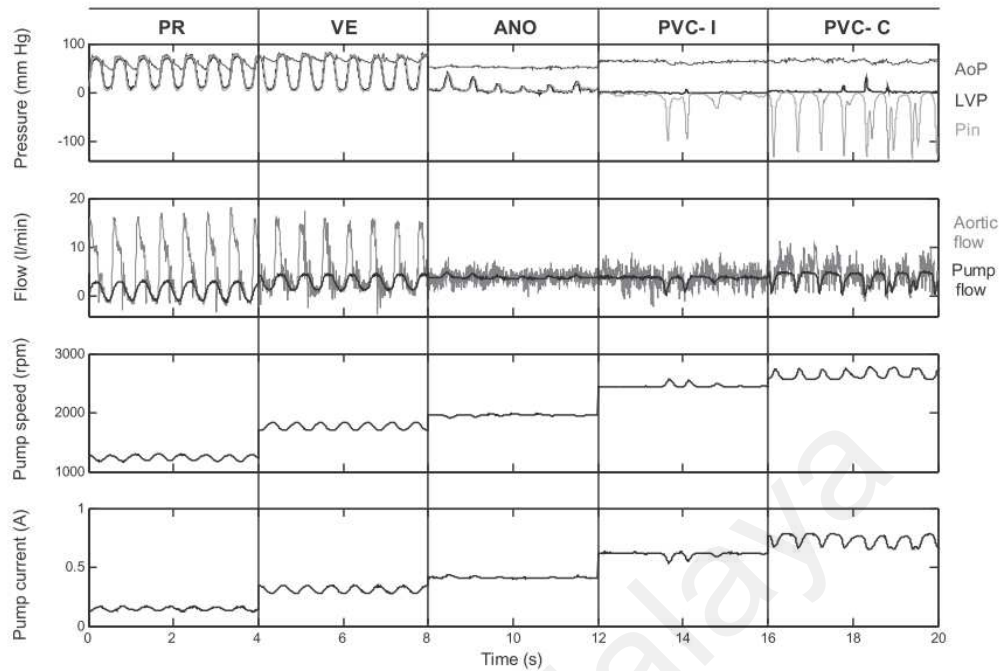


Figure 2.5: Waveforms of noninvasive signals (speed and current) and invasive signals (aortic pressure (AoP), left ventricular pressure (LVP), pump inlet pressure (Pin), aortic flow (Qa) and pump flow (Qp)) for different pumping states (Karantonis, Lovell, et al., 2006).

provide overall decision regarding the presence of suction occurrence. It was found from the study that fuzzy logic method achieved the highest classification rate, albeit resulting in some uncertain classification.

Suction detection scheme based on power spectral density analysis was applied by (Yuhki et al., 1999) through obtaining the waveform deformation index (WDI). The proposed method did not require any external flow or pressure sensors and the experiment was conducted on goats as subjects. With the assumption that undistorted motor current waveform can be represented as a pure sine wave, various waveforms were synthesized including the one that highly resembled the distorted motor current waveform obtained from mock loop study. As shown in Figure 2.6, patterns of different pump states were identified from the relationship of signals. From the pump speed adjustment based on the WDI algorithm, the risk of regurgitation and suction events have been successfully reduced. To detect suction occurrence in VAD, three indices, namely pulsatility index,

diminishing return index and harmonic index were proposed in an experimental study on calves (Baloa et al., 2000). Multiple hemodynamic variables were taken into consideration during the development of multi-objective optimization scheme (Baloa et al., 2000). The pulsatility index was set to hold speed slightly below the suction-inducing speed, and the difference between the reference and actual pulsatility is opted as control signal (Baloa et al., 2000). The diminishing return index measured the flow rate changes with respect to speed transition by assuming that the flow-speed relationship are the same throughout computation time of the control system (Baloa et al., 2000). Meanwhile, the harmonic index described loss of power in the first harmonic of the pump current waveform (Baloa et al., 2000).

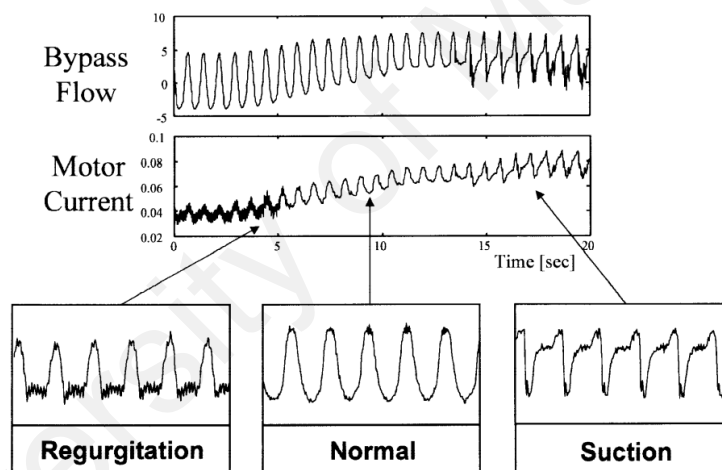


Figure 2.6: Patterns of different states (regurgitation, normal and suction) from deriving the relationship between bypass flow and motor current waveforms (Yuhki et al., 1999).

Data fusion with neural fuzzy logic was proposed by (Choi, 2003) in suction detection study to handle ambiguous signals. Half of the data from animal experiments was used for training the system to adjust the membership function by computing the mean pulsatility index, change in mean pulsatility index, mean value and change in mean value of the load coefficient (Choi, 2003). The resulting pump flow and load coefficient of pump derived from changes in pump speed from the study is shown in Figure 2.7. The findings from the work have been extended for regulation of pump speed (Choi et al., 2005) of an

axial flow blood pump for LVAD. By employing a model of cardiovascular system with implanted LVAD, reference control index of pulsatility controller was investigated with inclusion of changes in SVR (Choi et al., 2005). However, relationship between ventricular unloading and stroke volume is presumed by pulsatility-based controller. There were instances of such controllers failing to meet physiological demands of patients with various conditions due to the misleading reference pulsatility index that does not account for changes caused by altered contractility from sympathetic response or ventricular recovery (Choi et al., 2007). Hence, in order to solve this problem, pulsatility ratio of the pump flow and pressure difference (Choi et al., 2007) was suggested as a control index. Several different physiological disturbances involving afterload through SVR, preload through pulmonary vascular impedance (PVI), contractility of left heart and threshold pressure of suction resistor are taken into account during the simulation.

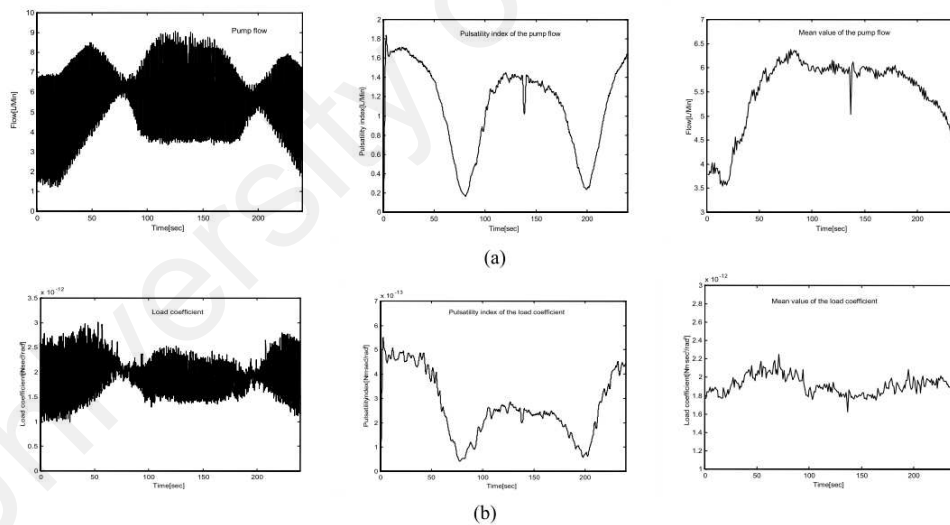


Figure 2.7: Resulting signal waveforms due to change in pump speed (a) pump flow (left), pulsatility index(center), and mean value of the pump flow (right) (b) load coefficient (left), pulsatility index of the load coefficient (center) and mean value of the load coefficient (right) (Choi, 2003).

Mock loop as well as in vitro experiments were used in the study by (Voigt et al., 2005) to identify suction events. Reliable detection algorithm with optimized parameters was found for solid suction detection under non-pulsatile conditions. However, due to the

overlapping boundaries at the working point of the proposed system, the algorithm lost its steadiness in the pulsatile states. Nevertheless, most suction occurrence happens shortly after the implantation of LVAD where the volume is not balanced due to hypovolemia. In many cases, the blood flow is non-pulsatile when there is rapid change in ventricular filling, which demanded pump speed adjustments (Voigt et al., 2005).

A control method to alleviate inflow suction by increasing right pump flow in biventricular bypass configuration was proposed by (Tanaka et al., 2006) for implementation between the ventricles and arteries. Particularly during the first few days after operation, the circulatory system of patients may be slightly unstable. This approach allows the circulatory control to be maintained while maximizing the flow rate simultaneously.

A discriminant analysis model was proposed by (Ferreira, Chen, et al., 2006) in a suction detection study with pump flow signal. The model combined several indices from the frequency domain, time domain and time-frequency domain. Frequency indices were used for sensing indirect changes in the harmonic and subharmonic energy content of the investigated signal during suction events. Based on a beat-to-beat analysis and first derivative of pump flow, the time domain indices identified the changes in pulsatility. Meanwhile, time-frequency indices were used to find the standard deviation variations of the instantaneous frequency of pump flow signal. Some of the identified indices with potential were extended to the subsequent work that focused on frequency indices supplemented by time-frequency indices via feature extraction algorithm (Ferreira, Simaan, et al., 2006). The acquired information was combined into a weighted decision system and preliminary analysis was shown to be rather positive. This work was further extended to the design of a rule-based controller for LVAD (Ferreira et al., 2007). With a lumped parameter model of the circulatory system coupled with LVAD, several levels of activity and contractility were tested on the system. By Mamdani's approach (Mamdani, 1974), the design of the said controller required membership sets for the input and output variables as

well as construction of rule-base and selection of defuzzification method (Ferreira et al., 2007). Fuzzy associative memory bank was used to organize the rule base, associating the input variables with output variables (Ferreira et al., 2009). Hemodynamic analysis was performed to verify the proposed method by computation of cardiac output and mean arterial pressure under all test conditions.

Based on beat-to-beat analysis of the pump flow signal, (Vollkron et al., 2005) developed a reliable suction system with optimization on different algorithms. The six resulting suction indicators were asymmetry criteria, plateau criteria, slew rate criteria, low-flow criteria, mean-min-max criteria, and saddle criteria. The proposed approach achieved specificity of 85% to 95% for certain suction state and possible suction state (Voigt et al., 2005). Clinical experiments was conducted to further improve the automatic suction detection system (Vollkron et al., 2007). Additional criterion derived from existing indicators was used and numerically optimized nonlinear characteristic curve dependent on heart rate was applied to substitute threshold in previous study (Vollkron et al., 2005). In (Vollkron et al., 2007), arrhythmia events was included for the investigation to gauge its effectiveness in practical applications. Ventricular arrhythmia is the change of the heart contraction from its normal rate, possibly reducing cardiac output and increasing heart work rate, hence requiring more oxygen than usual. It may occur as a transient effect during partial or full ventricular collapse with periods of reduced venous return due to excessive unloading of continuous left ventricular support, and was reported to vanish within five minutes after suction (Vollkron et al., 2007). Different types of arrhythmia such as ventricular extrasystolic, monomorphic ventricular tachycardia, polymorphic ventricular tachycardia and ventricular fibrillation were taken into consideration to accommodate the varying physiological conditions on patients.

Compared to previous studies that only include normal and suction state, (Karantonis, Cloherty, et al., 2006) initially considered a large variation of pump state. A non-

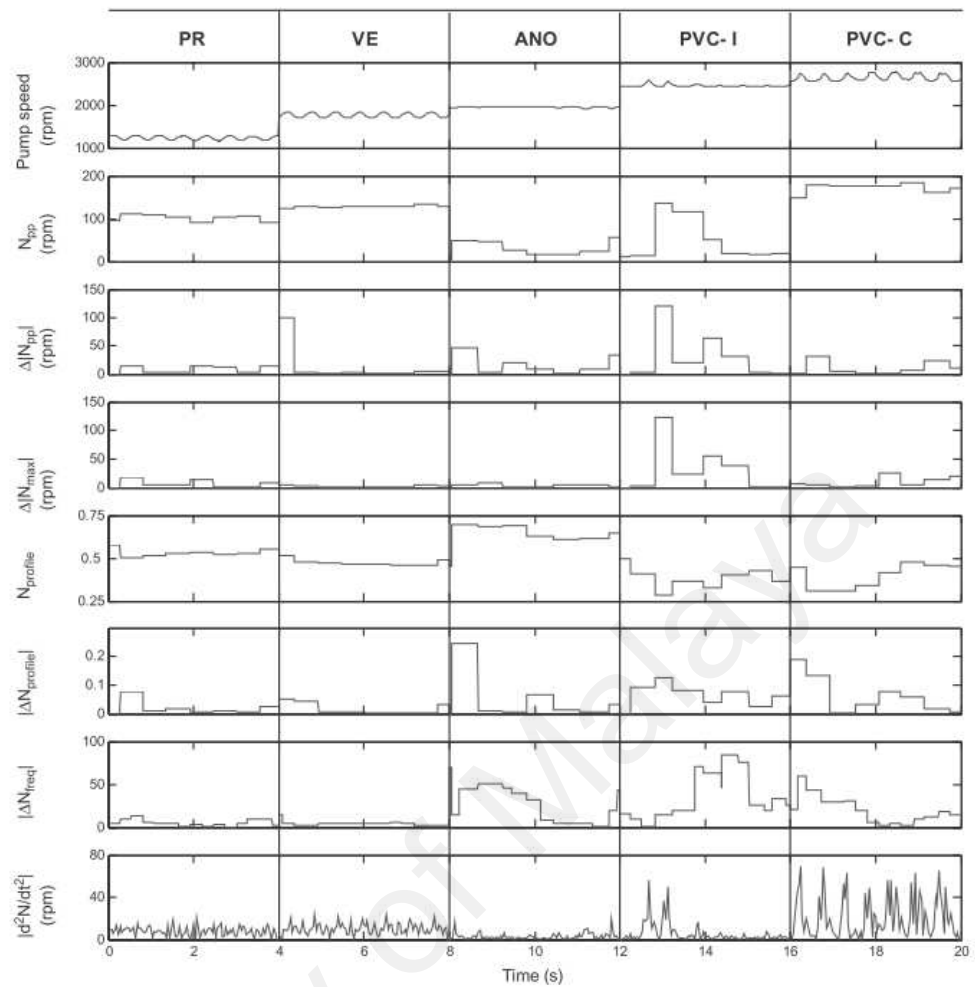


Figure 2.8: Waveforms of indices based on pump speed to determine different pump states with porcine data (Karantonis, Cloherty, et al., 2006).

invasive strategy involving the use of seven indices was proposed as shown in Figure 2.8. Porcine experiments were carried out with LVAD from VentrAssist, employing classification and regression tree (CART) for detection of different states via pruning of classification tree. The indices used were speed pulsatility, change in speed pulsatility, difference in consecutive change in speed pulsatility, speed amplitude symmetry, change in speed amplitude symmetry, number of samples between successive crossings of filtered and averaged signal as well as second derivative of the speed signal. Initially, the detection performance was evaluated for each and every states tested. Rather than individual states, the identification result is observed to be improved when the states were grouped. VE and ANO states were categorized as non-suction state whereas both PVC-I and PVC-C

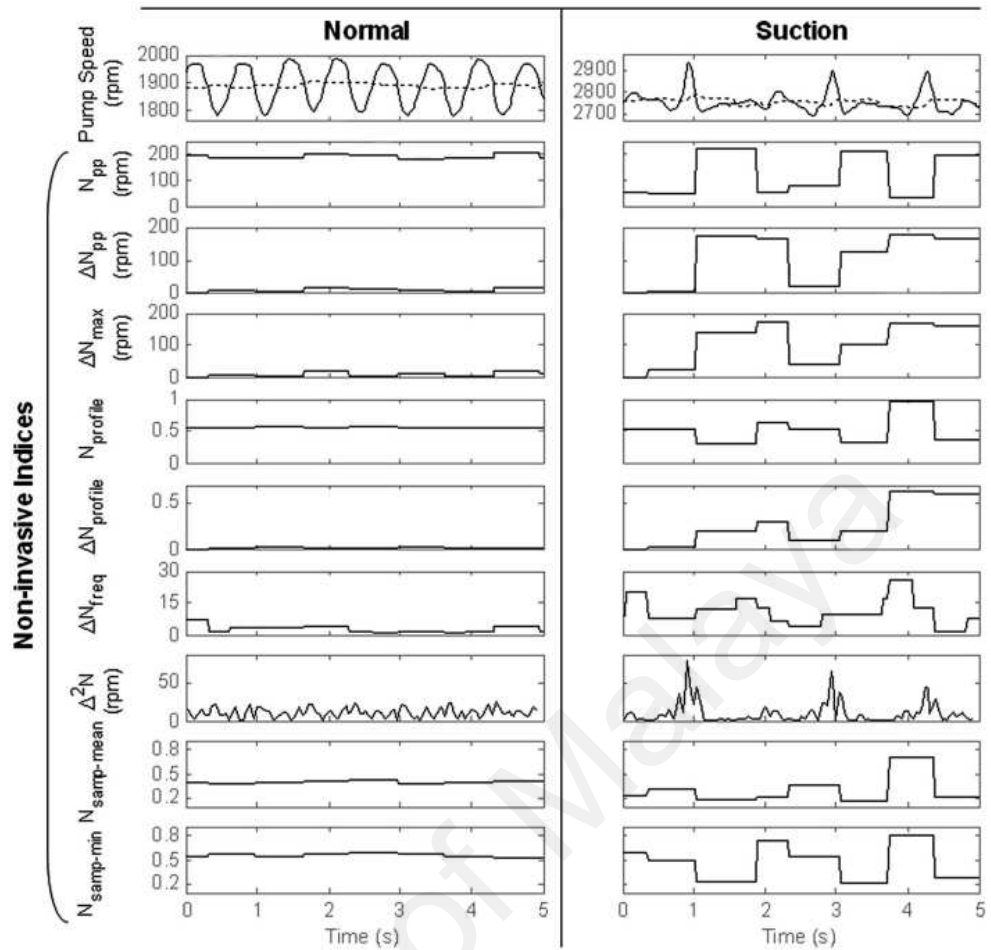


Figure 2.9: Waveforms of indices based on pump speed to determine normal and suction states on human data (Karantonis, Mason, et al., 2007).

fall under suction state. This proposed method was extended to data obtained from heart patients in intensive care unit (Karantonis, Mason, et al., 2007), as shown by the pump speed index waveforms in Figure 2.9. It was observed that inter-patient and intra-patient variability posed a significant challenge for the automated state detection algorithms. It is noted from the patient trials (Karantonis, Lovell, et al., 2006; Karantonis, Mason, et al., 2007) that the wide variation in cardiac conditions of the study had caused a lower performance than the previous study (Karantonis, Cloherty, et al., 2006) that achieved 100% accuracy. In order to account for more cardiac rhythm disturbances, a study (Karantonis, Lovell, et al., 2007) included arrhythmia occurrence with the same approach. Arrhythmic occurrence is a result of disturbance of normal electrical conduction system of the heart and may cause suction at left ventricular myocardium. While non-arrhythmic suction is

due to excessive withdrawal of blood from left ventricle by the pump, suction induced by arrhythmia originates naturally in the native heart itself and appeared as interspersed brief periods of suction in lower speed (Karantonis, Lovell, et al., 2007). Nevertheless, these two were categorized as the same state due to suction characteristics (Karantonis, Lovell, et al., 2007). With the additional suction from arrhythmia to be included in the training set, good results were obtained for the suction classification algorithm. To further extend the suction detection approach, artificial neural network (Karantonis et al., 2008) was used for evaluating the indices due to the classifier's ability to adaptively learn and self-organize training information. As with previous studies, the five different states were classified into 'suction' and 'normal' clusters with high sensitivity and specificity.

A study by (Mason et al., 2008) regarding suction detection conducted on human patients had proposed a combination of multiple indices. The presented work used indices such as minimum change in slope, maximum increase in successive maxima within snapshots, maximum slope, waveform deformation, waveform amplitude, number of high data samples relative to the snapshot mean and difference between maximum and mean (Mason et al., 2008). Each of the seven indices was assigned a threshold value for suction classification. All possible paired combinations were considered to increase sensitivity. Beat to beat variation in flow was identified and obtained via echocardiography while systolic notching at the arterial pressure waveform was used to aid the identification of suction events. Fixed threshold method was applied for both single index and combination of indices for evaluation purposes. The study concluded that combination of maximum increase in successive maxima within snapshots index and number of high data samples relative to the snapshot mean index cover suction onset as well as both early and late forms of ventricular collapse (Mason et al., 2008).

(Arndt et al., 2010) proposed the use of a pulsatility based preload-sensitive control algorithm with self-adapting pulsatility reference for implantable LVAD. The pulsatility

index was calculated as the mean absolute deviation from the mean pressure difference. The fast response provided by the pulsatility index to accommodate the pump output to venous return (Arndt et al., 2010).

By considering the complex relationship between heart rate, blood assistant index (BAI) and pump speed, the model-free adaptive control was proposed for the design of anti-suction controller (Gao, Gu, Zeng, & Chang, 2012). BAI is defined as the ratio of external work from ventricular assist device to the input power of the cardiovascular system, and act as an indicator to show occurrence of left ventricular suction under several physiological conditions. BAI signal implies the function of the native heart whereas heart rate signal reflects the blood demand of circulatory system. From the study it was observed that when the rotational speed of device increase leading to the decrease of LVP, the BAI increase correspondingly. On the other hands, when suction occurs, BAI exceeds 100%. The demonstrated positive correlation of the proposed index with respect to suction occurrence had prompted its incorporation with previous work involving heart rate (Gao, Nie, Chang, & Zeng, 2011) to propose the control algorithm.

In attempting to detect occurrence of ventricular suction, Gaussian Mixture Model (GMM) with constrained parameters was applied by (Tzallas et al., 2012) to model the reduction of pump flow signals baseline. The proposed methodological steps involve signal windowing, GMM classification and GMM adaptation (Tzallas et al., 2012). With the aim of tracking the signal baseline and rapid baseline degradation that is caused by suction occurrence (Tzallas et al., 2012), the approach was said to be simple for implementation and can be operated in real time. Performance of the method was quantified by using receiver operating condition with overall accuracy of 93% (Tzallas et al., 2012).

In the work of (Wang, Faragallah, Divo, & Simaan, 2011; Wang & Simaan, 2013), suction detection was identified by using Lagrangian support vector machine. A total of three pump states (no suction, approaching suction and suction) were identified via a two-

step classification. In the first step, discrimination was performed between suction state and non-suction state (no suction and approaching suction). Classification among 'no suction' state and 'approaching suction' state was implemented in the second step. In the study, both centrifugal pump and axial pump were used in calves data for comparisons.

Different types of suction and non-suction events was studied (Ng et al., 2013) with indices deriving from amplitude, duration, gradient and frequency of pump speed signal based on their irregularity. The suction events considered in the study included PVC-I as well as PVC-C with and without arrhythmia occurrences. It was found from the study that combination of two amplitude based indices, namely the maximum gradient change in positive slope and standard deviation of maximum amplitude for a cycle achieved sensitivity of 98.9% and specificity of 99.7% (Ng et al., 2013).

2.7 Aortic Valve Non-opening

Operating on the basis of bio-impedance changes to applied alternating current, impedance cardiography (DeMarzo & Lang, 1996) was used in the detection of aortic valve opening. However, the ambiguity due to variation of the signal impeded accurate identification on onset of VE.

In the study of different pumping states of LVAD, (Ayre et al., 2001) had proposed a state transition index (STI) in ovine experiments. In order to investigate the different pump states induced by the changes in the pump speed point of Figure 2.10 for hypertensive, normovolemic and hypovolemic physiological intervention, invasive measurements such as aortic pressure (AoP), LVP and aortic flow (AoQ) were taken as reference for determining the index of pump speed. Derived from the maximum instantaneous speed and the root mean square (rms) of the instantaneous speed (Ayre et al., 2001), the STI is low or negative when there is no state change. However, the STI value was significantly larger and positive during presence of state change.

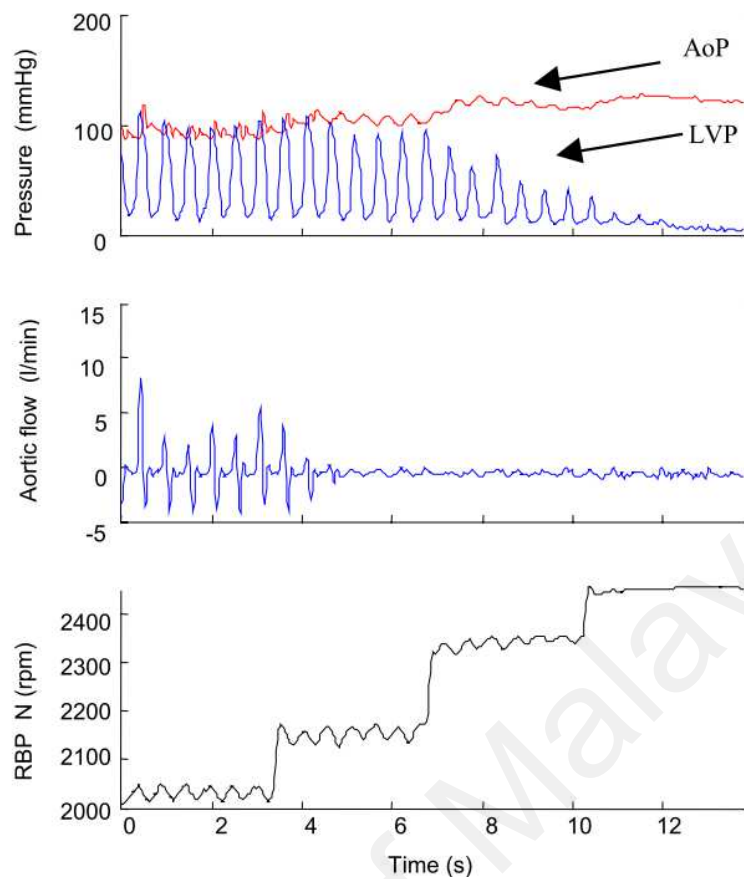


Figure 2.10: Transition of pump state from VE to ANO during the increase of pump speed (Ayre et al., 2001).

In (Lin et al., 2001), the cardiac cycle was divided into four stages according to the status of aortic valve and mitral valve. Optimal pump control index from computation of pump voltage was proposed for suction and backflow reduction purposes. It was found from the study that the proposed index (total time between mitral valve close to aortic valve open divided by total time between aortic valve close to mitral valve open) is a good indicator for controlling LVAD (Lin et al., 2001).

Optimal adjustment of operating point was investigated by using a control method (Arndt et al., 2008) that performs both full assist (FA) and partial assist (PA) with simulation model. FA provides maximum support with closed aortic valve but avoid suction occurrence by having adequate safety margin. Meanwhile, PA allows moderate transitioning support between the opening of aortic valve and a permanently closed aortic valve with better LV washout, moderate LV loading and near physiological LV volume

(Arndt et al., 2008). Pulsatility index was applied on the rotational speed signal to design a cascaded control loop transitioning from mode FA to PA.

In a study by (Bishop et al., 2010), it was hypothesized that electrical current waveforms would indicate the state of aortic valve due to the pressure change in the left ventricular. Data from six patients are collected and Fast Fourier transform analysis was performed. Karhunen-Loève, also known as principal component analysis was applied to project the pump electrical current signal, trend between aortic valve opening and current usage of LVAD (Bishop et al., 2010). By indicating shared signal behaviors, the eigenvectors can be used to determine the opening ratio of aortic valve without echocardiograms for minimal aortic valve regurgitation (Bishop et al., 2010). Despite achieving statistically significant results, prior calibration was required and patient-specific nature of the proposed approach is an undesirable factor that does not allow inter-patient variation during larger scale validation.

Skewness, kurtosis and crestfactor were proposed by (Granegger et al., 2011, 2013) for identification of aortic valve opening by employing nearest neighbor classifier. It was observed that partial support occurs during systole where the aortic valve open and the pump flow shows a flat plateau. On the contrary, sharper peak is displayed during full support, in which the aortic valve closes. From the validation on numerical model as well as animal experiments, the study reported accuracy of 95% for animal data and 99% for simulated numerical model. This approach allows pump speed adjustment for frequent opening of the aortic valve and thus avoids the adverse effect of ANO.

2.8 Current Limitations

The proposed pulsatility index (Arndt et al., 2008, 2010) has limited effectiveness in clinical study. Apparent pulsatility induced by suction is not highly distinguishable from the actual pulsatility from ventricular contraction and the vague selection criteria for

pulsatility index value poses feasibility issues for practical application.

While the work of (Yuhki et al., 1999) was able to establish suction event or re-gurgitation using WDI, this was actually done visually with reference to graph of WDI against speed. Meanwhile, (Endo et al., 2001) was able to detect the transition between partial and total assist of the native heart as well as the transition between total assist and suction. However, a coefficient peculiar to each individual would be needed and this hinders automated large scale implementation. Despite single index based suction detection mechanism was proposed by (Tanaka et al., 2006), there was no discussion made concerning inter-animal variation that requires a more robust algorithm. Since no automated process was involved and no statistical assessment was given for the said approach, there was no statistical basis that can be made regarding these works.

In the works of (Vollkron et al., 2005, 2007), analysis of pump flow signal was performed with inclusion of flow probe. Despite achieving high sensitivity and specificity, these methods are not preferable as such invasive sensors tend to reduce system reliability and increases costs.

Despite the inclusion of ANO state in previous suction study (Karantonis, Cloherty, et al., 2006) had achieved accuracy of 100%, it was suggested that the data available was highly limited. As mentioned in his later study (Karantonis, Mason, et al., 2007) involving human patients, the wide variation in cardiac conditions and dynamics was not taken into consideration in the previous study (Karantonis, Cloherty, et al., 2006). State identification involving arrhythmia events was later explored in the effort to validate the proposed algorithm in a more robust environment, in this instance the ANO data was omitted due to insufficient data.

While the work of (Tzallas et al., 2012) on suction detection has achieved accuracy of 93%, the implemented GMM approach lacks the robustness to outliers. The classification was performed under assumption that the signals in the suction state behave in Gaussian

distribution.

2.9 Summary

Due to the increasing usage of LVAD, it is imperative for these devices to have adequate perfusion for end-organ function. Ventricular collapse and ANO occurrence are some of the deleterious pump states that need to be rectified to avoid inducing complications during implementation of the IRBP. Despite the previous efforts on the subjects, there are very few automated algorithm that emphasized on studying their effectiveness with varying levels of preloads and afterloads. In this study, the detection of ventricular suction and ANO are conducted with consideration of a variety of physiological conditions for a more robust investigation.

University of Malaya

CHAPTER 3

METHODS

3.1 Overview

The chapter focuses primarily on the techniques and details on the implementation workflow performed on the study. Section 3.2 elaborates the acquisition process of the signals of interests for the classification task. Meanwhile, Section 3.3 gives explanation on the signal processing steps operated on the obtained signals in greater details by describing the overall workflow, cycle estimation as well as indices computation. The following section describes the various classification algorithms that are evaluated in the study. Next, validation approaches of the classification are presented in Section 3.5 on the related classifiers. Section 3.6 functions as a platform for detailing the selection methods of the extracted indices for optimal classification performance and improvement of combination set of indices. Section 3.7 includes the evaluative measures taken for the tested approaches in the study. Lastly, Section 3.8 gives the summarized remark for the chapter.

3.2 Signal Acquisition

In this study, different pump states are investigated for data taken from four greyhounds. These healthy, anesthetized and open-chest animals were acutely implanted with IRBP from *VentrAssistTM* (Ventracor Ltd, Sydney, Australia) with mechanical ventilation (Lim, 2010). With apico-aortic configuration, the IRBP was integrated with third-generation centrifugal pump and novel hydrodynamic bearing that gives a characteristically flat pump-head versus pump-flow curve (Lim, 2010). The pump speed of the IRBP was controlled by a proportional integral controller with time constant of about 3.5ms, allowing the pump speed to be modulated by cardiac cycle (Lim, 2010).

3.2.1 Acquisition of Non-invasive Pump Speed Signal

In the IRBP, there is an impeller with four blades, each of them were included with permanent magnet that works with stator coils for impeller rotation (Ayre, Mason, & Karantonis, 2007). Each stator coil set is fitted in pump housing on either side of the impeller (Ayre et al., 2007). While being rotated, the impeller is suspended by hydrodynamic thrust bearing provided by the pump (Ayre et al., 2007). A brushless DC motor formed from the stator coils and the magnets within the impeller will send six back electromotive force (emf) pulses per full revolution back to the controller, correlating with the different magnet positions as the stator coils are passed (Ayre et al., 2007). The instantaneous speed is thereby calculated from the detected back emf signal generated from the motor (Ayre et al., 2007). The experiment on the subjects under healthy condition started with a speed ramp from 1600 rpm, with increment of 100 rpm at each set point (Lim, 2010). Once all variables have reached steady state, perturbations on the cardiac contractility, afterload and preload are induced for different specified levels, that is, low, medium and high (Lim, 2010). Figure 3.1 is an example of speed ramp that transitions from VE state to ANO state.

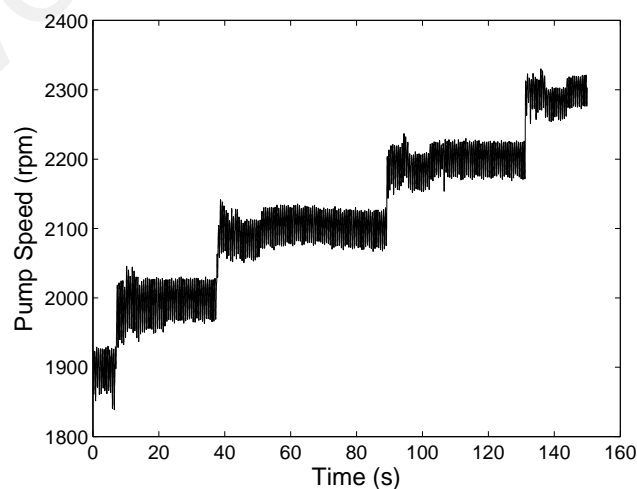


Figure 3.1: Snapshot of a speed ramp signal taken from greyhound data (Ooi et al., 2013).

3.2.2 Acquisition of Invasive Signals as Reference Signals

In the experiment, the subjects were instrumented with indwelling catheters and disposable Tru Wave pressure transducer (Edwards Life Sciences, Pty Ltd, Sydney, Australia) for readings of AoP, LVP, left atrial pressure (LAP), central venous pressure (CVP), pulmonary arterial pressure (PAP), inlet pressure (INP) and outlet pressure (OUP) (Lim, 2010). In order to record AoQ and pump flow rate, ultrasonic flow probe (Transonics perivascular and tubing flow sensors) were connected with T106 flowmeter (Transonic systems Inc, NY,USA)(Lim, 2010). While the initial acquisition system was set at sampling rate of 4 kHz, it was down-sampled to 200 Hz in accordance with most previous studies (Karantonis, Lovell, et al., 2006; Voigt et al., 2005; Vollkron et al., 2007; Ferreira et al., 2007; Mason et al., 2008).

3.3 Cardiac Signal Processing

Appropriate approaches are applied to the signal for the pre-processing steps as well as the actual realization of the indices extraction, forming an indispensable portion of the study. Two types of classification workflow are implemented in the study, namely multiclass classification and binary classification.

Multiclass classification approach is performed in order to differentiate all the available different pump states at one go. It is recommended for highly evident characteristics that are exclusively different for each pump state. As depicted in Figure 3.2, the data is classified into three different pump states, namely VE, ANO and suction. This method was previously applied in (Karantonis, Cloherty, et al., 2006; Karantonis, Lovell, et al., 2006, 2007; Ferreira, Chen, et al., 2006; Voigt et al., 2005; Choi, 2003) for determining different pump states with varying degree of success.

Another approach of performing the study is through nested binary classification. The study on over-pumping states is implemented in two stages. The data is first dis-

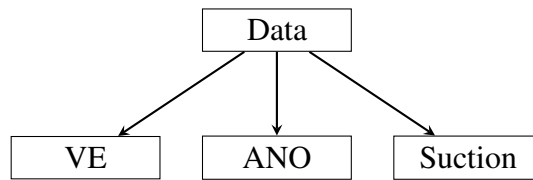


Figure 3.2: Multiclass classification strategy for overall classification of all pump states

criminated into two groups, namely suction state and non-suction states. In the second step, the resultant non-suction states are further classified into VE state and ANO state as shown in Figure 3.3. This strategy has been applied in a number of previous studies on suction detection (Karantonis, Mason, et al., 2007; Wang & Simaan, 2013) as well as ANO detection (Granegger et al., 2011, 2013; Ooi et al., 2014).

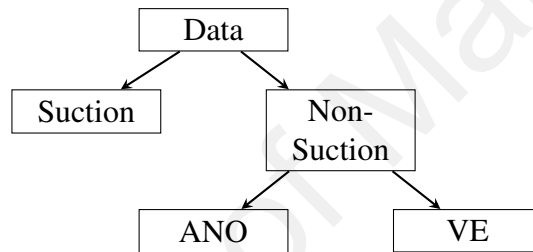


Figure 3.3: Nested binary classification strategy for overall classification of all pump states

Overall workflow of undertaken tasks involving the two stages for the study is illustrated in Figure 3.4. Initially, different pump states are appropriately categorized by using reference signals from gold standards established from existing knowledge (Ayre et al., 2001; Lim et al., 2012). This is imperative to ensure that no equivocal pump state or debatable case that may compromise the reliability or correctness of result are allowed in the study. This is followed by the process of estimating cycles from the signals that will be discussed in greater details. This pre-processing step allows different morphology-based indices to be computed on the respective cycles. Different characteristics of signals are expected to be extracted with regards to the identified cycles and proceed to the testing phase with various classification algorithms. Finally through repetitive testing and experimenting with the relevant parameters, the results from the classifiers will be optimized

for higher performance.

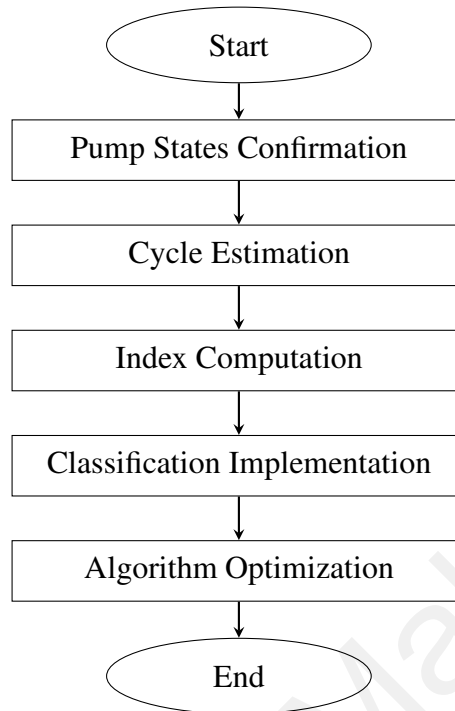


Figure 3.4: Flowchart of overall pump state classification

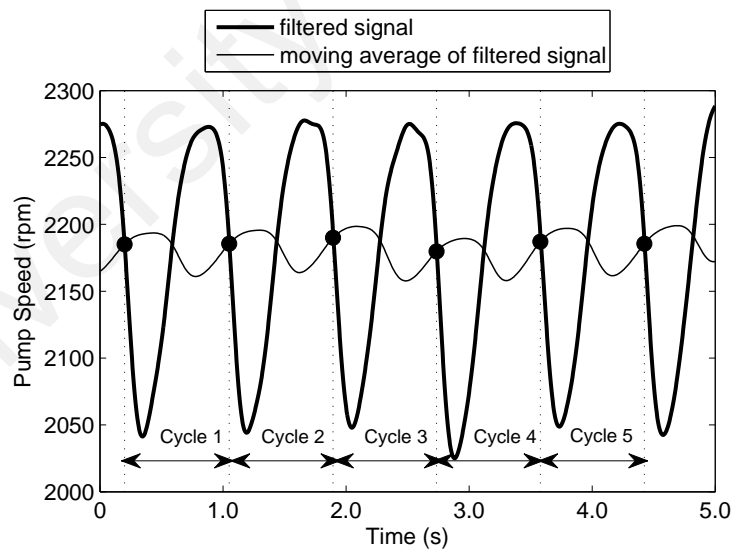


Figure 3.5: Implementation of pump speed waveform during cardiac cycle estimation for indices extraction.

Indices for the classification task are computed by deriving the data points from the estimated cycle. After filtering the signal with a low pass filter of 10 Hz cutoff frequency to remove noise, a moving average filter is applied to the signal. Intersection between a

filtered signal and moving average of the filtered signal is used to indicate the said cycles, which is identified from one crossing point to the successive alternate crossing point from the superimposition, as shown in Figure 3.5.

In the determination of cardiac cycles, different values for moving average size ranging from 0.25s to 4s are tested. When the moving average size is exceedingly small, over estimation of cycle may occur as shown in Figure 3.6(a) where there is a shift in baseline when the pump speed is ramped up. On the contrary in Figure 3.6(b), under estimation may occur from moving average size that is too large. An imperfect and irregular peak in the speed waveform may be mistakenly identified as multiple cycles, causing the incorrect derivation of indices.

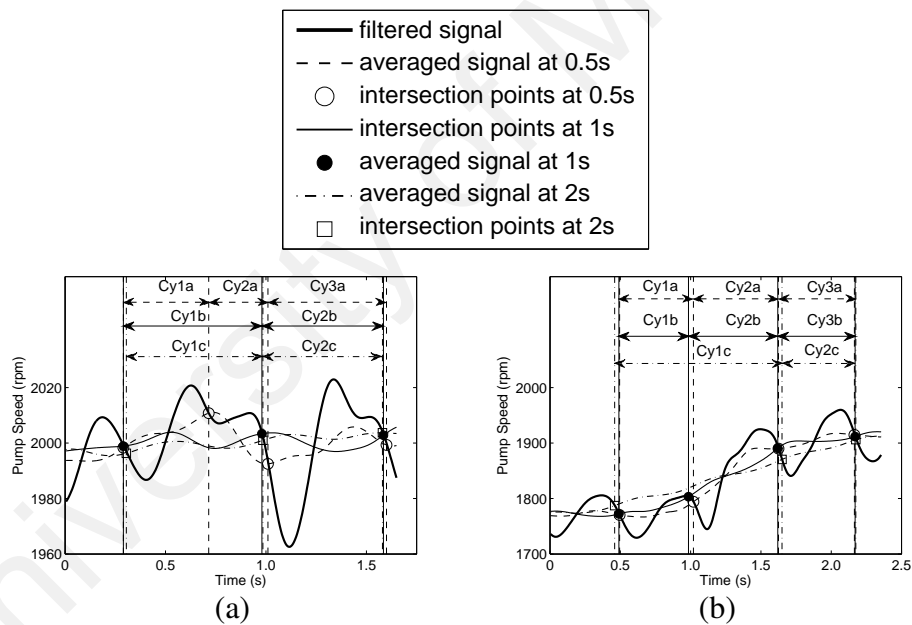


Figure 3.6: Effects of different moving average size on cycle estimation.(a) shows moving average of 0.5s has under-estimated the number of cycles and (b) shows moving average of 2s has over-estimated the number of cycles (Ooi et al., 2014).

Hence, finding suitable size of moving average is imperative in determining the cycle for future cycle extraction. In this study, the moving average size is set at 1s which is equivalent to 200 data points.

3.3.0 (a) Multiple Cycle Based Index Computation

Index computation from multiple cycles is attempted to compute indices from several cycles instead of only taking computation from each cycle. The approach is implemented when the featured characteristic of different states lies in between cycle. From Figure 3.7, it can be seen that a single segment comprises of several cycles that each compute different values for pump state index. These are combined to give an overall representation that describe the morphology of the segment. Such procedure is performed by taking the maximum, minimum, mean and standard deviation of all computed indices in the segment, which represented a single data in classification task. This is applied during the differentiation between suction state and non-suction state in the first step. A segment with duration of five seconds will be taken out and evaluated as a single data for the classification task.

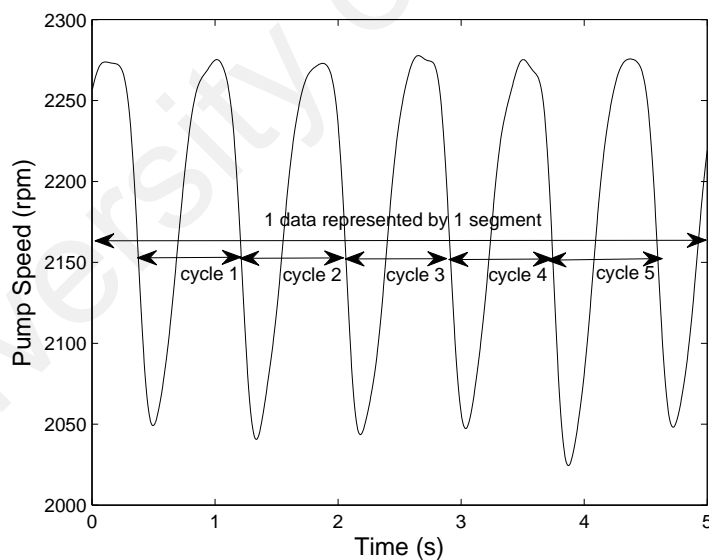


Figure 3.7: Single data represented by segment that consists of multiple cycles for indices computation.

3.3.0 (b) Single Cycle Based Index Computation

Single cycle based index computation is suitable for signals that display distinct shapes and morphology in each cycle. This approach allows different characteristic ex-

hibited to be taken into consideration, including the slight variation among the same state. As shown in Figure 3.8, indices are computed from every cycle. The indices computed from each of the estimated cycles (cycle 1, cycle 2 etc) are taken as separate data for distinguishing between different states. This method is used in the second stage to classify among ANO state and VE state.

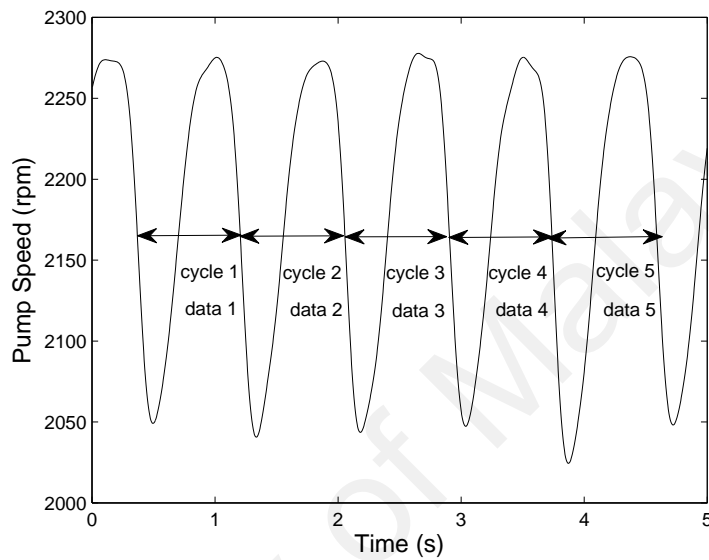


Figure 3.8: Five data represented by five individual cycles in single cycle index computation

3.4 Classification Algorithms

Classifiers are data mining tools applied to make automatic prediction of membership group for data instances (Qin, Xia, & Li, 2009). These techniques can be applied in a wide range of applications from astronomy (Folkes, Lahav, & Maddox, 1996) to fields of minuscule scale involving microorganisms (Beck & Foster, 2014). In this context, classifiers are implemented to distinguish between different states that take place throughout the course of implantation of rotary blood pump. Classifiers should be able to represent even the most complicated problem when supplied with sufficient data in order to make the appropriate decision (Michie, Spiegelhalter, & Taylor, 1994). Generally, supervised classifications are categorized into parametric and non-parametric classifiers. The former

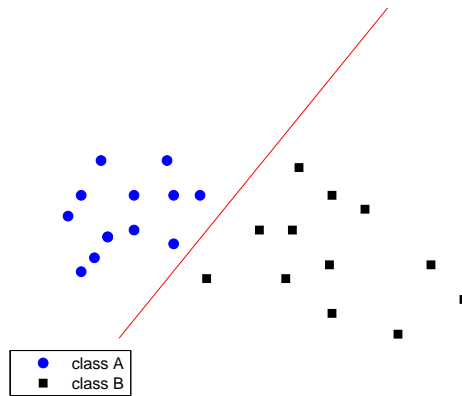


Figure 3.9: An example of LDA implementation on two classes that considers the between-class variance and within class variance.

is implemented with prior assumption on the data distribution whereas the latter does not rely on such assumption. In this study, both will be employed to the pump state classification for comparison. Linear Discriminant Analysis (LDA) and Logistic Regression (LR) are examples of parametric classifiers whereas both Back Propagation Neural Network (BPNN) and K-Nearest Neighbor (KNN) are categorized as non-parametric classifiers.

3.4.1 Linear Discriminant Analysis

LDA is one of the oldest classification procedures and the most commonly implemented (Michie et al., 1994). It works by searching for a set of weights to produce a linear discriminant boundary line by considering between-class variance as well as within-class variance. The objective is to develop an alternate subspace with lower dimension from statistical measure of mean value and variance so that the data points become separable (Xanthopoulos, Pardalos, & Trafalis, 2012). The separation is achieved from obtaining a boundary line that bisects the joining line between centers of the classes (Michie et al., 1994). Direction of the said line is affected by the shape of the clusters of points (Michie et al., 1994). As shown in Figure 3.9, the two types of data points are separated by classifier boundary line determined from distribution of data in the different classes. This is achieved by taking into consideration the cluster size and distribution of the two classes.

LDA solution can be acquired from a generalized eigenvalue system so fast and mas-

sive processing of data samples can be performed (Xanthopoulos et al., 2012). However, LDA was developed for use in normally distributed explanatory variables, hence good results may only be obtained when normality assumptions are fulfilled (Pohar, Blas, & Turk, 2004).

3.4.2 Logistic Regression

Logistic regression estimates the probability of occurrence of a particular event based on the dependent variable that is dichotomous, discrete or categorical (Antonogeorgos, Panagiotakos, Priftis, & Tzonou, 2009). Classes are labelled as '1' for positive event and '0' for negative event. Logistic function, also known as sigmoid function (Dreiseitl & Ohno-Machado, 2002) is applied to map the probability decision into the interval between $[0;1]$, as shown in Figure 3.10. When the value of the sigmoid function falls above 0.5, the class is represented by '1', yielding positive event. On the contrary, value of sigmoid function that exceeds 0.5 will cause the class to be counted as '0', leading it to be classified as negative event.

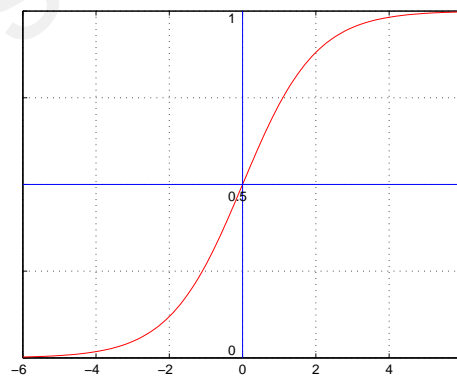


Figure 3.10: Plot of sigmoid function for the classification implementation

Overall flexibility of the classifier boundary is enhanced via its ability to obtain non-linear models. The main disadvantage of LR lies in its assumption of data following the logistic distribution and errors being binomially distributed (Hosmer & Lemeshow, 2004). This may not be the case for every practical application. Also, whenever faced

with large data set, there is a great chance of LR having overfitting problem (Geng, 1992).

LR is said to be sensitive to outliers too (S. Y. Park & Liu, 2011).

3.4.3 Back Propagation Neural Network

In BPNN, the ability to learn relationship between a series of input variables and the corresponding variables is achieved from the training of network (Tu, 1996). Internal weights within the network are adjusted (Tu, 1996) in accordance to the mathematical relationship between the inputs and outputs of a data set, as mapped in Fig 3.11. It is a model free estimator that does not depend on assumption of the tested data (Chang & Islam, 2000).

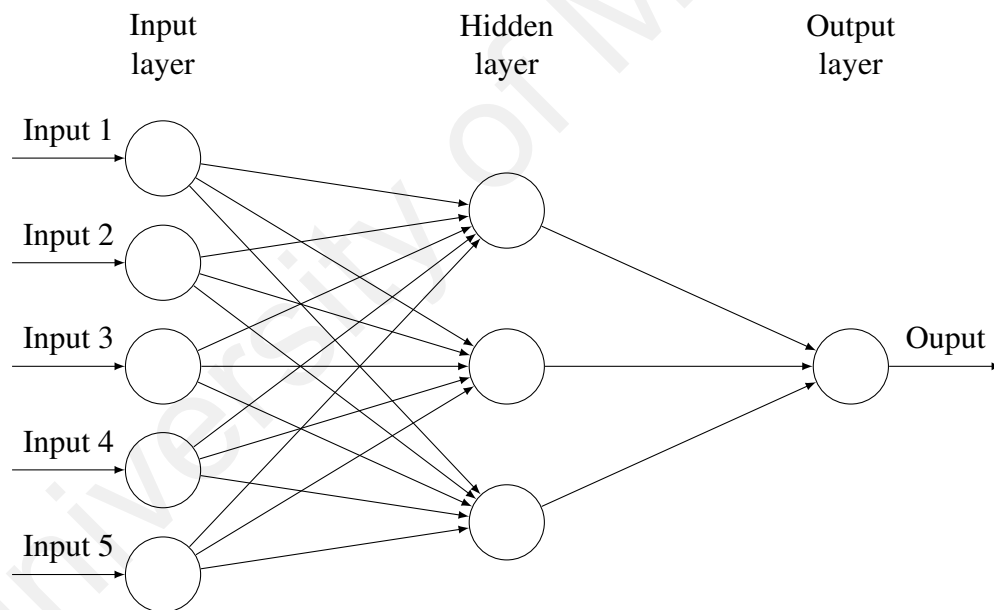


Figure 3.11: An example of a neural network model

The back propagation scheme comprises of forward activation and backward error flows (Moustafa, Alqadi, & Shahroury, 2011). Initiated by the random assignment of weights for symmetry breaking, the input patterns are fed to the network and output patterns are produced from the forward activation flow (Moustafa et al., 2011). Errors from the generated output are computed with respect to the desired output (Moustafa et al.,

2011). The errors are then summed over the complete set of training data to modify the weights in the hidden layer (Moustafa et al., 2011). The error in the form of cost function is gauged by the deviation of predicted classes from actual classes in supervised learning. Lower cost function would imply lower errors, where the predicted classes highly resemble actual classes with high accuracy. Gradient descent is applied to consecutively take the required steps in reaching the zero gradient which corresponds to a local minimum (Riedmiller & Braun, 1993). Learning rate that is too small will result in slow convergence during the search. On the contrary, excessively large learning rate may prevent the cost function from converging. In this classifier, less formal statistical training is required for this approach and implicit detection of complex non-linear relationship between input and output can be achieved (Tu, 1996). However, it is often seen as the black box testing due to its limited capability of performing explicit identification of possible causal relationship (Tu, 1996).

3.4.4 K-Nearest Neighbor

KNN predicts the state classification by referring to the majority votes of neighboring data points. Based on the assignment of label on predominance of a class in the neighborhood, the classifier finds a group of k objects in the training set that achieve the highest proximity with the test data. Similarity function is implemented to estimate the likeliness of the particular data point under test with regards to the decided cluster of training points by distance calculation. In this classification approach, there is no need for explicit training and the process only start taking place when testing data is available. In this classifier, the key elements are (i) types of distance metrics for similarity function (ii) the value of k , which determined the size of the number of nearest neighbor as well as (iii) the number class to be classified into.

When the value of parameter k is set at five as depicted in Figure 3.12, five nearest

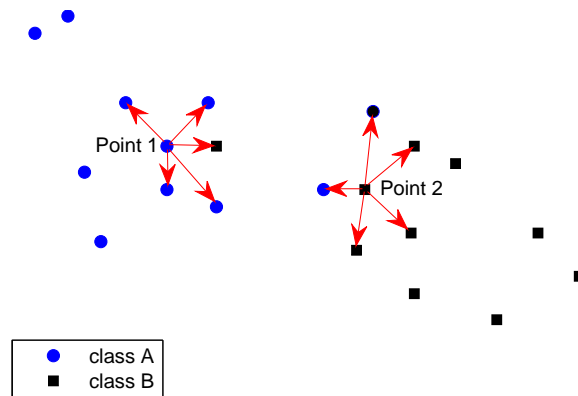


Figure 3.12: An example of nearest distance computation for KNN classification.

points from the neighboring region will be taken into consideration to determine the class of the tested data point. Point 1, for instance, is surrounded by four points from class A and one point from class B. Hence it will be predicted as class A based on the considered neighboring points. Meanwhile, Point 2 is close to three points from class B and two points from class A, as a result it is identified as class B due to the majority votes. This classification approach is easy to implement and debug due to its simplicity and transparency. However, the classifier suffers from poor run time when the training set is extremely large. The drawback of this classification method is the required intermediate distance calculation that may cause long computation time, especially when the size of data is large.

3.5 Validation of Classification

When the exact data is used for both training and testing, good classification rate is expected. However, this may not reflect the true performance of classification methods or robustness of the indices in providing indication of different pump states. Ideally an efficient and accurate classification algorithm is expected to perform well on unseen test data (Refaeilzadeh, Tang, & Liu, 2009). Application on the same data in this manner will result in serious over-fitting (Refaeilzadeh et al., 2009), where the classifier parameters are too sensitive to the training data such that it becomes unstable (Shakhnarovich, El-

Yaniv, & Baram, 2001). The fit will change significantly when part of the training data is removed (Shakhnarovich et al., 2001). In order to measure the true error rate of the classifier performance on the entire population, there are several validation methods that can be applied to avoid this problem.

In these validation approaches, the data is split into training set and testing set. Training set is a portion of the data that is used in adjustment of classifier parameters in repetitive manner to give a better fit during the test. Meanwhile, testing set is used to evaluate how well the classifiers perform with the adjusted parameters with respect to the presented indices. In some instances, there is an additional validation set that is neither applied to training or testing process. Prior to implementation on the testing set, experimentation with validation set prunes the parameters by repetitive evaluation until the optimal values are found.

By assuming that the training set and testing set are homogenous with same characteristics despite being separate entities of their own, ideally the classifier should be able to give good performance on the testing data based on the learning process on the training data. This process is imperative to generally gauge the ability of classification algorithm and for comparing performance of different classifiers. In order to ensure fairness for classifier implementation to give realistically good result, there are several approaches that can be used to apply the procedure, such as random subsampling, k fold cross validation and leave one out validation.

In hold out approach, the complete data is categorized into training set and testing set respectively for the purpose of classifier-independent learning and testing. The procedure is only performed once and no repetition is involved. However, setting aside a testing set from the training process in such way in practice may give misleading error rate during single training testing experiment, particularly when there is disparity on the distribution of data in the different sets. The results from the process can be influenced by the selected

training testing split and available data that is not fully utilized (Refaeilzadeh et al., 2009). As a result, the classifier may adjust the relevant parameters in favor of the training data excessively, causing possible over-fitting on the training set. When the holdout portion for the testing data is set too small, the test is susceptible to change (Shakhnarovich et al., 2001). On the other hand, having a too large testing data will cause it to be overly pessimistic due to limited training (Shakhnarovich et al., 2001).

For random subsampling, the testing set is randomly extracted from the original raw data without replacement. The process is repeated for k times so that the result is not biased to a single fold. Hence, the testing set and training set will be different for each fold and the inherent variability from the separate fold will contribute to a more reliable result for the classification task.

In order to ensure the validity and fairness of classification result, k fold cross validation is performed by dividing the data into different subsets. In each fold, some subsets will act as training set whereas the rest will function as testing set. The successive round of implementation has the different subsets taking turns to be the testing set. This allows all data points to have the equal opportunity of being included in training set as well as testing set and thus each data point is validated by others (Refaeilzadeh et al., 2009). The final performance measures are taken by averaging result from all calculated folds. As shown in the Figure 3.13, the original data is first allocated into three subsets of equal size. Among them, one of the subset is used as a testing set whereas the others are used as a training set. The term 'k-fold' indicates that the classification procedure will be repeated for k times, each with different training set and testing set.

Similarly to k fold cross validation, leave one out cross validation operates by using different folds. However, in this case, the process of training and testing is repeated for k times where k is the total number of data in the study. In each iteration, each data point take turns to be testing set while the rest of the data function as the training set

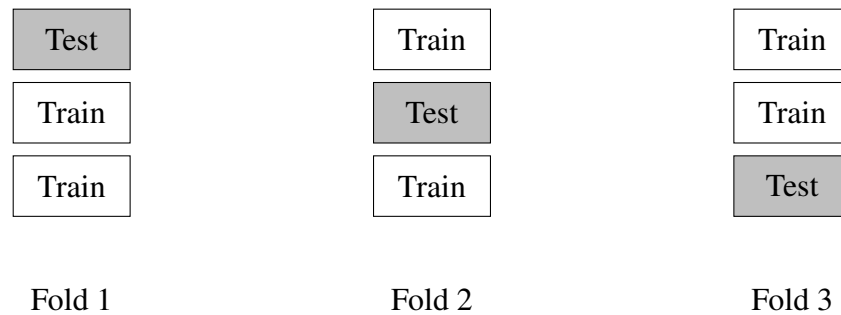


Figure 3.13: Working steps of k fold cross validation (k=3).

(Refaeilzadeh et al., 2009). This extreme approach is known to have high variance which could have caused unreliable estimate (Efron, 1983). It is usually used in applications where data are limited (Refaeilzadeh et al., 2009).

Overall, for validation approaches with iteration, the number of folds involved will affect the overall performance of the classification as well. Small number of fold will induce small variance and thus leading to large bias which are either conservative or higher than the true error rate. On the contrary, accuracy for repetition of larger number of folds will be higher due to the small bias on the classifiers. Due to the number of iteration taken, the overall computation time will be comparatively longer.

3.6 Feature Selection

In order to find the optimal set of combination of indices for the pump state classification without compromising the performance (Pudil, Novovičová, & Kittler, 1994), feature selection is a process of repetitive evaluation applied on the pump states study. Procedures that are more computationally feasible are applied in place of exhaustive search approach to save computation time and prevent redundancy. The purpose of this process is to select only a few indices that are meaningful and effective for the final implementation as computation involving a large number of indices is expensive. By applying appropriate feature selection on the index combinations, better performance can be obtained with reduced complexity and run time.

Sequential Forward Selection (SFS) starts from an empty set where indices are added sequentially during the search for the next best index. Since it is initialized from an empty set, a wide range of combination is potentially evaluated. As it works towards the full set, the region evaluated will be narrowed since most of the tested indices were already selected into the combination set. However, SFS is unable to remove indices that are rendered obsolete upon inclusion of newly found indices. It is best applied when the optimal subset is relatively small.

Meanwhile, Sequential Backward Selection (SBS) initiates its operation from the full set by sequentially removing the least significant index in the subset that potentially worsens the overall performance of the index combination. This approach is suitable for applying in cases when the optimal index subset is large. However, its drawback lies in its inability of reevaluation of a particular index upon removal. Since it originates from full set and mainly deals with large subsets, more computation is required compared to SFS.

Due to the nesting problem demonstrated by both SFS and SBS, alternative methods are proposed (Pudil et al., 1994) by combining them. Two such examples are Sequential Floating Forward Selection (SFFS) and Sequential Floating Backward Selection (SFBS). These methods are proposed in application of index combination in order to achieve optimal pairings that gives the best performance in the most efficient and least computationally expensive way. As shown in Figure 3.14, SFFS commences from an empty set, where each forward step to include new index is followed by removal of indices in a backward direction whenever certain conditions are not fulfilled (Pudil et al., 1994). The said conditions are having a minimum of two indices in the combination set as well as producing combination set that can achieve higher accuracy than the known existing index set thus far (Pudil et al., 1994). On the contrary, SFBS starts operating from a full set, each backward step of index removal will incur forward steps in succession, in an analogous

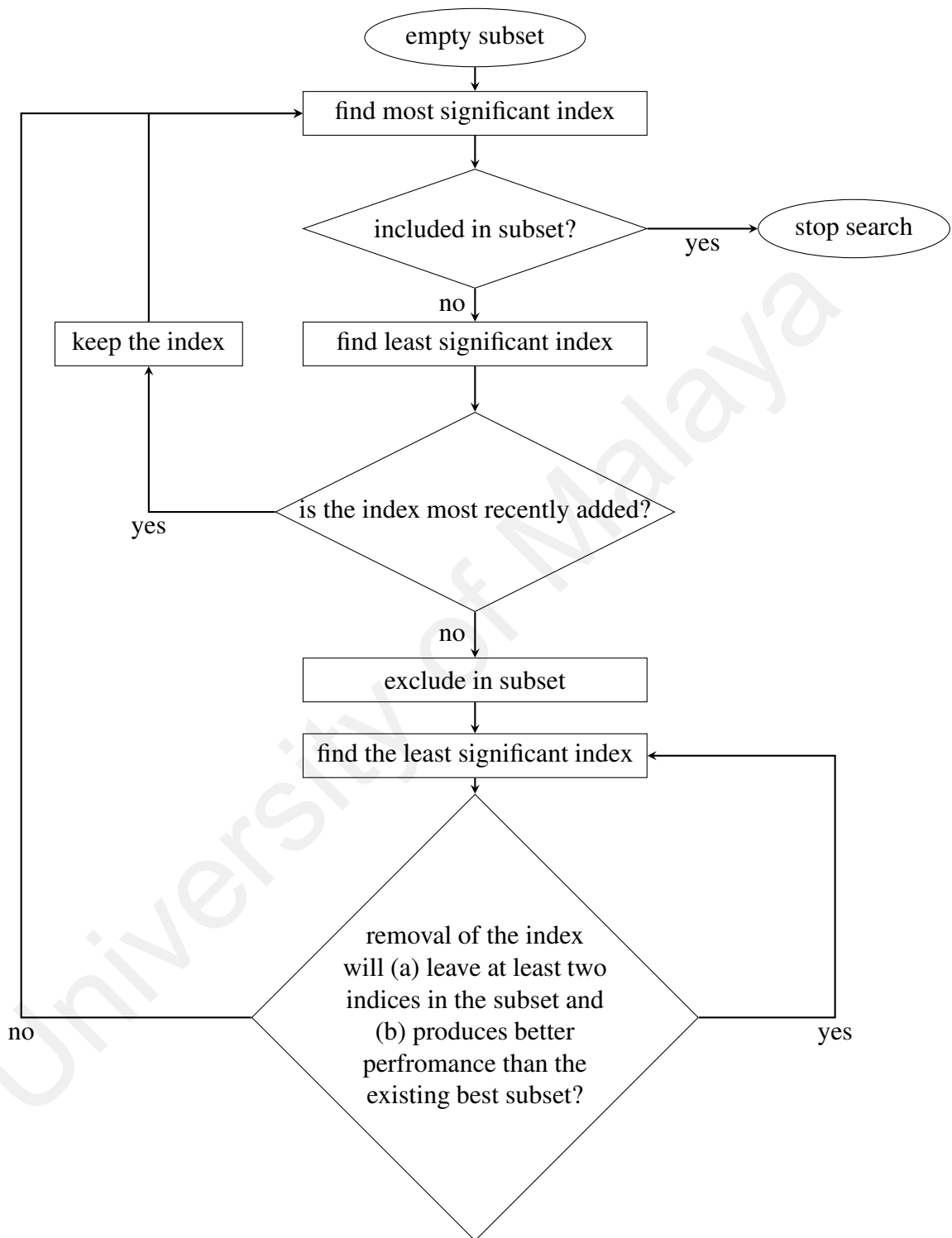


Figure 3.14: Workflow of SFFS in finding the optimal set of indices for the final implementation in pump state detection.

fashion as SFFS. During the search for the optimal combination, the dimensionality of the subset is floating up and down as it goes through the process of addition and removal of indices.

3.7 Assessment and Evaluation

In order to assess the effectiveness of the classifiers with regards to all the tested indices on the task of differentiating pump states, several evaluative criteria are used. Table 3.1 shows the confusion matrix that summarizes all the possible outcomes with regards to actual condition in classification.

Table 3.1: Confusion matrix of all possible classification outcomes.

		Actual Condition	
		Condition positive	Condition negative
Predicted Outcome	Test positive outcome	TP	FP
	Test negative outcome	FN	TN

As presented in Table 3.1, true positive (TP) is the case where the positive condition is predicted positive as it is. When negative condition is mistakenly predicted as positive condition, false positive (FP) occurs. On the contrary, false negative (FN) happens when positive condition is wrongly identified as negative condition. As implied by its name, true negative (TN) is the case where negative condition is correctly predicted as negative in the test outcome.

Accuracy quantifies the level of correctness when comparing the actual condition with respect to predicted condition in a classification test, as shown in Eq 3.1.

$$Accuracy = \frac{TP + TN}{TP + TN + FP + FN} \times 100\% \quad (3.1)$$

Sensitivity is a measure of possibility of detecting positive outcome when the actual condition is indeed positive, as indicated by Eq 3.2. In the context of this study, it illus-

trates how likely the indices are going to perform correct identification of over-pumping states with the help of classifier.

$$Sensitivity = \frac{TP}{TP + FN} \times 100\% \quad (3.2)$$

As denoted by Eq 3.3, specificity defines the possibility of identifying negative outcome from a group of negative condition. In this study, it basically gauges the ability of correct identification of normal pumping states.

$$Specificity = \frac{TN}{TN + FP} \times 100\% \quad (3.3)$$

In instances where the different classes constitute equal proportion in the data distribution, accuracy is capable of displaying the percentage of correctness from the classification by comparing the predicted class with regards to the actual class for all test data points. However, in some cases due to imbalanced distribution of data from different class, accuracy may not be sufficient to truly reflect the performance of the classification implementation. In situation where data points from class A (positive condition) far outweighing class B (negative condition), there is a possibility of misclassifying most of the points as class A instead of differentiating class B as it is. The computed accuracy may be very high but the predicted class is not able to give the actual representation of the distribution. The resultant sensitivity is extremely high but at the expense of specificity. On the contrary, when the data points from class B (negative condition) present in far greater amount than that of class A (positive condition), it will cause very high specificity and low sensitivity. Hence, ideally for correct classification, besides having high percentage of accuracy, it is desirable to have equally balanced sensitivity and specificity so that the overall accuracy is not biased by the uneven distribution of tested data.

3.8 Summary

The chapter organizes the workflow of the study in a systematic manner with the overall methodological steps shown with adequate explanations. Acquisition of signals is described with the required justification and substantial reasoning is provided for the application of classification algorithms. Different types of classifiers such as LDA, LR, BPNN and KNN are explored so as to provide greater understanding on the operations of the said classification algorithms. In addition, validation of the task and optimization of the index subsets are presented to ensure better and more reliable performance is achieved. Methods of evaluation on the study are given to assess the performance of the employed approaches. The framework of implementation of the study is documented and detailed for applications in the following chapters.

CHAPTER 4

VENTRICULAR SUCTION DETECTION

4.1 Overview

This chapter revolves around the detection of the ventricular suction pump state. Section 4.2 reveals the standard approach of checking this particular pump state to ensure that state determination is properly performed. Section 4.3 details the portrayal of suction state in pump speed waveform to achieve successful characterization. As for Section 4.4, all the evaluated indices that are employed on the suction classification tasks are elaborated in details. This leads to Section 4.5 that documents the observations and results for the pump state detection. The following discussion section gives an insight to the findings of the study with the required justifications. Finally Section 4.7 gives a conclusive remark regarding the identification of suction state from non-suction state.

4.2 Suction State Determination

Being a critically risky pump state, ventricular suction is one of the most undesirable pump state during the implantation of rotary blood pump (Boston et al., 2003). It is vital that this pump state is properly confirmed with the established standard before proceeding with the classification task. Table 4.1 illustrates the differences of waveform found in suction state and non-suction state by observing the signal taken from LVP distal.

Suction state exhibits negative spike whereas non-suction state does not show such occurrence. Excessive unloading (Yi, 2007) of suction event had emptied the ventricle and caused the ventricular walls to be forced into the inflow cannula. Such phenomenon is illustrated in the unusual presence of negative spike of LVP distal signal.

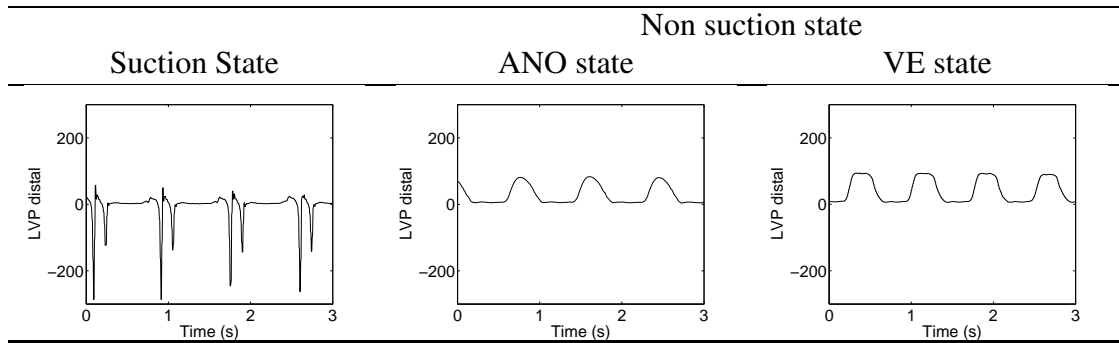


Figure 4.1: Reference signal used for distinguishing suction state and non-suction state.

4.3 Suction State in Pump Speed Waveform

Based on the extracted suction pump state examples, presence of saddles can be observed frequently. The overall speed waveform comprising of peaks and troughs are highly irregular or even erratic as shown in Figure 4.2.

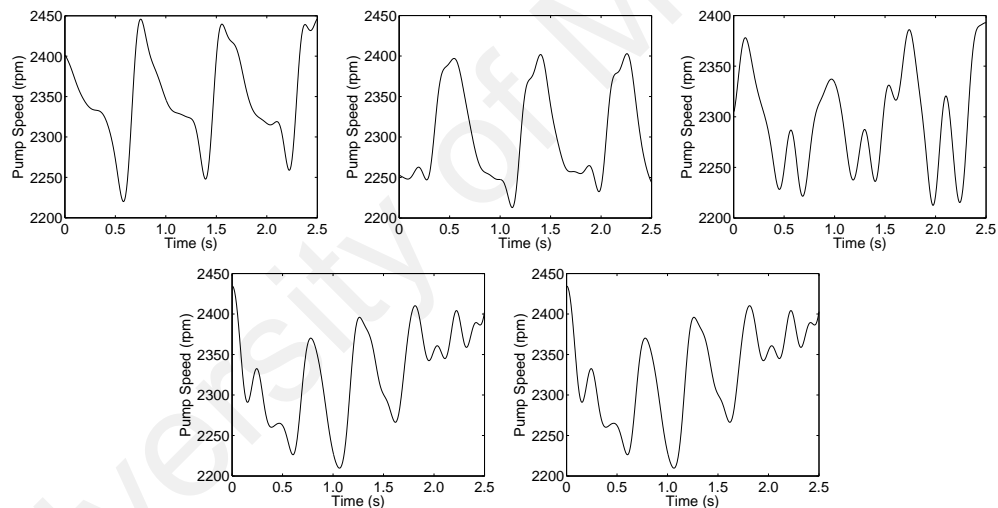


Figure 4.2: Examples of identified ventricular suction instances obtained from pump speed signal.

4.4 Suction Indices

A number of indices from eight categories are evaluated to test their ability to distinguish between suction state and non-suction state, as shown in Table 4.1. Computation of these indices are performed in respective multiple cycles in the data segment. These computed values will subsequently be taken by statistical measures (maximum, minimum, mean and standard deviation) as a representation of the particular data.

Table 4.1: Descriptions of all features used in the present study.

Indices	Descriptions	Formula
Bas_1	Maximum	$max(x)$
Bas_2	Minimum	$min(x)$
Bas_3	Mean	$mean(x)$
Ran_1	Range	$Bas_1 - Bas_2$
Ran_2	Lower range	$Bas_3 - Bas_2$
Ran_3	Upper range	$Bas_1 - Bas_3$
Dir_1	Lower range/range	Ran_2/Ran_1
Dir_2	Range/mean	Ran_2/Bas_3
Dir_3	Lower range/upper range	Ran_2/Ran_3
Sta_1	Standard deviation	$\sqrt{(\sum(x - Bas_3)^2)/n}$
Sta_2	Skewness	$\sum(x - Bas_3)^3/(n - 1)Sta_1^3$
Sta_3	Kurtosis	$\sum(x - Bas_3)^4/(n - 1)Sta_1^4$
Rms_1	Root mean square	$\sqrt{mean(x^2)}$
Rms_2	Maximum/root mean square	Bas_1/Rms_1
Rms_3	Minimum/root mean square	Bas_2/Rms_1
Rmr_1	Root mean and range	$\sqrt{Bas_3 * Ran_1}$
Rmr_2	Maximum/root mean and range	Bas_1/Rmr_1
Rmr_3	Minimum/root mean and range	Bas_2/Rmr_1
Dur_1	Duration of a cycle	$Num(x)$
Dur_2	Duration of half cycle	$Num(x_{half})$
Dur_3	Duration above min-max threshold	$Num(x > (Bas_1 + Bas_2)/2)$
Dur_4	Duration above mean -max threshold	$Num(x > (Bas_1 + Bas_3)/2)$
Gra_1	Gradient	$x(i + 1) - x(i)$
Gra_2	Maximum gradient	$max(x(i + 1) - x(i))$
Gra_3	Minimum gradient	$min(x(i + 1) - x(i))$
Gra_4	Absolute gradient difference	$abs(Gra_2 - abs(Gra_3))$
Gra_5	Gradient difference	$Gra_2 - Gra_3$
Gra_6	Maximum gradient change in negative slope	$max((x_{nhalf}(i + 1) - x_{nhalf}(i)) - (x_{nhalf}(i) - x_{nhalf}(i - 1)))$
Gra_7	Maximum gradient change in positive slope	$max((x_{phalf}(i + 1) - x_{phalf}(i)) - (x_{phalf}(i) - x_{phalf}(i - 1)))$

Bas indices are applied in this study to investigate their potential in reflecting the changes from non-suction states to suction states by means of statistical measures on the pump speed waveform. The statistical values are expected to give indications on the detected pump states and were previously applied in the works of (Karantonis, Cloherty, et al., 2006; Karantonis, Lovell, et al., 2006, 2007; Karantonis, Mason, et al., 2007; Karantonis et al., 2008; Mason et al., 2008; Ng et al., 2013). Indices from *Ran* group are tested due to the characteristic changes of pump speed amplitude among suction state and non-suction state. The gradual changes in the pump speed waveform may be detected by observing the changes, as discussed in (Karantonis, Cloherty, et al., 2006; Karantonis, Lovell, et al., 2006, 2007; Karantonis, Mason, et al., 2007; Karantonis et al., 2008; Mason et al., 2008; Ng et al., 2013; Baloa et al., 2000).

Dir indices take into consideration of ranges from the changes in amplitude with respect to the statistical measures so as to better capture the trend between suction state and non-suction state. It is also proposed for distinguishing between ANO state and VE state (Vollkron et al., 2007; Yuhki et al., 1999; Vollkron et al., 2007). Meanwhile, *Sta* indices that were previously proposed in (Granegger et al., 2011, 2013; Ooi et al., 2014) for ANO detection are also applied in the classification task due to its potential in detecting the irregularities present in the suction state. Prior to this, Rms_2 (crestfactor) was previously introduced for classifying ANO states (Granegger et al., 2011, 2013; Ooi et al., 2014). By integrating rms with statistical measures, *Rms* indices are therefore included in the study for analysis of suction identification. *Rmr* indices (Ooi et al., 2014) are essentially derivation and permutation from *Rms* indices counterparts. Attempts were made to replicate its structure with alternative components for capturing the differences between suction state and non-suction states. For *Dur* indices, estimation of the duration of cycle is gauged in each tested data for detecting suction state based on the observed trend. It is previously applied in (Karantonis, Cloherty, et al., 2006; Karantonis, Lovell,

et al., 2006, 2007; Karantonis, Mason, et al., 2007; Karantonis et al., 2008; Mason et al., 2008; Ng et al., 2013). By adjusting the threshold for the *Dur* indices such as *Dur*₃ and *Dur*₄, presence of saddles may be detected for the classification task. Gradient from the pump speed waveforms are approximated in order to distinguish between the different states. *Gra* indices are proposed by (Ng et al., 2013; Vollkron et al., 2007; Ferreira, Chen, et al., 2006) to observe the different gradient as well as maximum change of gradient in positive and negative slope. This index group is intended to differentiate between suction state and non-suction via estimation of saddles in the waveform.

4.5 Results

4.5.1 Classification Strategy

In order to classify all available pump states in the study, multi class classification is applied to the greyhound data to detect VE state, ANO state and suction state.

Table 4.2: Statistical performance of index mean of *Dur*₃ for multi-class classification. Sensitivity, specificity and accuracy are denoted as P1, P2 and P3 respectively.

Indices	VE			ANO			Suction		
	P1	P2	P3	P1	P2	P3	P1	P2	P3
mean of <i>Dur</i> ₃	43.8	79.1	66.9	55.5	75.1	68.5	93.7	91.5	92.2

Table 4.2 shows example of indices performance applied on all pump states via multi class classification. It can be observed that while index mean of *Dur*₃ performs well for detecting suction state with accuracy of 92.2%, it has some problems in differentiating VE state and ANO state by reaching accuracy of only 66.9% and 68.5% respectively. The full list of statistical performance in terms of sensitivity, specificity and accuracy for all tested indices to detect all states can be found in the Appendix A.

Some indices are more effective in distinguishing suction state whereas others may perform optimally for other pump state. Results from this study found that there is no particular index that achieves the highest accuracy for all pump states. It can be seen that some indices are more effective in detecting suction states whereas others are more

prone to classifying between ANO state and VE state. Hence the following effort on the study will be focused in nested binary classification approach that makes advantage of the potential indices for successful pump state detections.

4.5.2 Individual Index

The different individual suction indices are evaluated by using different classifiers from binary classification, as combined in Table 4.3. The full result for each of the different classifiers can be found at the Appendix B. The performance with respect to the different statistical measures (max, min, mean and std) in terms of accuracy is illustrated in Figure 4.3.

Bas indices generally give accuracy that ranges from 71.2% to 84.5%. Standard deviation of these groups generally gives poorer performance than the rest. Meanwhile, *Ran* indices focused on finding the periodical changes observed in the pump speed amplitude, yielding accuracy from 70.6% to 85.3%. For *Dir* indices, accuracy falls between 72.9% and 91.9%, which are achieved by taking into consideration the division of different range and statistical components. *Sta* indices are able to produce accuracy from 62.2% to 91.9% by categorizing the different pump states based on the statistical distribution of pump speed amplitude. By taking into account square roots and division operation among the statistical measures, *Rms* indices manage to obtain accuracy that ranges between 68.2% and 87.7%. *Rmr* indices, which comprise of mean and range of pump speed amplitude, indicate the change of different pump states with accuracy from 75% to 83.5%. Computation of duration of cycles forms *Dur* indices, which distinguish the different pump states with regards to the duration and computed duration with respect to certain threshold. The resultant accuracy is between 69.4% and 94.%. Mean value taken from the different cycles of these indices are quite effective as all computed accuracies for this category exceed 90%. *Gra* indices evaluate different gradient permutations

Table 4.3: Statistical performance of binary classification of different indices on greyhound data from taken from compared classifiers. Results are arranged as sensitivity/specificity(accuracy)

	max	min	mean	std
<i>Bas</i> ₁	76.2 / 85.9 (82.7)	81.9 / 87.4 (85.5)	78.3 / 87.2 (84.2)	57.5 / 82.5 (74.5)
<i>Bas</i> ₂	76.2 / 84.4 (81.7)	76.6 / 84.0 (81.5)	82.1 / 85.7 (84.5)	55.4 / 78.9 (71.2)
<i>Bas</i> ₃	75.5 / 86.7 (83.1)	68.4 / 85.8 (80.1)	67.5 / 84.8 (79.1)	56.6 / 81.0 (73.0)
<i>Ran</i> ₁	62.5 / 84.5 (77.2)	69.7 / 86.6 (81.1)	69.0 / 87.4 (81.3)	51.0 / 80.4 (70.8)
<i>Ran</i> ₂	57.4 / 84.8 (75.8)	65.2 / 83.7 (77.7)	61.7 / 85.6 (77.8)	51.4 / 79.9 (70.6)
<i>Ran</i> ₃	66.5 / 86.4 (79.9)	79.6 / 88.0 (85.3)	72.2 / 88.4 (83.1)	48.5 / 78.3 (68.6)
<i>Dir</i> ₁	51.5 / 83.2 (72.9)	82.4 / 95.5 (91.3)	84.3 / 95.6 (91.9)	71.0 / 78.8 (76.3)
<i>Dir</i> ₂	74.0 / 86.6 (82.5)	74.0 / 86.6 (82.5)	74.0 / 86.6 (82.5)	51.0 / 98.0 (82.7)
<i>Dir</i> ₃	69.0 / 88.0 (81.9)	70.5 / 80.7 (77.3)	87.7 / 91.6 (90.3)	40.8 / 79.9 (67.2)
<i>Sta</i> ₁	60.9 / 85.4 (77.4)	72.5 / 84.7 (80.7)	70.8 / 87.1 (81.8)	53.6 / 79.1 (70.8)
<i>Sta</i> ₂	78.3 / 93.3 (88.4)	48.7 / 81.5 (70.8)	85.7 / 94.6 (91.7)	74.5 / 81.6 (79.2)
<i>Sta</i> ₃	65.3 / 78.9 (74.4)	51.5 / 84.2 (73.6)	62.2 / 79.8 (74.0)	67.3 / 79.8 (75.7)
<i>Rms</i> ₁	76.7 / 85.4 (82.5)	70.0 / 85.7 (80.5)	69.3 / 85.0 (79.8)	54.7 / 79.7 (71.5)
<i>Rms</i> ₂	61.3 / 84.4 (76.9)	73.2 / 83.2 (79.9)	68.3 / 84.0 (78.9)	49.5 / 77.8 (68.6)
<i>Rms</i> ₃	86.5 / 88.3 (87.7)	70.2 / 87.1 (81.6)	80.7 / 88.5 (86.0)	51.1 / 76.4 (68.2)
<i>Rmr</i> ₁	62.3 / 84.5 (77.2)	63.6 / 87.7 (79.9)	64.2 / 86.2 (79.0)	63.9 / 80.6 (75.0)
<i>Rmr</i> ₂	75.3 / 87.4 (83.4)	69.2 / 85.3 (80.0)	75.9 / 86.7 (83.2)	70.5 / 83.8 (79.3)
<i>Rmr</i> ₃	75.0 / 87.1 (83.1)	67.2 / 85.8 (79.7)	75.0 / 86.7 (82.9)	72.6 / 85.0 (81.0)
<i>Dur</i> ₁	42.2 / 98.8 (80.4)	7.7 / 98.3 (68.8)	86.9 / 92.8 (90.8)	73.0 / 88.6 (83.5)
<i>Dur</i> ₂	28.5 / 99.4 (76.3)	21.6 / 99.2 (74.0)	86.0 / 93.4 (90.9)	47.2 / 80.2 (69.4)
<i>Dur</i> ₃	51.1 / 98.8 (83.3)	4.4 / 99.3 (68.5)	89.5 / 96.6 (94.2)	73.7 / 86.7 (82.4)
<i>Dur</i> ₄	53.9 / 99.1 (84.5)	0.0 / 100.0 (67.5)	89.2 / 95.1 (93.1)	70.7 / 86.4 (81.2)
<i>Gra</i> ₁	50.4 / 85.7 (74.2)	58.4 / 83.6 (75.4)	59.2 / 79.8 (73.1)	56.2 / 84.6 (75.3)
<i>Gra</i> ₂	59.6 / 86.5 (77.7)	74.6 / 81.1 (79.0)	60.4 / 86.2 (77.8)	60.0 / 81.2 (74.3)
<i>Gra</i> ₃	79.2 / 90.1 (86.4)	60.1 / 84.8 (76.7)	65.0 / 87.6 (80.2)	47.3 / 81.4 (70.2)
<i>Gra</i> ₄	90.6 / 87.5 (88.5)	53.3 / 81.1 (72.0)	79.7 / 90.5 (87.0)	52.9 / 81.2 (72.0)
<i>Gra</i> ₅	55.6 / 85.1 (75.5)	85.5 / 90.4 (88.8)	67.5 / 86.1 (80.0)	52.3 / 82.2 (72.5)
<i>Gra</i> ₆	57.0 / 86.4 (76.7)	71.5 / 84.3 (80.1)	59.6 / 87.5 (78.4)	52.2 / 82.0 (72.3)
<i>Gra</i> ₇	80.6 / 94.2 (89.8)	52.6 / 84.6 (74.2)	58.6 / 86.1 (77.1)	59.3 / 86.7 (77.7)

from series of differentiation of neighboring points from the pump speed signal, achieving accuracy between 70% and 90.2%

4.5.3 Optimization of Classifiers

In order to ensure that the tested classifiers are operating optimally for best performance, some parameters for the algorithm settings are tested and compared.

For classification involving LR, regularization parameters are introduced to prevent over-fitting from occurring in order to obtain good generalization performance (Lee, Lee,

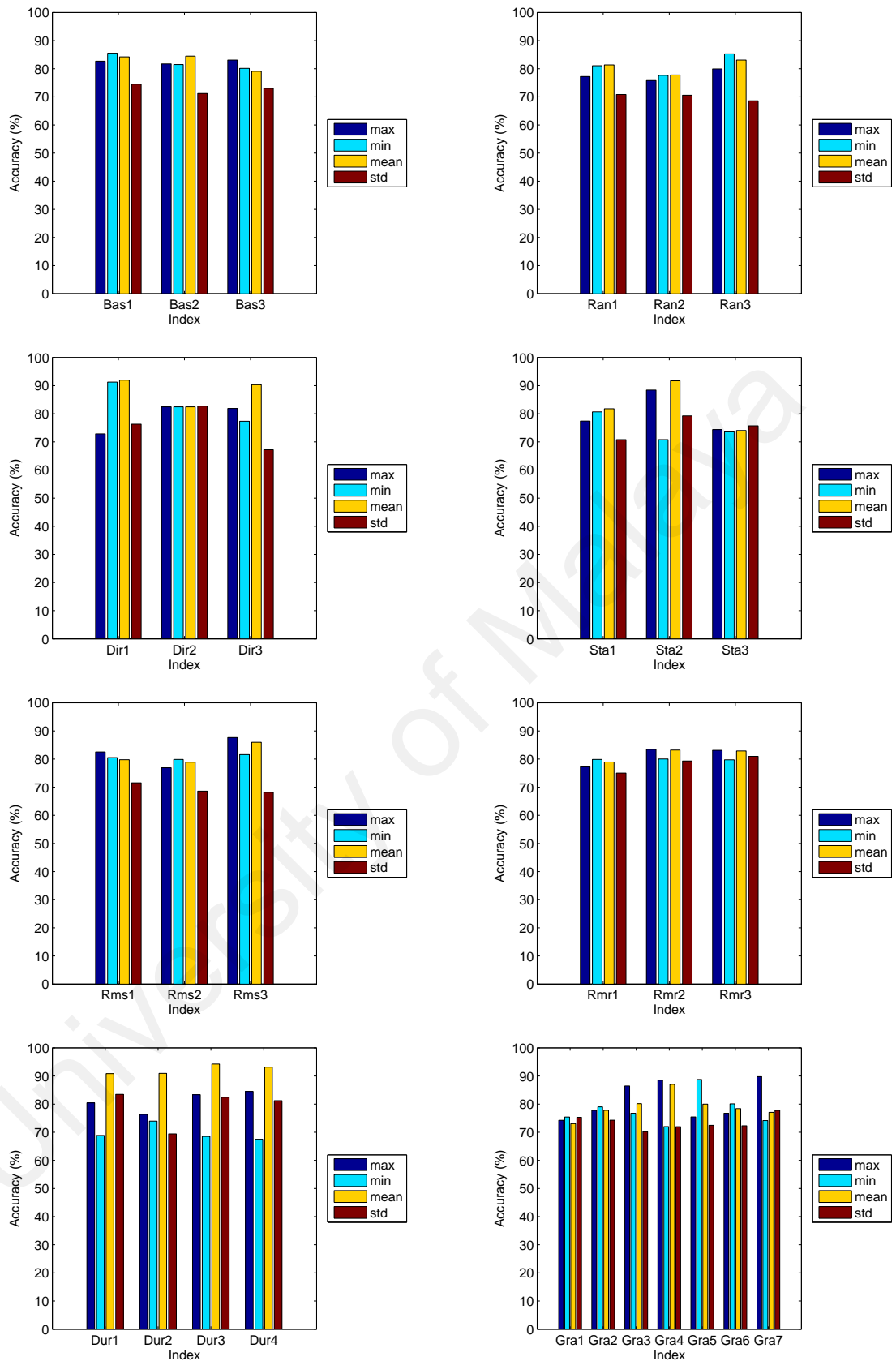


Figure 4.3: Accuracy of suction classification for all tested indices for greyhound data.

Abbeel, & Ng, 2006). Different regularization parameters ranging from 0.001 to 0.3 are tested in the implementation of LR in suction detection. As shown in Table 4.4, there is

Table 4.4: Comparison of statistical performance for different regularization under LR.

Regularization parameter	Sensitivity	Specificity	Accuracy
0.001	90.3	95.7	94.0
0.003	90.4	95.8	94.0
0.01	90.4	95.8	94.0
0.03	90.3	95.7	94.0
0.1	90.3	95.8	94.0
0.3	90.5	95.7	94.0

not much difference for the sensitivity and specificity, resulting in accuracy of 94% for all the tested values. Thus, in this study the regularization parameter for LR is set at 0.01.

During BPNN classification, learning rate of different values ranging from 0.001 to 0.3 are compared. It is observed in Table 4.5 that low learning rate resulted in slightly inferior performance. Meanwhile, high value of learning rate is observed to cause the overall result to deteriorate marginally. Thus, the learning rate for BPNN is set at 0.01 throughout the rest of the study.

Table 4.5: Comparison of statistical performance for different learning rate under BPNN.

Learning rate	Sensitivity	Specificity	Accuracy
0.001	80.1	97.3	91.7
0.003	88.5	97.1	94.3
0.01	88.7	97.0	94.3
0.03	88.5	97.1	94.3
0.1	88.8	96.9	94.2
0.3	88.8	96.8	94.2

In the algorithm, gradient descent is applied for the iterative reduction of cost function. Higher learning rate will enable the local minimum in the cost function to be reached sooner by taking larger iterative steps in finding the said minimum point but at the expense of possible cases of missing convergence. On the contrary, lower learning rate takes small gradual step at reaching the minimum gradient such that it may cause the computation time to be unnecessarily long.

In addition, different values of the maximum number of iteration are attempted during BPNN application. Higher iteration will lead to larger processing time and thus be

Table 4.6: Comparison of statistical performance for different number of iteration under BPNN.

Maximum number of iteration	Sensitivity	Specificity	Accuracy
50	79.2	97.3	91.3
200	88.7	97.0	94.3
500	88.7	97.0	94.2
1000	88.7	97.0	94.3
1500	80.3	97.3	91.7
2000	88.7	97.0	94.3
5000	88.7	97.0	94.3

more computationally expensive. An optimized solution is achieved when sufficiently good classification result can be obtained with minimal iteration. Hence, it is vital to ensure the threshold that set the appropriate number of iteration works well. From the study observation as shown in Table 4.6, variation of the maximum number of iteration does not alter much the overall performance of the classification. It can be observed that all the compared maximum number of allowed iteration produces similar results.

Table 4.7: Comparison of statistical performance for different hidden under BPNN.

Hidden nodes	Sensitivity	Specificity	Accuracy
1	88.4	97.0	94.2
2	88.7	97.0	94.3
3	88.7	97.0	94.3
4	88.7	97.0	94.3
5	88.7	97.0	94.3
6	88.6	97.0	94.3
7	88.7	97.0	94.3
8	88.5	97.0	94.2
9	88.6	97.0	94.3
10	88.6	97.0	94.3

For BPNN, the suitable combination of weights will substantially aid the classification. Minimal computational effort that does not compromise the performance of the classification task is intended. Hence, different number of hidden nodes are tested and compared during the implementation of suction detection with BPNN. As observed in Table 4.7, pump state detection with hidden node from 1 and 10 has yielded accuracy that fluctuates between 94.2% and 94.3%. Due to the similar result produced from the different number of hidden nodes, computation of BPNN will apply one hidden node

throughout the study.

In KNN, Euclidean distance is applied in the computation of distance between the different data points. Different k parameters in odd numbers ranging from 1 to 19 are heuristically evaluated as displayed in Table 4.8. Since it is binary classification with two known classes, odd number is necessary to ensure that classification decision can be made effectively without complications. It is observed that similar results are given from all the tested k parameters.

Table 4.8: Comparison of statistical performance for different values of k parameter under KNN.

k parameter	Sensitivity	Specificity	Accuracy
1	91.0	97.8	95.6
3	94.1	96.1	95.4
5	90.2	95.4	93.7
7	91.5	96.8	95.1
9	89.6	96.3	94.1
11	88.3	96.4	93.7
13	89.0	97.0	94.4
15	88.9	96.7	94.2
17	88.3	97.1	94.2
19	88.6	97.4	94.5

4.5.4 Comparison of Different Classifiers

For binary classification of individual performance, all the tested classifiers give similar trend. There is not much variation in terms of sensitivity, specificity and accuracy despite non-parametric classifiers such as BPNN and KNN are noted to produce slightly higher percentage as shown in Figure 4.4.

When combinations of several indices are implemented in the study, small gradual improvements are observed in terms of sensitivity, specificity and accuracy as indicated in Table 4.9. Among the four classifiers, the increase in accuracy in KNN is the most prominent as shown in Figure 4.5.

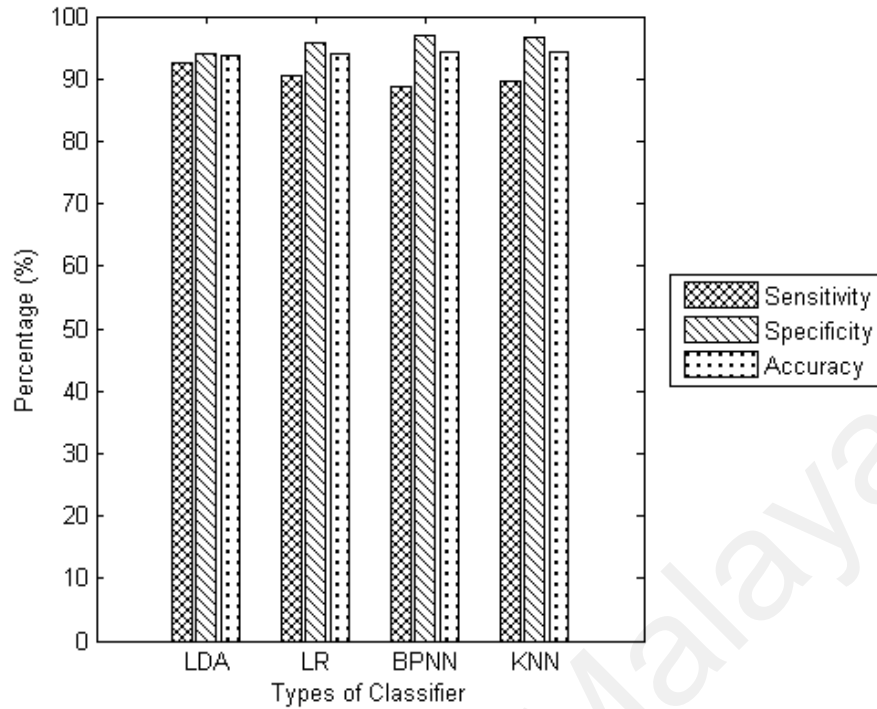


Figure 4.4: Comparison of different classifiers in terms of sensitivity, specificity and accuracy for individual index implementation.

Table 4.9: Statistical Performance of multiple indices for suction detection. Sensitivity, specificity and accuracy are denoted as P1, P2 and P3 respectively.

No.	LDA			LR			BPNN			KNN		
	P1	P2	P3	P1	P2	P3	P1	P2	P3	P1	P2	P3
1	92.8	94.1	93.6	90.4	95.8	94.1	87.1	96.0	93.1	89.7	96.4	94.2
2	92.6	97.6	96.0	92.7	97.8	96.1	92.7	97.7	96.1	97.9	97.3	97.5
3	94.1	97.6	96.5	94.7	97.6	96.7	94.8	97.6	96.7	98.7	97.9	98.2
4	94.7	98.0	96.9	94.5	98.0	96.9	95.6	97.6	96.9	98.7	98.1	98.3
5	95.6	97.8	97.1	95.7	98.0	97.2	95.9	97.7	97.1	100.0	99.2	99.5

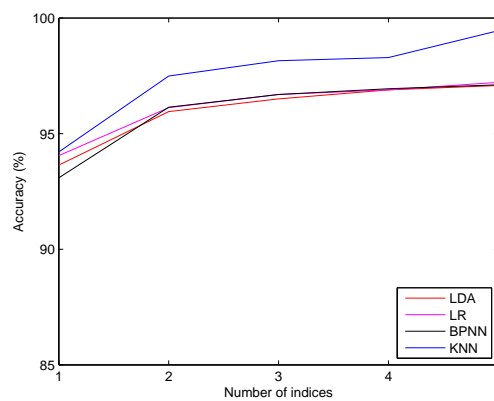


Figure 4.5: Comparison of accuracy from different classifiers when implemented with multiple indices.

4.5.5 Classification Time

For a total of 3636 segments of data, it comprises of 3273 segments of training data and 363 segments of testing data in accordance to train-test ratio of 9:1 in cross validation. Overall, the implementation of classification involving two indices are slightly greater than that of single index as shown in Table 4.10. The total duration taken varies depending on different type of classification method. LDA requires a total of 3.9×10^{-2} s for single index and 4.1×10^{-2} s for two indices. For LR classifier, 5.7×10^{-2} s and 4.4×10^{-1} s are taken for single index and two indices respectively. A total of 4.5s is taken by BPNN for single index and 5.6s is used for combination of two indices. KNN, meanwhile, appears to require longer time with 1.4×10^1 s for single index and 1.9×10^1 s for paired indices. Parametric classifiers such as LDA and LR are observed to give shorter time for completing the task whereas non-parametric classifiers like BPNN and KNN are expected to require more time. Due to the nature of KNN classifier, only testing time is available for the classification where intermediate distances are computed between the training data and testing data to decide the class of the tested state.

Table 4.10: Comparison of computation time for all classifiers during the implementation of suction indices.

Classifier	Training (3273 segments)		Testing (363 segments)		Total (3636 segments)	
	1 index	2 indices	1 index	2 indices	1 index	2 indices
LDA	1.3×10^{-3}	1.7×10^{-3}	3.8×10^{-2}	3.9×10^{-2}	3.9×10^{-2}	4.1×10^{-2}
LR	3.3×10^{-2}	4.1×10^{-1}	2.4×10^{-2}	2.4×10^{-2}	5.7×10^{-2}	4.4×10^{-1}
BPNN	4.4	5.6	2.5×10^{-2}	2.8×10^{-2}	4.5	5.6
KNN	NA	NA	1.4×10^1	1.91×10^1	1.4×10^{-3}	1.91×10^1

4.6 Discussion

As with other muscles in the body, the cardiac muscles are subjected to the production of contractions that forms the series of rhythmic contractions and relaxation. During the evaluation of its contractile properties, preload is used to denote the degree of muscular stretched tension when the contraction is initiated (Guyton & Hall, 2006) during the

diastole phase. The preload level is often associated with level of venous return because the higher volume of blood return to the heart during diastole, the higher is the preload level. It is commonly implied as the end diastolic pressure on the filled ventricle (Guyton & Hall, 2006). Afterload, meanwhile, is the applied tension on the wall of ventricle during ejection. It is often referred as the end load against which blood ejection occurred from the heart contraction. Since the levels for the afterloads and preloads varies throughout the course of normal beating of the heart, this study emphasizes inclusion of such variation in order to give a more robust representation of pump state detection without limiting to any particular cardiac condition. Although there are a number of works (Karantonis, Cloherty, et al., 2006; Mason et al., 2008; Ferreira et al., 2007; Voigt et al., 2005; Vollkron et al., 2007) presented previously on the topic of pump state detections on LVAD, most of them do not include these different perturbations.

Among the different pump states encountered in rotary blood pump, ventricular suction is perhaps one of the most hazardous pump states (Boston et al., 2003) that will have serious consequence in health condition of the heart. Hence, it is imperative that detection of such pump state is effectively performed and rectified as soon as possible.

Cross validation is applied during the application of the various classification algorithms to ensure that the distribution of the training and testing data do not affect the final result of the classification. Such repetition of fold implementation is necessary to ensure that the true performance comparison of the different indices is executed fairly in evaluation of inter-subject robustness without bias. Ten-fold cross validation is naturally chosen in this case as it is a popular rule of thumb and was previously applied in the work of (Karantonis, Lovell, et al., 2006; Karantonis, Cloherty, et al., 2006; Karantonis, Mason, et al., 2007). Setting the number of fold at 10 will stratify the cross validation during large experimentation (Kohavi et al., 1995).

Additionally, SFFS is applied in the study to find the optimal set for the index com-

bination. This searching algorithm combines the advantage of inclusion of new indices as well as exclusion of existing indices in the set to make the searching process more efficient and optimal. In terms of indices evaluation, *Bas* indices do not perform outstandingly with none of them producing accuracy that exceeds 90%. These indices are previously applied by (Karantonis, Cloherty, et al., 2006; Karantonis, Lovell, et al., 2006, 2007; Karantonis, Mason, et al., 2007; Karantonis et al., 2008; Ng et al., 2013; Ferreira et al., 2007). While *Bas*₁ was reported among the indices proposed by (Karantonis, Cloherty, et al., 2006; Karantonis, Lovell, et al., 2006, 2007; Karantonis, Mason, et al., 2007; Karantonis et al., 2008), it was unclear whether the good performance achieved was solely or partly contributed by this index. The exact role played by this index in the acquiring of perfect classification rate is not explicitly stated. Similarly, *Bas*₂ is among one of the few proposed indices proposed by (Ferreira, Chen, et al., 2006) without clear indication of performance for each indices. Meanwhile, *Bas*₃ was tested in (Ng et al., 2013) and performed mediocly.

As for *Ran* indices, overall the indices does not give promising performance in identifying suction states from non-suction states despite being used in a number of previous work (Karantonis, Cloherty, et al., 2006; Karantonis, Lovell, et al., 2006, 2007; Karantonis, Mason, et al., 2007; Karantonis et al., 2008; Mason et al., 2008; Ng et al., 2013). *Ran*₁ was applied in the work of (Karantonis, Cloherty, et al., 2006; Karantonis, Lovell, et al., 2006, 2007; Karantonis, Mason, et al., 2007; Karantonis et al., 2008; Ng et al., 2013; Ferreira et al., 2007) as it is believed to be able to characterize the suction state based on the amplitude change of the pump speed signal. *Ran*₂ was proposed by (Mason et al., 2008) in similar fashion and tested in (Ng et al., 2013) as well but neither studies indicated exceptional performance. *Ran*₃ was evaluated in (Ng et al., 2013) and performs poorly in that study.

Meanwhile the *Dir* indices operates on the basic indices but with a different mode of

operation: division. In the present study, both minimum of Dir_1 and mean of Dir_1 are able to achieve detection with high accuracy of 92%. Prior to this, a number of suction works (Karantonis, Cloherty, et al., 2006; Karantonis, Lovell, et al., 2006, 2007; Karantonis, Mason, et al., 2007; Karantonis et al., 2008; Ng et al., 2013; Ferreira et al., 2007; Tanaka et al., 2006) have applied Dir_1 in their investigation with varying degree of success. The index gauges the deformation of waveform upon state transition to ventricular suction and performs reasonably well among other tested indices in (Mason et al., 2008). As demonstrated in (Tanaka et al., 2006), it has the potential of performing suction detection whilst maintaining the circulatory control. However, individual performance of this index was not specifically stated in (Karantonis, Cloherty, et al., 2006; Karantonis, Lovell, et al., 2006, 2007; Karantonis, Mason, et al., 2007; Karantonis et al., 2008) despite being one of the tested indices in the investigation that concludes with high accuracy. Performance of Dir_2 index in the present study does not give much competition compared to the rest of the test indices despite being proposed in a study (Endo et al., 2001) to acquire a flexible control method based on the index. Nevertheless, the index is reported to perform poorly in evaluation conducted by (Ng et al., 2013).

Sta indices, meanwhile, have been proposed for identifying ANO state from normal ventricular states in the works by (Granegger et al., 2011, 2013; Ooi et al., 2014). While these indices may be effective in performing such detection, their application in classifying suction data from non-suction ones does not yield satisfactory result.

Rms indices have primarily been applied in pump state detection involving the detection of ANO state (Granegger et al., 2011, 2013; Ooi et al., 2014) due to its characteristic morphology. However, there is no observed good performance when implemented to differentiate between suction state and non-suction state. Adopting similar characteristics of *Rms*, *Rmr* indices (Ooi et al., 2014) generally do not show promising classification accuracy in the suction detection of the present study. While the described indices above

show the tendency to capture the waveform erraticism observed in the suction data, similar characteristics are also exhibited in non-uniformities found in ANO state. Confusion arising from these two pump states may have caused the indices to perform poorer than expected when implemented to distinguish ventricular suction state from others.

The accuracy for mean of Dur_1 is moderately high in present study but is observed to give subpar results in the reported evaluation by (Ng et al., 2013). The same trend is observed for Dur_2 . Dur_2 was implemented a number of previous studies (Karantonis, Cloherty, et al., 2006; Karantonis, Lovell, et al., 2006, 2007; Karantonis, Mason, et al., 2007; Karantonis et al., 2008; Ng et al., 2013) on suction state. This index is applied to test the changing pulsatility on pump speed signal. While it is part of the contributing index that resulting in perfect result attained in the said study (Karantonis, Lovell, et al., 2006), it was implicitly implemented in such a way that it has become difficult to compare and gauge the effectiveness of this particular index separately.

As for Dur indices, the mean of Dur_3 appears to be the index that gives the highest accuracy (94%) with sensitivity of 89% and specificity of 97%. Similar to Dur_4 , it applies computation of duration and compare with determined threshold in order to spot unusual ripples found in the peaks of speed signals. In this study, the good performance of the index is largely contributed by the presence of saddles in the suction data as opposed to non-suction data. Such threshold method was previously applied in the work of (Mason et al., 2008) with excellent result. It was also tested in (Ng et al., 2013), albeit with suboptimal performance and did not stand out from other tested indices. This may be caused by the different data distribution under test, as pointed out by (Ng et al., 2013) that data containing arrhythmia may not work very well under this index. While the tested data in the study is noted to have combined normal and arrhythmia data, (Karantonis, Lovell, et al., 2006; Karantonis, Cloherty, et al., 2006; Karantonis, Lovell, et al., 2007; Ng et al., 2013), the porcine data size was still very limited.

Gra indices were proposed by (Ng et al., 2013) to identify suction data by searching for irregularities such as presence of saddles. Unfortunately, this group of indices does not give exceptional classification performance in present study.

Generally it can be observed that the mean of the evaluated indices show greater potential as an indicator in extracting the indices for effective classification of pump states. This statistical measure gives good representation of all the participating cycles so that indices that reflect closely the overall segment is produced. On the other hand, standard deviation for the indices appears to the poorest indicators of all. Computation of the dispersion of the obtained indices for all the data cycles in segments is performed and from observation this does not seem to be a good measure to categorize suction data and non-suction data.

From the tested indices on greyhound data, it can be observed that accuracy is increased when indices are added. In fact the improvement can be observed to reach accuracy of approximately 99.5% when five indices are combined to check for suction state.

4.7 Summary

Due to the possible health risks involved, ventricular suction is a critical pump state caused by over-pumping that should not be overlooked. In this study, a number of methods have been applied to investigate suction detection in greyhound data. By implementing direct statistical computation on the different computed indices in the pump speed waveform amplitude, changes from suction states to non-suction states may be detected with varying degree of success. Different types of indices are evaluated in conjunction with parametric classifiers and non-parametric classifiers to test their effectiveness at distinguishing suction data from non-suction data. Generally, it was observed that mean is the better indicator at extracting the information presented from the multiple cycles in the data segment. From the pump speed signal, presence of saddles was identified in suction

data by application of single index with accuracy of 94.3%. Combination of indices with up to five components will further increase the classification rate to 99.5%.

University of Malaya

CHAPTER 5

ANO DETECTION

5.1 Overview

This chapter centers on identification of ANO pump state. The common approach of determining this pump state is discussed in details in Section 5.2. This is followed by Section 5.3 that explains the morphology of pump speed waveform with respect to the pump states. On the other hand, Section 5.4 describes the investigation of ANO state from the perspective of indices evaluation, supported by results and discussion. Lastly, Section 5.5 summarizes the gist of the chapter with the main findings presented.

5.2 ANO State Determination

As defined in Chapter 2, ANO can be attributed to the over-pumping of LVAD that causes blood flow to completely neglect the native route of the heart. Due to the lack of activity of aortic valve, there are risks of several complications such as aortic stenosis, aortic regurgitation (Granegger et al., 2011) or even the aortic fusion (Rose et al., 2000) that critically endangered the lives of patients if left untreated. There are several standard requirements for determining the pump state of the signals. In ANO state as shown in Figure 5.1, the AoP is greater than the maximum LVP (Ayre et al., 2001). This is in contrast from VE state where the maximum LVP exceeds AoP, driving the rhythmic opening and closing of aortic valve in the cycle. Due to obstruction of blood flow in the prolonged closure of aortic valve in ANO state, the net aortic flow is almost zero as compared to the normal positive flow in the VE state (Ayre et al., 2001). In VE state, there is a dip and a transient rise due to elastic recoil against the valve cusps before the gradual decline of aortic pressure, causing dicrotic notch in the signal (Boron & Boulpaep, 2008). On the

contrary, there is no such notch during ANO state (Lim et al., 2012).

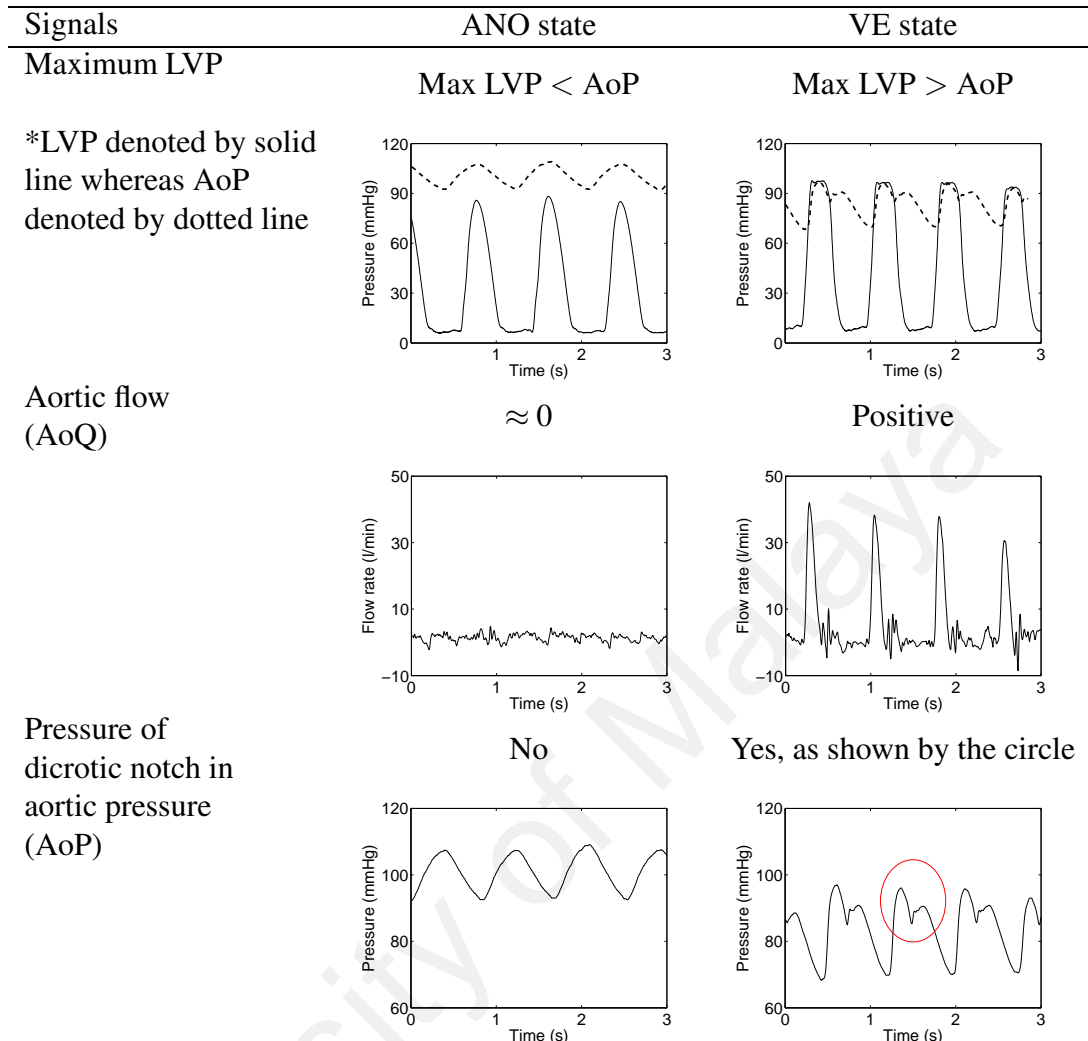


Figure 5.1: Reference signal criteria between ANO and VE state

5.3 ANO Pump State in Pump Speed Waveform

In this study, pump speed signal is investigated for applications on different classification algorithms. This noninvasive signal originated from a reliable method of acquisition from the detected back emf signal from the motor of the IRBP controller (Ayre et al., 2007), so that there are no complications that could compromise the stability of signal reading in the long term. This is in contrast with invasive signals that involve the use of external flow probes or transducers.

Due the variation of levels of preloads and afterloads found in the greyhound data, pump speed signals exhibit variation of different changes throughout the transition. Fig-

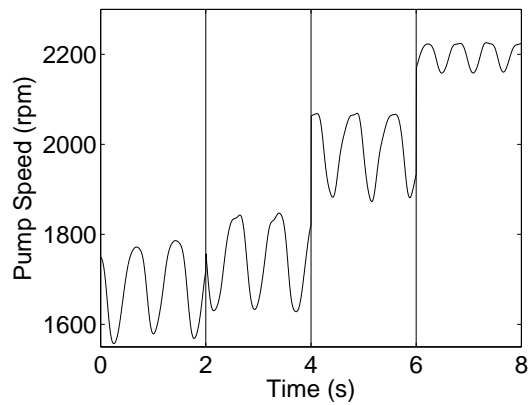


Figure 5.2: Transition from VE state to ANO state for pump speed waveform (Ooi et al., 2014).

Figure 5.2 shows the transition of VE state from lower speed range to ANO state in higher pump speed range (Ooi et al., 2014). As the pump speed transitions from low to high as shown in Figure 5.2, there is a gradual change in the morphology of the waveform of the signal. The initial stages of early ANO state is showing a rather even shape, with some peaks slightly flatten while remaining its original shape in the troughs. The irregularities continue to become more obvious with the presence of dual peak formation. Saddle-like features are observed in the peaks of pump speed signal in some instances. Figure 5.3

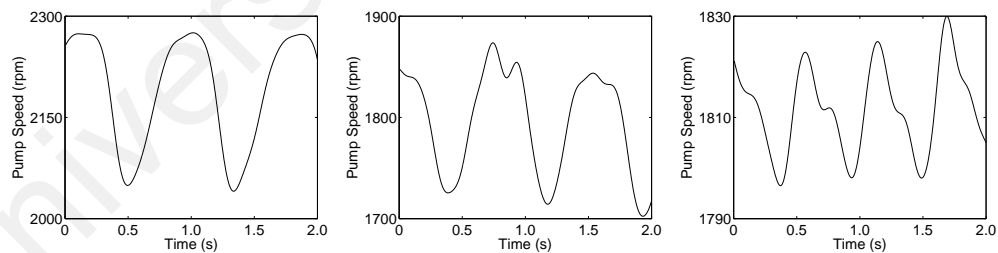


Figure 5.3: Examples of identified ANO instances obtained from pump speed signal (Ooi et al., 2014).

shows several variation of pump speed waveform found in the greyhound data. Some of them shows flat plateau with sharp trough whereas others display dual peaks and slight saddles in the peak (Ooi et al., 2014).

Table 5.1: List of evaluated ANO indices with respective description and formula (Ooi et al., 2014).

Indices	Descriptions	Formula
Ran_1	range	$max(x) - min(x)$
Ran_2	lower range	$mean(x) - min(x)$
Ran_3	upper range	$max(x) - mean(x)$
Dir_1	range / mean	$Ran_1 / mean(x)$
Dir_2	lower range / range	Ran_2 / Ran_1
Sta_1	standard deviation	$\sqrt{\frac{\sum(x - mean(x))^2}{n}}$
Sta_2	skewness	$\frac{\sum(x - mean(x))^3}{(n - 1)Sta_1^3}$
Sta_3	kurtosis	$\frac{\sum(x - mean(x))^4}{(n - 1)Sta_1^4}$
Rms_1	root mean square	$\sqrt{mean(x^2)}$
Rms_2	maximum / rms	$max(x) / Rms_1$
Rms_3	minimum / rms	$min(x) / Rms_1$
Rmr_1	root mean and range	$\sqrt{mean(x) * Ran_1}$
Rmr_2	maximum / rmr	$max(x) / Rmr_1$
Rmr_3	minimum / rmr	$min(x) / Rmr_1$

5.4 ANO Indices

In this study, ANO indices are computed to distinguish between ANO state and VE state. The indices, categorized in different groups, are motivated by the different morphology exhibited in the different states for the classification. A total of 10321 cycles of ANO data and 9976 cycles of VE data are pooled together for the detection.

Ran indices are tested in this study as ANO state was previously observed to exhibit smaller amplitude comparatively as demonstrated by Ran_1 (Karantonis et al., 2008; Karantonis, Mason, et al., 2007; Karantonis, Lovell, et al., 2007, 2006; Karantonis, Clougherty, et al., 2006) and Ran_3 (Endo et al., 2001). Ran_2 is added to the group to test its potential in the pump state recognition. The calculated range is expected to reflect the dissimilarity between the two different pump states. Dir indices are included as these indices are previously proposed in literature to reflect the differences in amplitude change among the pump states. By describing the statistical properties from the morphology of speed waveforms, Sta indices have the potential of performing effective separation be-

tween ANO and VE states. Sta_2 and Sta_3 indices were previously proposed in (Granegger et al., 2013, 2011) for ANO study whereas Sta_1 index is newly introduced in this study. Indices from Rms type includes crestfactor (Rms_2) that was proposed by (Granegger et al., 2013, 2011) and its similar permutations (Rms_3). By modifying the indices of the Rms type, Rmr indices are derived by replacing the square root of multiplication from the mean and the range. By taking into consideration the mean and range component in the data point of the speed cycle, ANO state may be distinguished from the VE state. Table 5.1 shows a complete list of the ANO indices and their respective equations.

5.5 Results

5.5.1 Individual Index

Table 5.2 shows the statistical performance of the individually tested ANO indices in terms of sensitivity, specificity and accuracy when different classifiers are applied.

Table 5.2: Statistical performance of individual ANO indices during implementation in greyhound data. Sensitivity, specificity and accuracy are denoted as P1, P2 and P3 respectively.

	LDA			LR			BPNN			KNN		
	P1	P2	P3	P1	P2	P3	P1	P2	P3	P1	P2	P3
Ran_1	68.0	50.3	59.3	67.6	51.1	59.5	47.9	97.2	72.1	60.1	86.5	73.0
Ran_2	66.4	54.7	60.6	66.2	55.4	60.9	47.3	96.4	71.5	56.0	86.5	71.0
Ran_3	68.6	47.2	58.1	68.3	48.3	58.5	49.3	95.1	71.8	61.4	85.0	73.0
Dir_1	73.4	62.6	68.1	72.7	64.1	68.5	56.5	95.5	75.7	60.5	90.1	75.1
Dir_2	62.5	54.8	58.7	62.6	54.6	58.7	51.1	65.6	58.2	57.3	56.1	56.7
Sta_1	68.7	50.5	59.7	68.0	51.5	59.9	50.8	97.1	73.5	62.6	86.2	74.2
Sta_2	63.4	50.8	57.2	63.3	50.8	57.2	51.1	64.8	57.9	58.2	57.0	57.6
Sta_3	58.2	68.9	63.5	60.4	66.8	63.6	66.5	60.5	63.5	66.0	58.6	62.4
Rms_1	55.9	93.1	74.2	56.8	91.1	73.3	61.2	82.4	71.5	63.4	85.8	74.4
Rms_2	0.0	100.0	49.1	70.6	67.0	68.8	58.1	90.6	74.1	58.7	89.6	73.9
Rms_3	0.0	100.0	49.1	73.1	61.4	67.4	57.5	93.6	75.3	61.3	88.6	74.7
Rmr_1	63.3	44.1	53.9	63.3	44.4	54.0	44.9	95.6	69.8	67.7	82.4	74.9
Rmr_2	58.8	91.7	75.0	65.7	76.5	71.0	54.8	97.5	75.8	60.4	90.5	75.2
Rmr_3	59.3	90.7	74.7	65.8	76.2	70.9	54.8	97.5	75.8	60.3	90.1	75.0

For greyhound data, accuracy of Ran indices generally falls between 58% and 73%, with sensitivity higher than specificity. As indicated by Table 5.2, the individual indices

show only slight difference in terms of overall index values in the different states. For *Dir* indices, Dir_1 index reaches the higher accuracy compared to Dir_2 index. The higher sensitivity values indicate that these two are more inclined to detect the ANO state based on the range permutation from the pump speed amplitude. Overall the accuracy ranges from 57% to 75%. *Sta* indices oversee the different pump states with accuracy that ranges from 60% to 74%. Despite the good result reported in previous work (Granegger et al., 2011, 2013), there is very little improvement in differentiating the two different pump states in the greyhound data of varying levels of preloads and afterloads. Meanwhile, the *Rms* indices are observed to be the ones with the better classification result with accuracy ranging from 72% to 75% for non-parametric classifiers. Classification result from parametric classifier, however, does not perform that well as it falls in the range of 50% to 69%. Similarly, *Rmr* indices give classification accuracy that lies between 54% and 75% and is one of the better index group overall. By taken into consideration on the performance of indices that exceed 70% accuracy, both BPNN and KNN deliver ten such indices whereas parametric classifiers such as LDA and LR only produce three each.

5.5.2 Combination of Indices

In order to further improve the result of the classification task, different pairings of the individual indices are combined for the testing. Table 5.3 shows the accuracy of index pairings from all index groups.

It can be seen from the Table 5.3 that when the individual indices are paired for comparisons, *Rms* indices and *Rmr* indices stand out as the most frequent component in combinations that achieve accuracy of more than 90%. Particularly, when paired with Rms_1 index, ten of such combinations are able to achieve high accuracy. This is followed by Rmr_1 and Sta_1 that show high potential in distinguishing ANO states from VE states.

Table 5.3: The highest classification accuracy among the compared classifiers for each combination is displayed (Ooi et al., 2014). The last row indicates the number of combination set that exceed 90% accuracy.

Index	<i>Ran</i> ₁	<i>Ran</i> ₂	<i>Ran</i> ₃	<i>Dir</i> ₁	<i>Dir</i> ₂	<i>Sta</i> ₁	<i>Sta</i> ₂	<i>Sta</i> ₃	<i>Rms</i> ₁	<i>Rms</i> ₂	<i>Rms</i> ₃	<i>Rmr</i> ₁	<i>Rmr</i> ₂	<i>Rmr</i> ₃
<i>Ran</i> ₁	-	76.4	76.2	91.2	76.6	76.9	77.4	76.8	92.0	87.4	87.9	91.2	91.0	91.0
<i>Ran</i> ₂	76.4	-	76.5	86.9	76.7	77.2	77.3	75.3	90.8	90.0	83.1	87.9	86.6	86.7
<i>Ran</i> ₃	76.2	76.5	-	89.1	76.8	77.4	77.6	77.3	92.0	85.5	91.1	87.6	89.3	89.4
<i>Dir</i> ₁	91.2	86.9	89.1	-	77.5	91.8	78.2	78.2	92.1	77.5	77.7	91.5	76.2	76.2
<i>Dir</i> ₂	76.6	76.7	76.8	77.5	-	77.6	63.2	66.0	78.5	77.7	77.7	78.0	77.3	77.3
<i>Sta</i> ₁	76.9	77.2	77.4	91.8	77.6	-	78.3	77.1	92.8	87.9	89.2	91.6	91.6	91.6
<i>Sta</i> ₂	77.4	77.3	77.6	78.2	63.2	78.3	-	67.0	78.7	78.0	78.4	79.0	78.2	78.1
<i>Sta</i> ₃	76.8	75.3	77.3	78.2	66.0	77.1	67.0	-	80.0	76.2	78.5	80.0	78.2	78.4
<i>Rms</i> ₁	92.0	90.8	92.0	92.1	78.5	92.8	78.7	80.0	-	90.7	91.8	92.1	92.1	92.1
<i>Rms</i> ₂	87.4	90.0	85.5	77.5	77.7	87.9	78.0	76.2	90.7	-	77.8	90.2	77.7	77.8
<i>Rms</i> ₃	87.9	83.1	91.1	77.7	77.7	89.2	78.4	78.5	91.8	77.8	-	90.2	77.7	77.8
<i>Rmr</i> ₁	91.2	87.9	87.6	91.5	78.0	91.6	79.0	80.0	92.1	90.2	90.2	-	91.4	91.4
<i>Rmr</i> ₂	91.0	86.6	89.3	76.2	77.3	91.6	78.2	78.2	92.1	77.7	77.7	91.4	-	75.8
<i>Rmr</i> ₃	91.0	86.7	89.4	76.2	77.3	91.6	78.1	78.4	92.1	77.8	77.8	91.4	75.8	-
> 90%	5	1	2	4	0	5	0	0	10	2	3	8	4	4

Table 5.4: Combinations of indices performs well in terms of overall accuracy from the different classifiers (Ooi et al., 2014). Number of indices is stated in the second row. X denotes the presence of the specified index in the combination sets with respect to each classifier. The last row shows the accuracy obtained from the corresponding index combination sets as indicated in each column.

Classifier	LDA					LR					BPNN					KNN				
Indices	1	2	3	4	5	1	2	3	4	5	1	2	3	4	5	1	2	3	4	5
<i>Ran</i> ₁		X	X	X	X				X	X									X	X
<i>Ran</i> ₂																		X		
<i>Ran</i> ₃																				
<i>Dir</i> ₁		X	X	X	X															
<i>Dir</i> ₂																				
<i>Sta</i> ₁				X	X		X	X	X			X	X	X	X		X	X		
<i>Sta</i> ₂																				X
<i>Sta</i> ₃			X		X					X					X				X	X
<i>Rms</i> ₁						X	X	X	X	X		X	X	X	X		X	X	X	X
<i>Rms</i> ₂														X	X					X
<i>Rms</i> ₃								X	X	X			X	X	X				X	X
<i>Rmr</i> ₁				X	X					X										
<i>Rmr</i> ₂	X															X				
<i>Rmr</i> ₃											X									
Accuracy	75.0	88.2	89.7	90.0	90.1	73.7	89.8	89.9	90.0	90.2	75.8	90.8	90.8	90.7	90.8	75.2	92.8	93.8	94.3	94.6

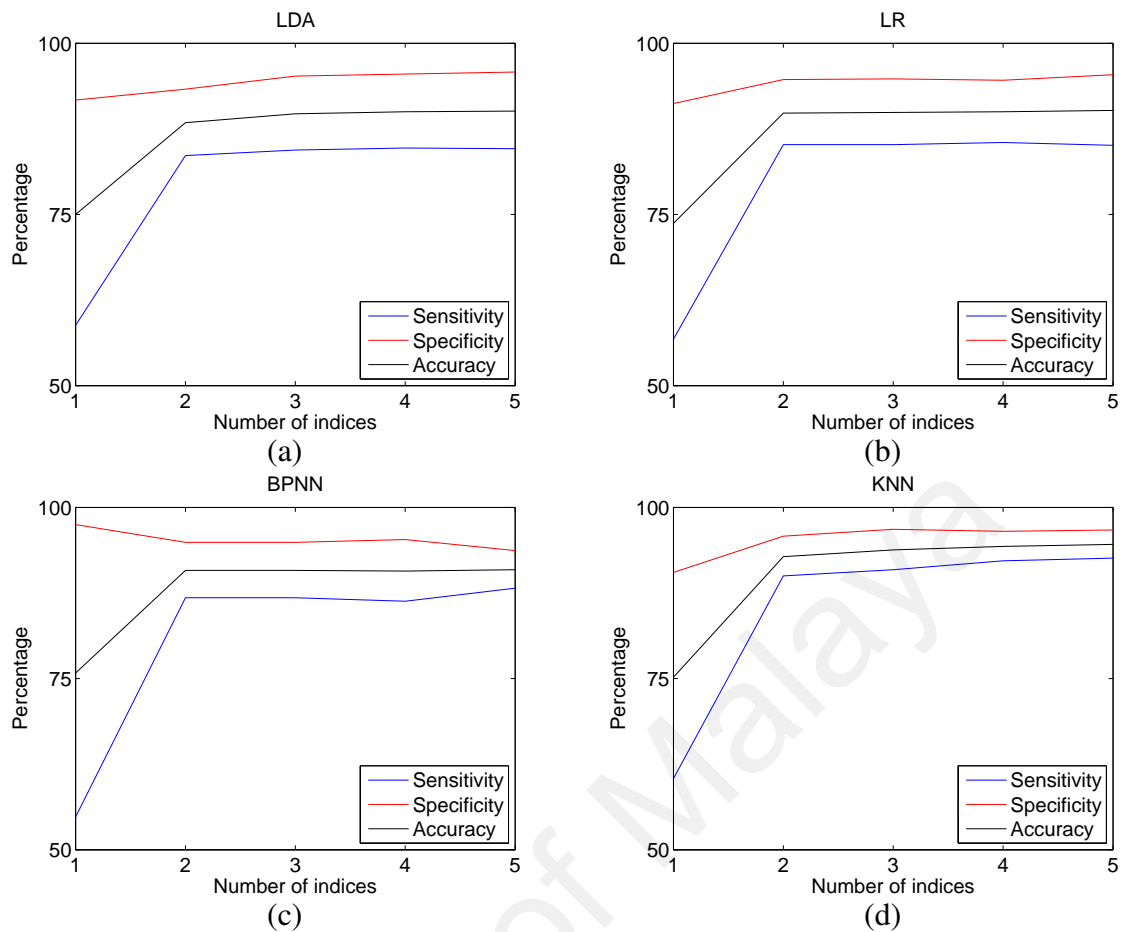


Figure 5.4: Percentage of statistical performance during implementation of combination of multiple ANO indices for (a) LDA, (b) LR, (c) BPNN and (d) KNN

Table 5.4 displays the accuracy and its respective component indices in combination when tested with different classifiers. Though there are slight variations among the different classification methods, it can be seen that indices from the *Rms* group and *Sta*₁ play a role in improving its classification performance for most classifiers.

Figure 5.4 shows the comparison of accuracy of different classifiers when combinations of multiple indices are tested. For both parametric classifiers and non-parametric classifiers, combinations of different indices are observed to give improvement in classification performance. While the exact improvement varies, significant increase in accuracy is observed when two indices are combined for all classifiers as displayed in Figure 5.4. On the other hand, subsequent increments of indices only give minimal improvement. Performance of different classifiers varies when experimented on the greyhound

data, due to their own characteristic way of implementation. Overall it is observed that non-parametric classifiers such as BPNN and KNN yield higher accuracy for the state classification task. As indicated in Figure 5.5, the plotted boundary lines for these classification methods are curvature and more flexible to give a better and optimized fit to the distribution to the computed index combination. On the contrary, parametric classifiers such as LDA and LR have the tendency to produce more rigid straight lines in the boundary between the different pump states. While the general trend is consistent for all classification methods, accuracy of KNN has particularly stand out among them by producing the highest rate of correct classification as the number of indices in the pairings increased.

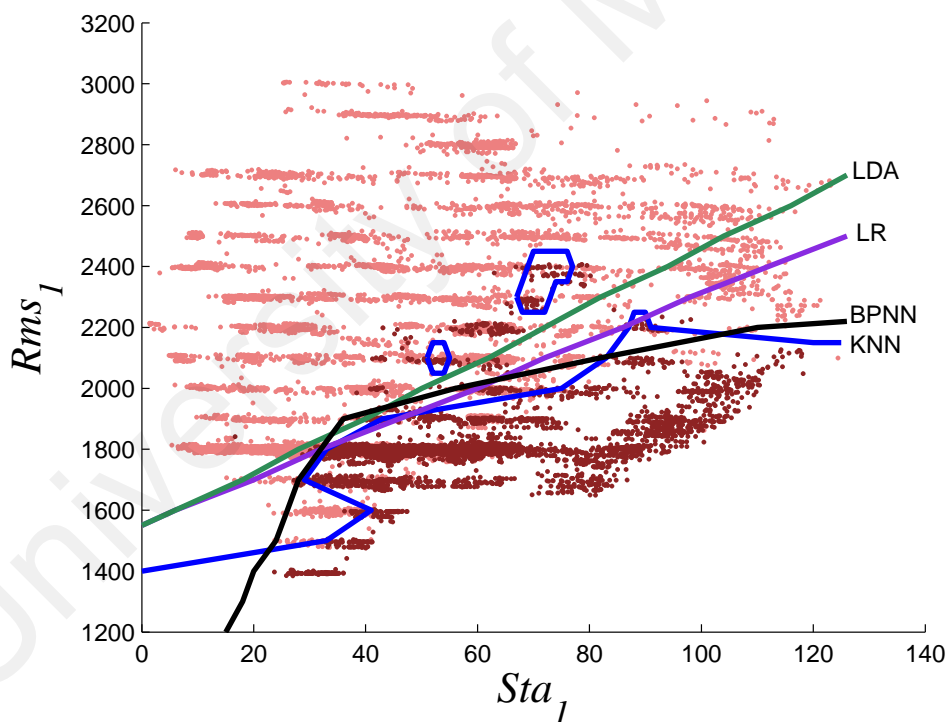


Figure 5.5: Decision boundaries of evaluated classification algorithms for ANO detection (Ooi et al., 2014). Distribution of data with VE state is represented by darker dots whereas distribution of data with ANO state is denoted by dots with lighter color.

5.5.3 Computation Time

From a total of 20297 cycles of data, it is split into 18268 cycles as training data and 2029 cycles as testing data according to train-test ratio of 9:1 in cross validation. Training time is the required duration for parameters in the different classifiers to adapt according to the presented training set. Testing time is the time when classifiers make discrimination decisions on the test data based on the adapted parameters. The total implementation time includes the training time on the 18268 cycles of data as well as 2029 cycles of testing data.

Table 5.5: Comparison of computation time for all classifiers during the implementation of ANO indices.

Classifier	Training (18268 data)		Testing (2029 data)		Total (20297 data)	
	1 index	2 indices	1 index	2 indices	1 index	2 indices
LDA	3.4×10^{-3}	3.1×10^{-3}	2.1×10^{-2}	2.2×10^{-2}	2.1×10^{-2}	2.2×10^{-2}
LR	5.2×10^{-2}	5.9×10^{-2}	5.2×10^{-2}	1.1×10^{-1}	1.0×10^{-1}	7.1×10^{-1}
BPNN	3.0×10^1	3.1×10^1	1.3×10^{-1}	1.3×10^{-1}	3.0×10^1	3.1×10^1
KNN	NA	NA	8.9×10^2	1.0×10^3	8.9×10^3	1.0×10^3

For LDA, LR and BPNN, total implementation time consists of training time and testing time as indicated in Table 5.5. There is no explicit training in KNN so its implementation only consists of the testing stage where intermediate computations of the testing data points are made with regards to the training data points during the classification process. For single index classification, LDA takes 3.4×10^{-3} s of training time and testing time of 2.1×10^{-1} s, hence the total implementation time is 2.1×10^{-1} s. LR requires 5.2×10^{-2} s for both training and testing leading to total time taken of 1.0×10^{-1} s. BPNN classifier takes 3.02×10^1 s of training and 1.3×10^{-1} s of testing, resulting in a total of 3.0×10^1 s for complete implementation. Comparatively, testing of KNN takes more time, which is 8.9×10^2 s, leading to the longest implementation among all tested classifiers in the study. All the classifiers show the trend of increasing total implementation time when two indices are used instead of single index. For LDA classifier, the required training time

of 3.1×10^{-3} s and testing time of 2.1×10^{-1} s contribute to total implementation time of 2.2×10^{-1} s. Training time of 5.9×10^{-1} s and testing time of 1.1×10^{-1} s are observed in LR, resulting in complete implementation that takes 7.1×10^{-1} s. BPNN requires training time of 3.1×10^1 s and testing time of 1.4×10^{-1} s, leading to 3.1×10^1 s of total implementation time. KNN uses up the most testing time at 1.0×10^3 s and requires the largest implementation time overall. Overall, it can be observed that implementation time for non-parametric classifiers (BPNN and KNN) is greater than parametric classifiers (LDA and LR).

5.6 Discussion

IRBP functions by directing blood out of ventricle into an alternative route to the aorta to supply oxygen to all the living cells in the body through circulation. Despite the advances of IRBP, the device still lacks the intrinsic ability to automatically adapt to variation of preload levels and changes in venous. Therefore, there is an ongoing effort in control strategy of IRBP to perform reliable and accurate detection of pumping states that may be detrimental to patient well-being.

In this study, a total of 14 indices originated from five different groups are tested and compared using greyhound data that comprises of various operating conditions, namely different levels of preloads and afterloads (low, medium, high) respectively (Ooi et al., 2014). Variation in afterload is achieved by altering the SVR whereas variation in preload is attained by changing the total blood volume.

Among the tested indices, *Rms* group shows great potential numerous time in different classifiers when testing is performed to find the best performing pairings. This is possibly due to its ability to reflect the amplitude of the pump speed signal as it transitions from one pump state to another.

In the field of pumping state detection of IRBP, only a number of research works

have concentrated on ANO state despite its consequence and potential risk to patients health. The study by (Ayre et al., 2001) is among the few earliest works on ANO state applied on three acute ovine models by proposing the use of STI. The proposed indicator is defined as the ratio of difference between maximum and rms value to difference of mean speed between two successive cycles. Meanwhile, detection of transition point between PA and FA previously proposed by (Endo et al., 2001) is the ratio of the current amplitude to the mean current, which is the equivalent of Dir_1 index in this study. While it performs reasonably well in this study, the performance is not outstanding with accuracy of 75.7%. Due to its dependency on cardiac contractibility and afterload of its absolute value (Endo et al., 2001), inter-subject and cardiac conditions robustness may be compromised. Despite their potential for further study, these works are limited due to the lack of automated system for the classification and thus prevented statistical based comparison (Yuhki et al., 1999; Endo et al., 2001).

Combinations of several indices were proposed by (Karantonis, Cloherty, et al., 2006; Karantonis, Lovell, et al., 2006, 2007; Karantonis, Mason, et al., 2007; Karantonis et al., 2008) and (Granegger et al., 2011, 2013) to accommodate the large variations found in the waveform patterns of the tested pump signal. While implementation of CART on six ex vivo porcine experiments reported 100% accuracy, the experimental measurements were obtained from healthy pigs with limited variability. On the other hand, the greyhound data in the present study comprises of subjects with induced heart failure of different levels of preloads and afterloads. This explains the result discrepancies when testing the Ran_1 and Dir_2 indices, which yielded lower accuracy of 73.2% and 58.7% respectively. It can be deduced that the proposed indices for ANO from (Karantonis, Cloherty, et al., 2006; Karantonis, Lovell, et al., 2006, 2007; Karantonis, Mason, et al., 2007; Karantonis et al., 2008) and (Granegger et al., 2011, 2013) were influenced by the different physiological conditions. In order to ensure the robustness of indices in per-

forming efficient and accurate detection of pump states, different levels of perturbations should not be overlooked.

The work of (Granegger et al., 2011, 2013) has proposed the use of skewness (Sta_2), kurtosis (Sta_3) and crest factor (Rms_2) on both numerical model and animal experiments with reported accuracy of 95%. When the proposed indices are implemented in the current study's pump speed signal, accuracy of 84.3% is obtained. The different accuracy of the same indices in different data sets could be due to the type of waveforms as pump flow signal was used in (Granegger et al., 2011, 2013). Different types of pump models could be the possible contributors as the present study uses centrifugal pump whereas axial pump was used in (Granegger et al., 2011, 2013). The proposed Rms_2 index may be more suitable for use in pump flow signal as it is more sensitive to changes in waveforms that are in higher proximity to the x-axis, as opposed to waveforms of higher magnitudes such as pump speed signal.

Among tested classification algorithms in this study, parametric classifiers such as LDA and LR are noted to obtain lower accuracy than non-parametric classifiers such as BPNN and KNN. This may be contributed by the assumption of parametric classifiers that the data is normally distributed, which may not be true for all practical applications.

Longer implementation time is observed to achieve higher classification accuracy, as illustrated by the fact that non-parametric classifiers generally require more computation time to complete the pump state detection task.

It can be observed that KNN gives the highest accuracy in this application, especially when the number of indices involved is increased. Similarly, previous work from (Granegger et al., 2011, 2013) has also reported that KNN came out as the best performing classifier when their ANOVA study is conducted in different data involving ovine animals.

With the suitable indices that characterize the different pump states effectively, the testing points from the indices will be distributed in such a way that makes it distinguish-

able from one pump state to another. Due to KNN classifier tendency to associate classes from the proximity of the neighboring training points, reliable prediction was performed on the tested data that achieved good classification results. Thus it can be deduced that KNN is a suitable classification algorithm for implementation of pump state classification.

Comparatively, the total time taken for execution of KNN classifier is slightly longer than the others, with 892 seconds for entire population of 20297 data. While the overall computation time of KNN may be slightly longer than the other classifiers, it still works sufficiently well to differentiate the distinction between normal VE state and ANO state. Although ideally shorter time is preferred for any application in real time, common medical experience with human subjects assisted by IRBP indicates that an estimate of valve opening at every five to ten heart beats is sufficient (Dr. Robert Salamonsen) (Ooi et al., 2014).

Previous clinical study involving four patients implanted with VAD has revealed that formation of partial aortic valve fusion takes about 26 days to 689 days (Rose et al., 2000). In another unaffiliated study (Connelly, Abrams, Klima, Vaughn, & Frazier, 2003) conducted on 17 patients, presence of commissural fusion of aortic valves of various severities is found in implantation duration that ranges from four days to 787 days. This implies that formation of aortic fusion itself takes time and close monitoring on the different pump states will be able to prevent such undesirable occurrence. From experience, clinical experts surmised that ability to estimate valve opening at every five to ten heart beats is adequately effective for prevention of life threatening consequences in patients.

5.7 Summary

Investigation on ANO detection has been employed with the aid of various classification algorithms performance by testing different indices. Combination of two indices (Rms_1 and Sta_1) is capable of reaching accuracy of 93% during the classification between

ANO state and VE state. Further addition of indices to five will even lead to accuracy of 95%. This is due to the ability of the index combination to characterize the morphology of the pump speed signal for ANO state. It can be seen that non-parametric classifier, in particular KNN, is able to perform the detection with high classification rate compared to the rest of the tested classifiers, despite the slightly longer computation time.

University of Malaya

CHAPTER 6

CONCLUSION

6.1 Overview

Despite the significance of LVAD as treatment for patients facing heart problems, automatic detection of different states remains one of the aims that researchers all over the world have been keen in achieving. The problem of over-pumping states has long been a dilemma that hinders the implementation of fully automation of the device without intervention from physicians. In this study, detection of two over-pumping states, namely ventricular suction and ANO that encompassed varying levels of operating conditions are investigated as an effort to seek potential approaches that can further improve the status quo of LVAD control system.

For suction identification, the pump state is characterized by the emergence of saddles and erraticism in morphology of pump speed signals. Presence of such features is successfully detected by the mean of Dur_3 . Other indices that fall under Dur types show prospective capabilities on classifying suction occurrence as well. It can be observed that employment of the index individually produces accuracy of 94%. Further improvement in accuracy of up to 99.5% can be achieved when combination of five indices are applied.

The task of ANO detection is implemented in similar fashion as ventricular suction. Classification is successfully performed between ANO and VE upon evaluation of different indices. However, unlike ventricular suction, at least two indices (Rms_1 and Sta_1) are required for the detection in order to achieve accuracy that is acceptable (93%). Being the intermediate transition stage between VE and ventricular suction, ANO state is easy to be mistakenly taken as either of them, especially for early stage ANO and end stage

ANO occurrence. Increase of accuracy to up to 95% can be observed when five indices are combined for the classification.

Evaluation of various classification algorithms in this study has found KNN to be the best performing classifier for both ventricular suction and ANO. This approach is simple to implement and it was relatively easy to visualize the way the different state are distinguished based on the distribution of the indices implemented.

Aside from IRBP, these indices may be implemented on temporary heart assist devices or artificial hearts. Additionally, the life support system that plays major role in supporting functions of heart and lung during surgeries may benefit from the findings from the present study. These indices could be helpful in controlling blood flow re-routing during coronary artery bypass procedure.

In conclusion, the study has successfully achieved the objectives specified are achieved for both investigated pump states as high accuracy of classification rate are obtained.

6.2 Recommendation for Future Work

While the study has addressed the key objectives, there remains several prospective directions where further research effort would be valuable and of immense interest.

For future endeavor, the classification study under various operating conditions can be expanded to include occurrence of under-pumping state as well. Aside from over-pumping states such as ventricular suction and ANO state investigated in the study, under-pumping state indicates that the power of the VAD is insufficient to operate normally. Detection of this pump state in consideration of varying operating conditions will allow novel approach being proposed to alleviate all the undesired pump states, thus leading to another breakthrough in the control system.

Inclusion of wider studies on patient trials in these aspects for more clinical data would be fruitful to identify the true potential of the proposed methods as well as to ver-

ify their viability in applications concerning heart disease patients. Real time detection system of the different pump states may even be designed as an extension upon incorporating the inputs and findings of these studies in adjusting the appropriate setting for IRBP.

All in all, there is still room for improvement for the progress made in pump state detection mechanism of the IRBP. Extended studies can be conducted to overcome the current constraints that limit the true potential of the device for the sake of mankind.

University of Malaysia

Appendices

University of Malaya

APPENDIX A

COMPLETE LIST OF RESULT FOR SUCTION DETECTION WITH MULTI CLASS CLASSIFICATION

Table A.1: List of statistical performance for multiclass classification. Sensitivity, specificity and accuracy are denoted as P1, P2 and P3 respectively. Statistical measures from the first column are used to extract indices computed in the multiple cycle that are found in second column

		VE			ANO			Suction		
		P1	P2	P3	P1	P2	P3	P1	P2	P3
max	<i>Bas</i> ₁	92.5	64.7	74.2	16.9	91.0	66.2	63.2	80.7	75.0
	<i>Bas</i> ₂	96.1	65.3	75.8	20.5	92.5	68.5	64.9	83.1	77.2
	<i>Bas</i> ₃	93.0	66.3	75.4	20.2	90.2	66.9	62.9	81.7	75.6
	<i>Ran</i> ₁	54.2	70.6	65.0	16.5	75.6	55.7	68.6	73.2	71.7
	<i>Ran</i> ₂	65.0	69.1	67.7	14.9	80.1	58.2	61.2	71.3	67.8
	<i>Ran</i> ₃	50.2	73.1	65.4	18.3	73.2	54.8	73.7	74.6	74.2
	<i>Dir</i> ₁	44.0	68.1	59.9	29.0	85.7	66.6	49.3	57.5	54.5
	<i>Dir</i> ₂	59.4	82.6	74.7	33.4	69.2	57.2	76.1	82.4	80.3
	<i>Dir</i> ₃	49.6	77.1	67.7	21.5	80.7	60.9	79.4	67.2	71.1
	<i>Sta</i> ₁	53.5	71.7	65.4	16.4	75.3	55.5	70.4	72.9	72.0
	<i>Sta</i> ₂	38.4	70.9	59.8	63.8	72.4	69.5	71.0	92.7	85.6
	<i>Sta</i> ₃	7.9	89.8	61.8	77.2	62.1	67.1	63.3	72.0	69.2
	<i>Rms</i> ₁	93.0	66.2	75.3	20.0	90.1	66.7	62.7	81.6	75.5
	<i>Rms</i> ₂	100.0	0.0	34.1	0.0	100.0	66.6	0.0	100.0	67.5
	<i>Rms</i> ₃	100.0	0.0	34.0	0.0	100.0	66.6	0.0	100.0	67.5
	<i>Rmr</i> ₁	55.2	61.2	59.1	8.2	82.4	57.4	58.2	67.2	64.3
	<i>Rmr</i> ₂	76.0	59.3	64.7	18.8	71.6	53.8	54.0	93.2	80.4
	<i>Rmr</i> ₃	75.0	59.9	64.9	19.6	71.0	53.6	54.2	93.2	80.6
	<i>Dur</i> ₁	58.7	75.6	69.7	46.0	74.4	64.8	64.5	84.4	78.0
	<i>Dur</i> ₂	61.7	58.9	58.7	14.0	87.7	62.2	61.5	71.3	68.2
	<i>Dur</i> ₃	65.7	65.7	65.3	35.3	84.1	67.3	75.5	87.8	83.7
	<i>Dur</i> ₄	55.6	72.2	66.4	36.6	78.0	64.1	73.8	82.4	79.6
	<i>Gra</i> ₁	54.7	66.9	62.7	65.2	49.0	54.0	3.7	96.0	65.6
	<i>Gra</i> ₂	59.5	62.4	61.3	66.9	51.8	56.7	0.2	99.4	67.1
	<i>Gra</i> ₃	53.1	79.6	70.6	25.3	71.8	56.3	85.5	80.0	81.8
	<i>Gra</i> ₄	79.6	49.0	59.2	27.9	90.8	69.4	64.1	95.4	85.3
	<i>Gra</i> ₅	59.8	68.5	65.5	15.3	79.6	58.0	58.2	68.6	65.2
	<i>Gra</i> ₆	53.6	59.8	57.5	60.6	47.5	51.7	0.0	100.0	67.5
<i>Gra</i> ₇	72.6	76.5	75.1	53.6	84.2	73.9	80.9	92.5	88.7	
min	<i>Bas</i> ₁	93.2	64.2	74.1	16.5	91.4	66.4	61.3	80.1	74.0
	<i>Bas</i> ₂	96.4	65.8	76.3	20.6	92.5	68.5	64.5	82.6	76.8
	<i>Bas</i> ₃	93.7	65.6	75.2	20.1	90.8	67.2	62.1	81.8	75.3
	<i>Ran</i> ₁	53.3	75.1	67.6	19.5	89.7	66.1	83.0	62.7	69.3
	<i>Ran</i> ₂	54.0	65.3	61.4	3.9	99.3	67.4	86.7	57.4	67.0
	<i>Ran</i> ₃	53.0	78.5	69.6	22.6	84.9	64.0	90.8	69.4	76.3

<i>Dir</i> ₁	43.4	76.0	64.8	63.2	74.3	70.5	82.3	93.3	89.7	
<i>Dir</i> ₂	59.6	82.5	74.7	33.5	69.3	57.2	76.1	82.4	80.3	
<i>Dir</i> ₃	13.3	57.5	42.5	62.1	75.6	71.1	43.7	75.9	65.4	
<i>Sta</i> ₁	54.0	72.9	66.4	16.2	96.3	69.4	90.6	60.8	70.5	
<i>Sta</i> ₂	44.9	73.9	64.0	61.1	50.5	52.9	14.5	86.0	61.5	
<i>Sta</i> ₃	30.6	78.7	62.3	60.0	69.7	66.5	55.9	74.8	68.7	
<i>Rms</i> ₁	93.6	65.6	75.1	20.0	90.8	67.1	62.5	81.8	75.5	
<i>Rms</i> ₂	100.0	0.0	34.1	0.0	100.0	66.6	0.0	100.0	67.5	
<i>Rms</i> ₃	100.0	0.0	34.1	0.0	100.0	66.6	0.0	100.0	67.5	
<i>Rmr</i> ₁	56.8	58.6	57.9	14.1	93.7	67.1	70.8	68.2	69.0	
<i>Rmr</i> ₂	93.8	64.9	74.7	33.3	83.6	66.7	49.9	90.3	77.1	
<i>Rmr</i> ₃	92.7	65.3	74.6	33.8	83.1	66.6	50.3	90.1	77.2	
<i>Dur</i> ₁	2.6	95.9	64.1	71.9	71.0	71.3	91.6	65.5	74.0	
<i>Dur</i> ₂	0.2	94.0	61.9	72.6	70.9	71.4	84.5	63.3	70.2	
<i>Dur</i> ₃	21.3	88.3	65.3	67.0	73.8	71.5	92.3	77.4	82.3	
<i>Dur</i> ₄	17.0	91.3	66.0	67.8	73.2	71.4	93.2	73.9	80.2	
<i>Gra</i> ₁	48.3	72.4	64.2	15.5	82.4	59.9	70.6	62.2	64.8	
<i>Gra</i> ₂	10.5	80.4	56.2	35.8	75.6	62.0	95.3	63.6	73.9	
<i>Gra</i> ₃	58.8	73.1	68.2	18.7	76.1	56.9	69.9	74.4	72.8	
<i>Gra</i> ₄	50.3	73.9	65.8	76.4	40.7	52.5	0.7	99.4	67.2	
<i>Gra</i> ₅	49.9	77.9	68.3	25.4	80.9	62.4	93.6	75.0	81.0	
<i>Gra</i> ₆	13.4	75.0	54.1	49.9	73.0	65.4	71.3	68.8	69.7	
<i>Gra</i> ₇	74.2	63.4	66.9	78.8	64.9	69.5	0.5	99.0	66.9	
mean	<i>Bas</i> ₁	92.7	64.7	74.3	16.7	90.9	66.1	62.5	80.4	74.5
	<i>Bas</i> ₂	96.5	65.9	76.4	20.8	92.3	68.4	64.8	82.9	77.0
	<i>Bas</i> ₃	93.5	66.2	75.5	20.1	90.0	66.6	62.2	81.9	75.5
	<i>Ran</i> ₁	49.2	72.9	64.7	19.6	73.4	55.3	75.0	75.2	75.1
	<i>Ran</i> ₂	55.2	70.8	65.4	18.3	77.4	57.5	71.1	73.6	72.7
	<i>Ran</i> ₃	46.7	79.6	68.3	23.2	67.9	52.9	78.7	76.5	77.2
	<i>Dir</i> ₁	58.8	76.2	70.2	50.7	77.5	68.4	86.9	93.8	91.6
	<i>Dir</i> ₂	59.7	82.7	74.8	33.4	69.3	57.3	76.2	82.4	80.3
	<i>Dir</i> ₃	54.3	72.7	66.3	31.4	83.4	66.0	94.1	83.1	86.7
	<i>Sta</i> ₁	48.8	75.3	66.2	21.0	72.4	55.2	76.2	75.0	75.5
	<i>Sta</i> ₂	88.5	53.6	65.1	4.6	93.2	63.5	87.6	92.9	91.2
	<i>Sta</i> ₃	12.3	83.4	59.1	76.9	58.5	64.6	50.8	77.7	69.0
	<i>Rms</i> ₁	93.3	66.1	75.4	20.1	89.9	66.6	62.2	82.0	75.5
	<i>Rms</i> ₂	100.0	0.0	34.1	0.0	100.0	66.6	0.0	100.0	67.5
	<i>Rms</i> ₃	100.0	0.0	34.1	0.0	100.0	66.6	0.0	100.0	67.5
	<i>Rmr</i> ₁	52.5	65.6	61.0	12.6	75.7	54.5	64.6	73.2	70.4
	<i>Rmr</i> ₂	88.3	67.3	74.4	38.4	78.9	65.3	54.7	94.4	81.5
	<i>Rmr</i> ₃	87.1	68.0	74.4	38.8	78.2	64.8	55.1	94.3	81.5
	<i>Dur</i> ₁	36.8	78.2	64.2	54.1	74.1	67.3	90.9	87.8	88.9
	<i>Dur</i> ₂	37.5	77.6	63.7	52.4	73.8	66.5	91.7	88.5	89.5
	<i>Dur</i> ₃	43.8	79.1	66.9	55.5	75.1	68.5	93.7	91.5	92.2
	<i>Dur</i> ₄	43.1	75.9	64.6	48.1	76.2	66.7	94.4	89.8	91.2
	<i>Gra</i> ₁	80.6	13.7	36.0	11.9	86.5	61.1	1.2	96.8	65.7
	<i>Gra</i> ₂	51.5	71.3	64.4	15.7	78.0	57.1	68.9	68.3	68.5
	<i>Gra</i> ₃	56.6	77.0	70.1	22.1	71.6	55.0	74.9	78.0	77.0
	<i>Gra</i> ₄	52.7	79.5	70.3	28.1	79.5	62.3	88.2	75.0	79.3
	<i>Gra</i> ₅	53.8	74.2	67.3	20.9	73.1	55.7	70.9	75.2	73.7

	<i>Gra</i> ₆	49.2	65.4	59.8	10.0	89.5	62.8	69.8	59.4	62.8
	<i>Gra</i> ₇	72.5	69.8	70.7	64.6	56.3	58.9	2.4	94.2	64.2
std	<i>Bas</i> ₁	72.1	45.7	53.9	29.5	85.8	66.0	43.5	90.4	75.2
	<i>Bas</i> ₂	11.3	83.9	59.1	78.0	49.1	58.7	27.9	75.5	59.8
	<i>Bas</i> ₃	20.9	88.0	65.1	81.7	53.6	62.9	40.1	79.7	66.8
	<i>Ran</i> ₁	47.4	73.7	64.7	81.2	42.9	55.6	2.4	99.2	67.6
	<i>Ran</i> ₂	46.3	79.6	68.2	84.9	42.7	56.8	9.5	98.3	69.3
	<i>Ran</i> ₃	50.0	67.8	61.7	76.7	45.7	56.0	0.0	100.0	67.5
	<i>Dir</i> ₁	9.4	82.4	57.5	75.3	67.4	70.1	63.1	73.7	70.3
	<i>Dir</i> ₂	50.3	69.9	63.2	69.0	39.9	49.6	0.0	100.0	67.5
	<i>Dir</i> ₃	47.9	77.1	67.1	87.7	43.8	58.5	2.7	98.6	67.3
	<i>Sta</i> ₁	47.1	75.0	65.4	81.7	41.3	54.7	1.8	99.5	67.6
	<i>Sta</i> ₂	6.4	82.6	56.5	76.5	62.5	67.1	50.2	71.3	64.4
	<i>Sta</i> ₃	6.6	87.1	59.6	77.7	60.6	66.3	55.0	71.6	66.2
	<i>Rms</i> ₁	21.5	87.8	65.2	81.8	53.7	63.1	39.9	80.0	66.9
	<i>Rms</i> ₂	46.7	82.3	70.1	83.3	40.9	55.0	9.1	96.5	68.0
	<i>Rms</i> ₃	48.8	77.1	67.4	78.8	41.6	54.0	4.4	97.6	67.2
	<i>Rmr</i> ₁	1.2	78.2	51.9	70.1	57.5	61.7	40.6	70.0	60.4
	<i>Rmr</i> ₂	72.1	47.9	55.8	8.3	77.4	53.9	53.9	91.5	79.3
	<i>Rmr</i> ₃	72.8	46.9	55.3	6.8	78.2	54.0	54.4	91.4	79.4
	<i>Dur</i> ₁	38.4	56.9	50.6	72.6	55.1	60.9	1.8	94.4	64.1
	<i>Dur</i> ₂	55.2	56.4	55.8	9.2	93.9	65.4	50.8	57.2	55.0
	<i>Dur</i> ₃	1.7	81.0	53.9	72.1	58.3	62.8	36.4	65.6	56.1
	<i>Dur</i> ₄	7.2	72.1	49.8	70.2	56.2	60.9	20.1	70.3	53.9
	<i>Gra</i> ₁	58.2	69.4	65.5	14.5	79.5	57.7	64.5	69.6	67.9
	<i>Gra</i> ₂	11.8	84.6	59.7	84.0	55.5	65.0	42.2	78.5	66.6
	<i>Gra</i> ₃	50.2	78.2	68.4	65.4	61.3	62.5	31.5	84.3	67.1
	<i>Gra</i> ₄	19.6	85.2	62.8	80.6	54.3	63.1	38.4	79.8	66.3
	<i>Gra</i> ₅	22.9	85.4	64.0	83.4	57.9	66.4	44.3	81.6	69.3
	<i>Gra</i> ₆	13.2	86.4	61.4	83.4	52.2	62.5	35.3	77.3	63.6
	<i>Gra</i> ₇	47.8	80.9	69.6	81.7	66.1	71.3	46.7	91.0	76.6

APPENDIX B

COMPLETE LIST OF RESULT FOR SUCTION DETECTION WITH ALL EVALUATED CLASSIFIERS

Table B.1: Statistical performance of the evaluation of the individual suction indices using LDA. The results are shown as sensitivity / specificity (overall accuracy).

	max	min	mean	std
<i>Bas</i> ₁	52.6 / 86.3 (75.4)	49.7 / 86.0 (74.2)	51.1 / 86.2 (74.8)	31.3 / 95.5 (74.7)
<i>Bas</i> ₂	60.6 / 87.1 (78.5)	60.0 / 85.9 (77.4)	61.0 / 86.3 (78.0)	7.8 / 96.0 (67.3)
<i>Bas</i> ₃	54.6 / 86.1 (75.9)	52.0 / 86.3 (75.2)	54.0 / 86.3 (75.8)	25.3 / 92.3 (70.6)
<i>Ran</i> ₁	44.4 / 92.3 (76.7)	64.5 / 89.5 (81.4)	59.8 / 88.9 (79.4)	0.0 / 100.0 (67.5)
<i>Ran</i> ₂	22.2 / 98.8 (73.9)	48.8 / 91.0 (77.2)	51.6 / 89.8 (77.4)	0.0 / 100.0 (67.5)
<i>Ran</i> ₃	51.9 / 91.5 (78.7)	74.4 / 89.0 (84.2)	68.1 / 89.9 (82.8)	0.2 / 99.9 (67.5)
<i>Dir</i> ₁	0.0 / 100.0 (67.5)	80.0 / 96.5 (91.2)	82.6 / 96.4 (91.9)	39.7 / 81.5 (67.9)
<i>Dir</i> ₂	74.1 / 86.0 (82.1)	74.1 / 86.0 (82.1)	74.1 / 86.0 (82.1)	0.0 / 100.0 (67.5)
<i>Dir</i> ₃	54.3 / 94.4 (81.3)	29.7 / 89.0 (69.7)	63.5 / 95.5 (85.1)	0.0 / 100.0 (67.5)
<i>Sta</i> ₁	39.5 / 93.8 (76.1)	62.5 / 89.6 (80.8)	63.4 / 89.4 (80.9)	0.0 / 100.0 (67.5)
<i>Sta</i> ₂	67.7 / 97.8 (88.0)	0.0 / 100.0 (67.5)	83.2 / 96.1 (91.9)	21.6 / 83.5 (63.3)
<i>Sta</i> ₃	37.3 / 84.6 (69.2)	36.3 / 92.4 (74.1)	26.9 / 88.2 (68.2)	30.2 / 85.8 (67.7)
<i>Rms</i> ₁	54.6 / 86.2 (75.9)	52.0 / 86.3 (75.2)	53.9 / 86.3 (75.8)	25.7 / 92.3 (70.7)
<i>Rms</i> ₂	0.0 / 100.0 (67.5)	0.0 / 100.0 (67.5)	0.0 / 100.0 (67.5)	0.0 / 100.0 (67.5)
<i>Rms</i> ₃	0.0 / 100.0 (67.5)	0.0 / 100.0 (67.5)	0.0 / 100.0 (67.5)	0.0 / 100.0 (67.5)
<i>Rmr</i> ₁	29.7 / 97.7 (75.6)	56.9 / 90.4 (79.5)	50.2 / 92.4 (78.7)	14.3 / 92.2 (66.9)
<i>Rmr</i> ₂	42.6 / 96.9 (79.2)	42.7 / 95.5 (78.3)	44.7 / 96.5 (79.6)	37.7 / 96.1 (77.1)
<i>Rmr</i> ₃	43.0 / 96.8 (79.3)	43.1 / 95.4 (78.4)	45.4 / 96.3 (79.8)	37.7 / 96.0 (77.1)
<i>Dur</i> ₁	49.5 / 97.1 (81.7)	69.2 / 71.1 (70.5)	89.0 / 90.7 (90.2)	0.0 / 99.9 (67.4)
<i>Dur</i> ₂	39.7 / 97.7 (78.8)	56.9 / 67.4 (63.9)	89.9 / 90.9 (90.6)	0.0 / 100.0 (67.5)
<i>Dur</i> ₃	64.9 / 97.1 (86.6)	86.7 / 89.0 (88.2)	92.6 / 94.1 (93.6)	3.8 / 95.5 (65.7)
<i>Dur</i> ₄	62.2 / 97.5 (86.1)	83.9 / 77.1 (79.4)	92.9 / 92.5 (92.6)	1.9 / 99.3 (67.6)
<i>Gra</i> ₁	0.0 / 100.0 (67.5)	0.0 / 100.0 (67.5)	0.0 / 100.0 (67.5)	39.5 / 92.5 (75.3)
<i>Gra</i> ₂	0.0 / 100.0 (67.5)	66.7 / 74.0 (71.3)	44.4 / 92.9 (77.1)	26.8 / 93.2 (71.6)
<i>Gra</i> ₃	81.2 / 87.9 (85.7)	50.2 / 88.1 (75.7)	63.7 / 86.4 (79.0)	11.5 / 98.6 (70.2)
<i>Gra</i> ₄	48.3 / 97.1 (81.2)	0.0 / 100.0 (67.5)	69.4 / 94.8 (86.5)	23.3 / 93.8 (70.9)
<i>Gra</i> ₅	16.0 / 99.8 (72.5)	85.1 / 90.8 (89.0)	56.4 / 88.6 (78.2)	28.5 / 94.2 (72.8)
<i>Gra</i> ₆	0.0 / 100.0 (67.5)	23.9 / 85.0 (65.1)	42.7 / 96.3 (78.8)	21.4 / 94.0 (70.4)
<i>Gra</i> ₇	75.4 / 96.5 (89.7)	9.9 / 100.0 (70.7)	0.0 / 100.0 (67.5)	37.4 / 96.7 (77.5)

Table B.2: Statistical performance of the evaluation of the individual suction indices using LR. The results are shown as sensitivity / specificity (overall accuracy).

	max	min	mean	std
<i>Bas</i> ₁	48.8 / 86.8 (74.5)	42.2 / 86.9 (72.4)	45.3 / 86.8 (73.3)	33.1 / 95.1 (75.0)
<i>Bas</i> ₂	54.4 / 87.9 (77.1)	56.4 / 87.3 (77.2)	58.4 / 87.6 (78.1)	6.6 / 96.3 (67.2)
<i>Bas</i> ₃	54.2 / 86.6 (76.1)	50.9 / 86.5 (74.9)	52.3 / 86.5 (75.4)	24.8 / 92.6 (70.7)
<i>Ran</i> ₁	45.8 / 91.5 (76.6)	67.4 / 88.3 (81.5)	60.3 / 88.5 (79.3)	0.0 / 100.0 (67.5)
<i>Ran</i> ₂	26.9 / 98.1 (74.9)	55.9 / 87.3 (77.0)	51.7 / 89.6 (77.2)	0.0 / 100.0 (67.5)
<i>Ran</i> ₃	53.3 / 89.8 (77.9)	75.8 / 88.9 (84.6)	68.8 / 89.4 (82.7)	0.1 / 100.0 (67.5)
<i>Dir</i> ₁	0.0 / 100.0 (67.5)	79.9 / 96.5 (91.1)	84.0 / 95.6 (91.8)	35.1 / 82.9 (67.3)
<i>Dir</i> ₂	73.2 / 87.3 (82.7)	73.2 / 87.3 (82.7)	73.2 / 87.3 (82.7)	0.0 / 100.0 (67.5)
<i>Dir</i> ₃	63.5 / 92.2 (82.8)	31.3 / 87.7 (69.3)	88.5 / 91.2 (90.3)	0.0 / 100.0 (67.5)
<i>Sta</i> ₁	43.4 / 92.5 (76.4)	66.5 / 86.1 (79.7)	64.6 / 88.8 (80.9)	0.0 / 100.0 (67.5)
<i>Sta</i> ₂	69.2 / 96.2 (87.3)	0.0 / 100.0 (67.5)	86.0 / 94.3 (91.6)	19.9 / 84.8 (63.6)
<i>Sta</i> ₃	34.9 / 85.9 (69.3)	36.6 / 92.4 (74.2)	25.6 / 89.1 (68.4)	27.3 / 87.1 (67.6)
<i>Rms</i> ₁	54.2 / 86.5 (76.0)	50.6 / 86.5 (74.8)	52.2 / 86.5 (75.4)	25.1 / 92.6 (70.7)
<i>Rms</i> ₂	48.9 / 87.1 (74.7)	59.6 / 88.1 (78.8)	59.6 / 86.7 (77.9)	0.0 / 100.0 (67.5)
<i>Rms</i> ₃	82.1 / 89.0 (86.7)	67.3 / 87.7 (81.0)	74.8 / 89.0 (84.4)	0.0 / 100.0 (67.5)
<i>Rmr</i> ₁	30.5 / 97.5 (75.7)	56.6 / 90.4 (79.4)	50.7 / 92.4 (78.8)	12.2 / 93.3 (66.9)
<i>Rmr</i> ₂	55.6 / 92.9 (80.7)	47.4 / 91.7 (77.2)	57.6 / 93.8 (82.0)	49.9 / 93.4 (79.2)
<i>Rmr</i> ₃	55.9 / 92.9 (80.8)	47.6 / 91.5 (77.2)	57.6 / 93.7 (81.9)	49.8 / 93.4 (79.2)
<i>Dur</i> ₁	51.3 / 96.3 (81.7)	60.7 / 74.0 (69.6)	84.2 / 93.3 (90.3)	0.0 / 100.0 (67.5)
<i>Dur</i> ₂	41.7 / 96.2 (78.5)	50.5 / 69.4 (63.3)	84.0 / 93.4 (90.3)	0.0 / 100.0 (67.5)
<i>Dur</i> ₃	67.2 / 96.4 (86.9)	81.2 / 93.4 (89.4)	90.4 / 95.8 (94.0)	3.4 / 96.0 (65.9)
<i>Dur</i> ₄	64.5 / 96.8 (86.3)	83.1 / 78.5 (79.9)	89.8 / 95.0 (93.3)	1.4 / 99.5 (67.7)
<i>Gra</i> ₁	0.0 / 100.0 (67.5)	25.7 / 99.1 (75.2)	0.0 / 100.0 (67.5)	40.4 / 92.3 (75.4)
<i>Gra</i> ₂	0.0 / 100.0 (67.5)	91.5 / 66.1 (74.2)	46.0 / 92.2 (77.1)	26.6 / 93.4 (71.7)
<i>Gra</i> ₃	79.5 / 89.2 (86.0)	51.7 / 87.7 (75.9)	63.8 / 86.5 (79.0)	11.4 / 98.5 (70.2)
<i>Gra</i> ₄	66.6 / 94.6 (85.6)	0.0 / 100.0 (67.5)	76.4 / 91.7 (86.7)	22.7 / 94.2 (71.0)
<i>Gra</i> ₅	18.6 / 99.7 (73.3)	83.5 / 91.4 (88.8)	57.2 / 88.2 (78.0)	28.4 / 94.0 (72.7)
<i>Gra</i> ₆	0.0 / 100.0 (67.5)	24.1 / 85.0 (65.2)	43.3 / 96.1 (78.9)	19.3 / 97.2 (71.8)
<i>Gra</i> ₇	74.6 / 96.5 (89.3)	7.8 / 100.0 (70.0)	0.0 / 100.0 (67.5)	35.9 / 96.8 (77.1)

Table B.3: Statistical performance of the evaluation of the individual suction indices using BPNN. The results are shown as sensitivity / specificity (overall accuracy).

	max	min	mean	std
<i>Bas</i> ₁	37.1 / 90.0 (72.9)	46.2 / 86.0 (72.8)	45.2 / 87.4 (73.6)	42.9 / 90.9 (75.3)
<i>Bas</i> ₂	56.4 / 86.4 (76.6)	51.5 / 86.4 (74.9)	58.8 / 84.2 (75.9)	0.0 / 100.0 (67.5)
<i>Bas</i> ₃	54.9 / 85.7 (75.7)	53.1 / 84.7 (74.4)	57.8 / 84.6 (75.8)	0.0 / 100.0 (67.5)
<i>Ran</i> ₁	41.9 / 93.0 (76.3)	63.3 / 90.1 (81.3)	55.1 / 92.9 (80.6)	0.0 / 100.0 (67.5)
<i>Ran</i> ₂	35.3 / 94.0 (74.8)	54.2 / 88.1 (77.1)	45.6 / 93.0 (77.5)	0.0 / 100.0 (67.5)
<i>Ran</i> ₃	49.1 / 92.8 (78.5)	71.8 / 89.6 (83.8)	62.2 / 92.6 (82.7)	3.6 / 99.0 (67.9)
<i>Dir</i> ₁	13.0 / 97.1 (69.8)	78.4 / 97.3 (91.1)	81.5 / 96.7 (91.8)	81.9 / 68.3 (72.7)
<i>Dir</i> ₂	72.2 / 87.9 (82.8)	72.2 / 87.9 (82.8)	72.2 / 87.9 (82.8)	0.0 / 100.0 (67.5)
<i>Dir</i> ₃	64.0 / 92.0 (82.8)	88.8 / 61.0 (70.1)	88.7 / 91.3 (90.5)	0.0 / 100.0 (67.5)
<i>Sta</i> ₁	43.3 / 92.7 (76.6)	64.2 / 88.6 (80.6)	56.9 / 92.6 (81.0)	1.3 / 99.6 (67.6)
<i>Sta</i> ₂	68.4 / 96.6 (87.4)	14.4 / 95.9 (69.4)	83.7 / 95.8 (91.9)	89.4 / 62.7 (71.4)
<i>Sta</i> ₃	89.8 / 63.4 (72.0)	33.6 / 93.8 (74.2)	79.6 / 64.9 (69.6)	87.6 / 63.3 (71.2)
<i>Rms</i> ₁	54.6 / 85.8 (75.6)	53.1 / 84.4 (74.2)	57.4 / 85.2 (76.1)	0.0 / 100.0 (67.5)
<i>Rms</i> ₂	47.5 / 88.5 (75.1)	62.3 / 86.4 (78.5)	58.2 / 87.3 (77.8)	0.0 / 100.0 (67.5)
<i>Rms</i> ₃	79.2 / 89.6 (86.2)	63.6 / 89.5 (81.0)	75.1 / 89.4 (84.7)	0.0 / 100.0 (67.5)
<i>Rmr</i> ₁	32.0 / 95.9 (74.9)	50.8 / 92.5 (78.9)	40.9 / 95.6 (77.8)	0.0 / 100.0 (67.5)
<i>Rmr</i> ₂	68.2 / 90.0 (82.9)	49.6 / 90.4 (77.1)	69.8 / 90.1 (83.5)	88.7 / 63.5 (71.7)
<i>Rmr</i> ₃	68.1 / 90.0 (82.9)	49.6 / 90.3 (77.0)	69.5 / 90.1 (83.4)	91.9 / 60.9 (71.0)
<i>Dur</i> ₁	41.1 / 97.1 (78.9)	95.9 / 63.1 (73.7)	81.9 / 94.2 (90.2)	72.4 / 64.4 (66.9)
<i>Dur</i> ₂	41.1 / 96.4 (78.4)	96.0 / 62.8 (73.6)	82.6 / 94.3 (90.5)	0.0 / 100.0 (67.5)
<i>Dur</i> ₃	59.8 / 97.0 (84.9)	78.8 / 94.6 (89.5)	88.6 / 97.0 (94.3)	64.0 / 68.9 (66.7)
<i>Dur</i> ₄	62.5 / 97.5 (86.1)	81.9 / 79.2 (80.1)	87.1 / 95.9 (93.1)	0.0 / 100.0 (67.5)
<i>Gra</i> ₁	24.3 / 96.8 (73.1)	40.7 / 93.0 (75.9)	0.0 / 100.0 (67.5)	36.1 / 94.9 (75.7)
<i>Gra</i> ₂	17.6 / 97.2 (71.3)	58.2 / 76.6 (70.7)	42.6 / 94.6 (77.6)	5.6 / 98.9 (68.5)
<i>Gra</i> ₃	74.3 / 90.8 (85.4)	43.0 / 91.3 (75.5)	58.2 / 90.3 (79.8)	11.8 / 98.4 (70.2)
<i>Gra</i> ₄	82.4 / 88.5 (86.6)	22.9 / 95.0 (71.5)	75.1 / 93.2 (87.3)	19.7 / 96.9 (71.8)
<i>Gra</i> ₅	32.7 / 96.4 (75.6)	80.6 / 91.8 (88.2)	47.9 / 92.7 (78.0)	25.4 / 95.3 (72.6)
<i>Gra</i> ₆	33.7 / 95.6 (75.4)	38.0 / 75.6 (63.4)	44.8 / 94.3 (78.2)	19.5 / 96.8 (71.7)
<i>Gra</i> ₇	77.5 / 96.3 (90.2)	18.6 / 98.5 (72.5)	38.7 / 92.8 (75.1)	43.3 / 95.4 (78.5)

Table B.4: Statistical performance of the evaluation of the individual suction indices using KNN. The results are shown as sensitivity / specificity (overall accuracy).

	max	min	mean	std
<i>Bas</i> ₁	76.2 / 85.9 (82.7)	81.9 / 87.4 (85.5)	78.3 / 87.2 (84.2)	57.5 / 82.5 (74.5)
<i>Bas</i> ₂	76.2 / 84.4 (81.7)	76.6 / 84.0 (81.5)	82.1 / 85.7 (84.5)	55.4 / 78.9 (71.2)
<i>Bas</i> ₃	75.5 / 86.7 (83.1)	68.4 / 85.8 (80.1)	67.5 / 84.8 (79.1)	56.6 / 81.0 (73.0)
<i>Ran</i> ₁	62.5 / 84.5 (77.2)	69.7 / 86.6 (81.1)	69.0 / 87.4 (81.3)	51.0 / 80.4 (70.8)
<i>Ran</i> ₂	57.4 / 84.8 (75.8)	65.2 / 83.7 (77.7)	61.7 / 85.6 (77.8)	51.4 / 79.9 (70.6)
<i>Ran</i> ₃	66.5 / 86.4 (79.9)	79.6 / 88.0 (85.3)	72.2 / 88.4 (83.1)	48.5 / 78.3 (68.6)
<i>Dir</i> ₁	51.5 / 83.2 (72.9)	82.4 / 95.5 (91.3)	84.3 / 95.6 (91.9)	71.0 / 78.8 (76.3)
<i>Dir</i> ₂	74.0 / 86.6 (82.5)	74.0 / 86.6 (82.5)	74.0 / 86.6 (82.5)	51.0 / 98.0 (82.7)
<i>Dir</i> ₃	69.0 / 88.0 (81.9)	70.5 / 80.7 (77.3)	87.7 / 91.6 (90.3)	40.8 / 79.9 (67.2)
<i>Sta</i> ₁	60.9 / 85.4 (77.4)	72.5 / 84.7 (80.7)	70.8 / 87.1 (81.8)	53.6 / 79.1 (70.8)
<i>Sta</i> ₂	78.3 / 93.3 (88.4)	48.7 / 81.5 (70.8)	85.7 / 94.6 (91.7)	74.5 / 81.6 (79.2)
<i>Sta</i> ₃	65.3 / 78.9 (74.4)	51.5 / 84.2 (73.6)	62.2 / 79.8 (74.0)	67.3 / 79.8 (75.7)
<i>Rms</i> ₁	76.7 / 85.4 (82.5)	70.0 / 85.7 (80.5)	69.3 / 85.0 (79.8)	54.7 / 79.7 (71.5)
<i>Rms</i> ₂	61.3 / 84.4 (76.9)	73.2 / 83.2 (79.9)	68.3 / 84.0 (78.9)	49.5 / 77.8 (68.6)
<i>Rms</i> ₃	86.5 / 88.3 (87.7)	70.2 / 87.1 (81.6)	80.7 / 88.5 (86.0)	51.1 / 76.4 (68.2)
<i>Rmr</i> ₁	62.3 / 84.5 (77.2)	63.6 / 87.7 (79.9)	64.2 / 86.2 (79.0)	63.9 / 80.6 (75.0)
<i>Rmr</i> ₂	75.3 / 87.4 (83.4)	69.2 / 85.3 (80.0)	75.9 / 86.7 (83.2)	70.5 / 83.8 (79.3)
<i>Rmr</i> ₃	75.0 / 87.1 (83.1)	67.2 / 85.8 (79.7)	75.0 / 86.7 (82.9)	72.6 / 85.0 (81.0)
<i>Dur</i> ₁	42.2 / 98.8 (80.4)	7.7 / 98.3 (68.8)	86.9 / 92.8 (90.8)	73.0 / 88.6 (83.5)
<i>Dur</i> ₂	28.5 / 99.4 (76.3)	21.6 / 99.2 (74.0)	86.0 / 93.4 (90.9)	47.2 / 80.2 (69.4)
<i>Dur</i> ₃	51.1 / 98.8 (83.3)	4.4 / 99.3 (68.5)	89.5 / 96.6 (94.2)	73.7 / 86.7 (82.4)
<i>Dur</i> ₄	53.9 / 99.1 (84.5)	0.0 / 100.0 (67.5)	89.2 / 95.1 (93.1)	70.7 / 86.4 (81.2)
<i>Gra</i> ₁	50.4 / 85.7 (74.2)	58.4 / 83.6 (75.4)	59.2 / 79.8 (73.1)	56.2 / 84.6 (75.3)
<i>Gra</i> ₂	59.6 / 86.5 (77.7)	74.6 / 81.1 (79.0)	60.4 / 86.2 (77.8)	60.0 / 81.2 (74.3)
<i>Gra</i> ₃	79.2 / 90.1 (86.4)	60.1 / 84.8 (76.7)	65.0 / 87.6 (80.2)	47.3 / 81.4 (70.2)
<i>Gra</i> ₄	90.6 / 87.5 (88.5)	53.3 / 81.1 (72.0)	79.7 / 90.5 (87.0)	52.9 / 81.2 (72.0)
<i>Gra</i> ₅	55.6 / 85.1 (75.5)	85.5 / 90.4 (88.8)	67.5 / 86.1 (80.0)	52.3 / 82.2 (72.5)
<i>Gra</i> ₆	57.0 / 86.4 (76.7)	71.5 / 84.3 (80.1)	59.6 / 87.5 (78.4)	52.2 / 82.0 (72.3)
<i>Gra</i> ₇	80.6 / 94.2 (89.8)	52.6 / 84.6 (74.2)	58.6 / 86.1 (77.1)	59.3 / 86.7 (77.7)

LIST OF PUBLICATIONS AND PAPERS PRESENTED

- Ooi, H.-L., Ng, S.-C., Lim, E. (2013) "ANO detection with k-nearest neighbor using Minkowski distance." In *International Conference of Signal Processing Systems (ICSPS)* (Vol.1, pp. 208-211).
- Ooi, H.-L., Ng, S.-C., Lim, E., Salamonsen, R.F., Avolio, A.P. and Lovell, N.H. (2014) "Robust aortic valve non-opening detection for different cardiac condition," *Artificial Organs*, 38(3), E57-E67.

University of Malaysia

REFERENCES

- Allen, G. S., Murray, K. D., & Olsen, D. B. (1996). Control of the artificial heart. *ASAIO Journal*, 42(6), 932–937.
- AlOmari, A.-H. H., Savkin, A. V., Stevens, M., Mason, D. G., Timms, D. L., Salamonsen, R. F., & Lovell, N. H. (2013). Developments in control systems for rotary left ventricular assist devices for heart failure patients: a review. *Physiological Measurement*, 34(1).
- Andrade, J. G., Al-Saloos, H., Jeewa, A., Sandor, G. G., & Cheung, A. (2010). Facilitated cardiac recovery in fulminant myocarditis: pediatric use of the Impella LP 5.0 pump. *The Journal of Heart and Lung Transplantation*, 29(1), 96–97.
- Antonogeorgos, G., Panagiotakos, D. B., Priftis, K. N., & Tzonou, A. (2009). Logistic regression and linear discriminant analyses in evaluating factors associated with asthma prevalence among 10-to 12-years-old children: divergence and similarity of the two statistical methods. *International Journal of Pediatrics*.
- Arndt, A., Nüsser, P., Graichen, K., Müller, J., & Lampe, B. (2008). Physiological control of a rotary blood pump with selectable therapeutic options: control of pulsatility gradient. *Artificial Organs*, 32(10), 761–771.
- Arndt, A., Nüsser, P., & Lampe, B. (2010). Fully autonomous preload-sensitive control of implantable rotary blood pumps. *Artificial Organs*, 34(9), 726–735.
- Ayre, P., Lovell, N., Morris, R., Wilson, M., & Woodard, J. (2001). Identifying physiologically significant pumping state transitions in implantable rotary blood pumps used as left ventricular assist devices: an in-vivo study. In *Proceedings of the 23rd Annual International Conference of the IEEE Engineering in Medicine and Biology Society (EMBS)* (Vol. 1, pp. 445–448).
- Ayre, P., Mason, D., & Karantonis, D. (2007). *System and method of controlling a rotary blood pump* (No. EP 1847281 A1).
- Balao, L. A., Liu, D., Boston, J., Simaan, M., & Antaki, J. (2000). Control of rotary heart assist devices. In *Proceedings of the American Control Conference* (Vol. 5, pp. 2982–2986).
- Barr, M. L., Bourge, R. C., Orens, J. B., McCurry, K. R., Ring, W. S., Hulbert-Shearon, T. E., & Merion, R. M. (2005). Thoracic organ transplantation in the United States, 1994–2003. *American Journal of Transplantation*, 5(4p2), 934–949.
- Beck, D., & Foster, J. A. (2014). Machine learning techniques accurately classify microbial communities by bacterial vaginosis characteristics. *PloS One*, 9(2), e87830.
- Bishop, C. J., Mason, N. O., Kfoury, A. G., Lux, R., Stoker, S., Horton, K., ... Reid, B. B. (2010). A novel non-invasive method to assess aortic valve opening in heartmate ii left ventricular assist device patients using a modified Karhunen-Loève transformation. *The Journal of Heart and Lung Transplantation*, 29(1), 27–31.
- Boron, W., & Boulpaep, E. (2008). *Medical physiology*. Elsevier Health Sciences. Retrieved from <http://books.google.com.my/books?id=H1MJRw08ihgC> (Accessed: 2014-06-09)
- Borovetz, H., Kormos, R., Griffith, B., & Hung, T. (1988). Clinical utilization of the artificial heart. *Critical Reviews in Biomedical Engineering*, 17(2), 179–201.
- Boston, J., Antaki, J., & Simaan, M. (2003). Hierarchical control of heart-assist devices. *IEEE Robotics & Automation Magazine*, 10(1), 54–64.
- Boston, J., Balao, L., Liu, D., Simaan, M., Choi, S., & Antaki, J. F. (2000). Combination of data approaches to heuristic control and fault detection. In *Proceedings of the Control Applications* (pp. 98–103).

- Boston, J., Simaan, M. A., Antaki, J., Yu, Y.-C., & Choi, S. (1998). Intelligent control design for heart assist devices. In *Proceedings of Intelligent Systems and Semiotics (ISAS)* (pp. 497–502).
- Chang, D.-H., & Islam, S. (2000). Estimation of soil physical properties using remote sensing and artificial neural network. *Remote Sensing of Environment*, 74(3), 534–544.
- Choi, S. (2003). Suction detection in left ventricular assist system: data fusion approach. *International Journal of Control Automation and Systems*, 1(3), 368–375.
- Choi, S., Boston, J. R., & Antaki, J. F. (2005). An investigation of the pump operating characteristics as a novel control index for LVAD control. *International Journal of Control, Automation, and Systems*, 3(1), 100–108.
- Choi, S., Boston, J. R., & Antaki, J. F. (2007). Hemodynamic controller for left ventricular assist device based on pulsatility ratio. *Artificial Organs*, 31(2), 114–125.
- Connelly, J. H., Abrams, J., Klima, T., Vaughn, W. K., & Frazier, O. (2003). Acquired commissural fusion of aortic valves in patients with left ventricular assist devices. *The Journal of Heart and Lung Transplantation*, 22(12), 1291–1295.
- DeMarzo, A. P., & Lang, R. M. (1996). A new algorithm for improved detection of aortic valve opening by impedance cardiography. In *Computers in Cardiology* (pp. 373–376).
- Dixon, J. F., & Farris, C. D. (1991). The AbioMed BVS 5000 system. *AACN Advanced Critical Care*, 2(3), 552–561.
- Dreiseitl, S., & Ohno-Machado, L. (2002). Logistic regression and artificial neural network classification models: a methodology review. *Journal of Biomedical Informatics*, 35(5), 352–359.
- Efron, B. (1983). Estimating the error rate of a prediction rule: improvement on cross-validation. *Journal of the American Statistical Association*, 78(382), 316–331.
- Endo, G., Araki, K., Kojima, K., Nakamura, K., Matsuzaki, Y., & Onitsuka, T. (2001). The index of motor current amplitude has feasibility in control for continuous flow pumps and evaluation of left ventricular function. *Artificial Organs*, 25(9), 697–702.
- Farrar, D. J., Holman, W. R., McBride, L. R., Kormos, R. L., Icenogle, T. B., Hendry, P. J., . . . Frazier, H. (2002). Long-term follow-up of thoratec ventricular assist device bridge-to-recovery patients successfully removed from support after recovery of ventricular function. *The Journal of Heart and Lung Transplantation*, 21(5), 516–521.
- Ferreira, A., Boston, J. R., & Antaki, J. F. (2007). A rule-based controller based on suction detection for rotary blood pumps. In *Proceedings of the 29th Annual International Conference of the IEEE Engineering in Medicine and Biology Society (EMBS)* (pp. 3978–3981).
- Ferreira, A., Boston, J. R., & Antaki, J. F. (2009). A control system for rotary blood pumps based on suction detection. *IEEE Transactions on Biomedical Engineering*, 56(3), 656–665.
- Ferreira, A., Chen, S., Simaan, M. A., Boston, J. R., & Antaki, J. F. (2006). A discriminant-analysis-based suction detection system for rotary blood pumps. In *Proceedings of the 28th Annual International Conference of the IEEE Engineering in Medicine and Biology Society (EMBS)* (pp. 5382–5385).
- Ferreira, A., Simaan, M., Boston, J., & Antaki, J. (2006). Frequency and time-frequency based indices for suction detection in rotary blood pumps. In *Proceedings of the IEEE International Conference on Acoustics, Speech and Signal Processing (ICASSP)* (Vol. 2, pp. II–II).
- Folkes, S., Lahav, O., & Maddox, S. (1996). An artificial neural network approach to the classification of galaxy spectra. *Monthly Notices of the Royal Astronomical Society*, 283(2), 651–665.
- Gao, B., Gu, K., Zeng, Y., & Chang, Y. (2012). An anti-suction control for an intra-aorta pump using blood assistant index: A numerical simulation. *Artificial Organs*, 36(3), 275–282.

- Gao, B., Nie, L. Y., Chang, Y., & Zeng, Y. (2011). Physiological control of intraaorta pump based on heart rate. *ASAIO Journal*, 57(3), 152–157.
- Geng, M. (1992). *A comparison of logistic regression to random forests for exploring differences in risk factors associated with stage at diagnosis between black and white colon cancer patients*. Unpublished doctoral dissertation, The Graduate School of Public Health, University of Pittsburgh, Pennsylvania, United States.
- Granegger, M., Moscato, F., Mahr, S., Wieselthaler, G., & Schima, H. (2011). Assessment of the aortic valve opening during rotary blood pump support. *ASAIO Journal*, 57, 75.
- Granegger, M., Schima, H., Zimpfer, D., & Moscato, F. (2013). Assessment of aortic valve opening during rotary blood pump support using pump signals. *Artificial Organs*, 38(4).
- Guyton, A., & Hall, J. (2006). *Textbook of medical physiology*. Elsevier Saunders. Retrieved from <http://books.google.com.my/books?id=K8-d-KzxvTYC> (Accessed: 2014-06-09)
- Hosmer, D., & Lemeshow, S. (2004). *Applied logistic regression*. Wiley. Retrieved from <http://books.google.com.my/books?id=Po0RLQ7USIMC> (Accessed: 2014-06-09)
- Kamdar, F., Boyle, A., Liao, K., Colvin-adams, M., Joyce, L., & John, R. (2009). Effects of centrifugal, axial, and pulsatile left ventricular assist device support on end-organ function in heart failure patients. *The Journal of Heart and Lung Transplantation*, 28(4), 352–359.
- Karantonis, D. M. (2008). *Control of a rotary blood pump*. Unpublished doctoral dissertation, Ph. D. Dissertation, Graduate School of Biomedical Engineering, The University of New South Wales (UNSW), Sydney, Australia.
- Karantonis, D. M., Cloherty, S. L., Lovell, N. H., Mason, D. G., Salamonsen, R. F., & Ayre, P. J. (2008). Noninvasive detection of suction in an implantable rotary blood pump using neural networks. *International Journal of Computational Intelligence and Applications*, 7(03), 237–247.
- Karantonis, D. M., Cloherty, S. L., Mason, D. G., Salamonsen, R. F., Ayre, P. J., & Lovell, N. H. (2006). Automated non-invasive detection of pumping states in an implantable rotary blood pump. In *Proceedings of the 28th Annual International Conference of the IEEE Engineering in Medicine and Biology Society (EMBS)* (pp. 5386–5389).
- Karantonis, D. M., Lovell, N. H., Ayre, P. J., Mason, D. G., & Cloherty, S. L. (2006). Identification and classification of physiologically significant pumping states in an implantable rotary blood pump. *Artificial Organs*, 30(9), 671–679.
- Karantonis, D. M., Lovell, N. H., Ayre, P. J., Mason, D. G., & Cloherty, S. L. (2007). Classification of physiologically significant pumping states in an implantable rotary blood pump: effects of cardiac rhythm disturbances. *Artificial Organs*, 31(6), 476–479.
- Karantonis, D. M., Mason, D. G., Salamonsen, R. F., Ayre, P. J., Cloherty, S. L., & Lovell, N. H. (2007). Classification of physiologically significant pumping states in an implantable rotary blood pump: patient trial results. *ASAIO Journal*, 53(5), 617–622.
- Kohavi, R., et al. (1995). A study of cross-validation and bootstrap for accuracy estimation and model selection. In *International Joint Conference on Artificial Intelligence (IJCAI)* (Vol. 14, pp. 1137–1145).
- Kumpati, G. S., McCarthy, P. M., & Hoercher, K. J. (2001). Left ventricular assist device bridge to recovery: a review of the current status. *The Annals of Thoracic Surgery*, 71(3), S103–S108.
- Lee, S.-I., Lee, H., Abbeel, P., & Ng, A. Y. (2006). Efficient l_1 regularized logistic regression. In *Proceedings of the National Conference on Artificial Intelligence* (Vol. 21, p. 401).
- Lietz, K., Long, J. W., Kfoury, A. G., Slaughter, M. S., Silver, M. A., Milano, C. A., ... Miller, L. W. (2007). Outcomes of left ventricular assist device implantation as destination therapy in the post-

rematch era implications for patient selection. *Circulation*, 116(5), 497–505.

- Lim, E. (2010). *Characterisation of cardiovascular-rotary blood pump interaction*. Unpublished doctoral dissertation, Ph. D. Dissertation, Graduate School of Biomedical Engineering, The University of New South Wales (UNSW), Sydney, Australia.
- Lim, E., Dokos, S., Salamonsen, R. F., Rosenfeldt, F. L., Ayre, P. J., & Lovell, N. H. (2012). Numerical optimization studies of cardiovascular-rotary blood pump interaction. *Artificial Organs*, 36(5), E110–E124.
- Lin, Y., Chou, N.-K., Chen, Y.-Y., & Jan, G. (2001). A pump control index for reducing suction and backflow effect caused by the portable centrifugal blood pump. In *Proceedings of the 23rd Annual International Conference of the IEEE Engineering in Medicine and Biology Society (EMBS)* (Vol. 1, pp. 465–466).
- Long, J. W., Kfoury, A. G., Slaughter, M. S., Silver, M., Milano, C., Rogers, J., . . . Frazier, O. (2005). Long-term destination therapy with the heartmate xve left ventricular assist device: Improved outcomes since the REMATCH study. *Congestive Heart Failure*, 11(3), 133–138.
- Mackay, J., Mensah, G., Mendis, S., Greenlund, K., & Organization, W. H. (2004). *The atlas of heart disease and stroke*. World Health Organization. Retrieved from <http://books.google.com.my/books?id=JagK-qIWaZoC> (Accessed: 2014-02-25)
- Mamdani, E. H. (1974). Application of fuzzy algorithms for control of simple dynamic plant. In *Proceedings of the Institution of Electrical Engineers* (Vol. 121, pp. 1585–1588).
- Mason, D. G., Hilton, A. K., & Salamonsen, R. F. (2008). Reliable suction detection for patients with rotary blood pumps. *ASAIO Journal*, 54(4), 359–366.
- Matoba, Y., Okubo, H., & Nosé, Y. (2004). Therapeutic left ventricular assist device and apheresis on dilated cardiomyopathy. *Artificial Organs*, 28(2), 171–181.
- Mendis, S., Puska, P., Norrving, B., Organization, W. H., Federation, W. H., & Organization, W. S. (2011). *Global atlas on cardiovascular disease prevention and control*. World Health Organization in collaboration with the World Heart Federation and the World Stroke Organization. Retrieved from <http://books.google.com.my/books?id=ZRbKygAACAAJ> (Accessed: 2014-06-10)
- Michie, D., Spiegelhalter, D. J., & Taylor, C. C. (1994). *Machine learning, neural and statistical classification*. Ellis Horwood.
- Moustafa, A. A., Alqadi, Z. A., & Shahroury, E. A. (2011). Performance evaluation of artificial neural networks for spatial data analysis. *Contemporary Engineering Sciences*, 4(4), 149–163.
- Naiyanetr, P., Moscato, F., Vollkron, M., Zimpfer, D., Wieselthaler, G., & Schima, H. (2010). Continuous assessment of cardiac function during rotary blood pump support: A contractility index derived from pump flow. *The Journal of Heart and Lung Transplantation*, 29(1), 37–44.
- Navia, J. L., McCarthy, P. M., Hoercher, K. J., Smedira, N. G., Banbury, M. K., & Blackstone, E. H. (2002). Do left ventricular assist device (LVAD) bridge-to-transplantation outcomes predict the results of permanent lvad implantation? *The Annals of Thoracic Surgery*, 74(6), 2051–2063.
- Ng, S.-C., Lim, E., Mason, D. G., Avolio, A. P., & Lovell, N. H. (2013). Evaluation of suction detection during different pumping states in an implantable rotary blood pump. *Artificial Organs*, 37(8), E145–E154.
- Nosé, Y., Motomura, T., Miyamoto, H., Ohta, K., Takaba, J., & Sugita, Y. (2010). The need to change our objective for artificial heart development: from totally implantable permanent ventricular assist devices to wearable therapeutic ventricular assist devices. *Artificial Organs*, 34(12), 1069–1076.
- Nosé, Y., Yoshikawa, M., Murabayashi, S., & Takano, T. (2000). Development of rotary blood pump technology: past, present, and future. *Artificial Organs*, 24(6), 412–420.

- Ooi, H.-L., Ng, S.-C., & Lim, E. (2013). ANO detection with k-nearest neighbor using Minkowski distance. *International Journal of Signal Processing Systems (IJSPPS)*, 1(2), 208–211.
- Ooi, H.-L., Ng, S.-C., Lim, E., Salamonsen, R. F., Avolio, A. P., & Lovell, N. H. (2014). Robust aortic valve non-opening detection for different cardiac conditions. *Artificial Organs*, 38(3), E57–E67.
- Park, S. J., Tector, A., Piccioni, W., Raines, E., Gelijns, A., Moskowitz, A., ... others (2005). Left ventricular assist devices as destination therapy: a new look at survival. *The Journal of Thoracic and Cardiovascular Surgery*, 129(1), 9–17.
- Park, S. Y., & Liu, Y. (2011). Robust penalized logistic regression with truncated loss functions. *Canadian Journal of Statistics*, 39(2), 300–323.
- Pohar, M., Blas, M., & Turk, S. (2004). Comparison of logistic regression and linear discriminant analysis: a simulation study. *Metodolski Zvezki*, 1(1), 143–161.
- Pudil, P., Novovičová, J., & Kittler, J. (1994). Floating search methods in feature selection. *Pattern recognition letters*, 15(11), 1119–1125.
- Qin, B., Xia, Y., & Li, F. (2009). DTU: a decision tree for uncertain data. In *Advances in knowledge discovery and data mining* (Vol. 5476, pp. 4–15). Springer.
- Refaeilzadeh, P., Tang, L., & Liu, H. (2009). Cross-validation. In *Encyclopedia of database systems* (pp. 532–538). Springer.
- Riedmiller, M., & Braun, H. (1993). A direct adaptive method for faster backpropagation learning: The RPROP algorithm. In *Proceedings of IEEE International Conference on Neural Networks (ICNN)* (pp. 586–591).
- Rose, A. G., Park, S. J., Bank, A. J., & Miller, L. W. (2000). Partial aortic valve fusion induced by left ventricular assist device. *The Annals of Thoracic Surgery*, 70(4), 1270–1274.
- Salamonsen, R. F., Lim, E., Gaddum, N., AlOmari, A.-H. H., Gregory, S. D., Stevens, M., ... others (2012). Theoretical foundations of a Starling-like controller for rotary blood pumps. *Artificial Organs*, 36(9), 787–796.
- Salamonsen, R. F., Mason, D. G., & Ayre, P. J. (2011). Response of rotary blood pumps to changes in preload and afterload at a fixed speed setting are unphysiological when compared with the natural heart. *Artificial Organs*, 35(3), E47–E53.
- Schmid, C., Tjan, T. D., Etz, C., Schmidt, C., Wenzelburger, F., Wilhelm, M., ... Scheld, H. H. (2005). First clinical experience with the Incor left ventricular assist device. *The Journal of Heart and Lung Transplantation*, 24(9), 1188–1194.
- Shakhnarovich, G., El-Yaniv, R., & Baram, Y. (2001). Smoothed bootstrap and statistical data cloning for classifier evaluation. In *Proceedings of the 18th International Conference on Machine Learning (ICML)* (pp. 521–528).
- Tanaka, A., Yoshizawa, M., Olegario, P., Ogawa, D., Abe, K., Motomura, T., ... Nosé, Y. (2006). Detection and avoiding ventricular suction of ventricular assist devices. In *Proceedings of the 27th Annual International Conference of the IEEE Engineering in Medicine and Biology Society (EMBS)* (pp. 402–405).
- The Alfred Intensive Care Unit. (2011). *Artificial hearts*. <http://www.alfredicu.org.au/special-interest-groups/artificial-hearts/>. (Accessed: 2013-06-29)
- Tu, J. V. (1996). Advantages and disadvantages of using artificial neural networks versus logistic regression for predicting medical outcomes. *Journal of Clinical Epidemiology*, 49(11), 1225–1231.
- Tzallas, A. T., Rigas, G., Karvounis, E. C., Tsiouras, M. G., Goletsis, Y., Zielinski, K., ... Trivella, M. G.

- (2012). A Gaussian mixture model to detect suction events in rotary blood pumps. In *Proceedings of the 12th International Conference on Bioinformatics & Bioengineering (BIBE)* (pp. 127–131).
- Voigt, O., Benkowski, R. J., & Morello, G. F. (2005). Suction detection for the MicroMed DeBakey left ventricular assist device. *ASAIO journal*, *51*(4), 321–328.
- Vollkron, M., Schima, H., Huber, L., Benkowski, R., Morello, G., & Wieselthaler, G. (2005). Development of a reliable automatic speed control system for rotary blood pumps. *The Journal of Heart and Lung Transplantation*, *24*(11), 1878–1885.
- Vollkron, M., Voigt, P., Ta, J., Wieselthaler, G., & Schima, H. (2007). Suction events during left ventricular support and ventricular arrhythmias. *The Journal of Heart and Lung Transplantation*, *26*(8), 819–825.
- Wang, Y., Faragallah, G., Divo, E., & Simaan, M. A. (2011). Detection of ventricular suction in an implantable rotary blood pump using support vector machines. In *Proceedings of the 33rd Annual International Conference of the IEEE Engineering in Medicine and Biology Society (EMBS)* (pp. 3318–3321).
- Wang, Y., & Simaan, M. A. (2013). A suction detection system for rotary blood pumps based on the lagrangian support vector machine algorithm. *IEEE Journal of Biomedical and Health Informatics*, *17*(3), 654–663.
- Xanthopoulos, P., Pardalos, P., & Trafalis, T. (2012). *Robust data mining*. Springer. Retrieved from <http://books.google.com.my/books?id=CqMlwCO5yJcC> (Accessed: 2014-06-14)
- Yi, W. (2007). Physiological control of rotary left ventricular assist device. In *26th Chinese Control Conference (CCC)* (pp. 469–474).
- Yuhki, A., Hatoh, E., Nogawa, M., Miura, M., Shimazaki, Y., & Takatani, S. (1999). Detection of suction and regurgitation of the implantable centrifugal pump based on the motor current waveform analysis and its application to optimization of pump flow. *Artificial Organs*, *23*(6), 532–537.
- Zimpfer, D., Zrunek, P., Roethy, W., Czerny, M., Schima, H., Huber, L., ... Wieselthaler, G. (2007). Left ventricular assist devices decrease fixed pulmonary hypertension in cardiac transplant candidates. *The Journal of Thoracic and Cardiovascular Surgery*, *133*(3), 689–695.